PAPER • OPEN ACCESS

Progress and open questions in the physics of neutrino cross sections at intermediate energies

To cite this article: L Alvarez-Ruso *et al* 2014 *New J. Phys.* **16** 075015

New Journal of Physics
The open access journal at the forefront of physics
Deutsche Physikalische Gesellschaft DPG | IOP Institute of Physics

Progress and open questions in the physics of neutrino cross sections at intermediate energies

L Alvarez-Ruso[1], Y Hayato[2] and J Nieves[1]

[1] Instituto de Física Corpuscular (IFIC), Centro Mixto CSIC-Universidad de Valencia, E-46071 Valencia, Spain
[2] University of Tokyo, Institute for Cosmic Ray Research, Kamioka Observatory, Kamioka, Japan
E-mail: luis.alvarez@ific.uv.es

Received 17 March 2014, revised 5 May 2014
Accepted for publication 27 May 2014
Published 30 July 2014

New Journal of Physics **16** (2014) 075015

doi:10.1088/1367-2630/16/7/075015

Abstract

New and more precise measurements of neutrino cross sections have renewed interest in a better understanding of electroweak interactions on nucleons and nuclei. This effort is crucial to achieving the precision goals of the neutrino oscillation program, making new discoveries, like the CP violation in the leptonic sector, possible. We review the recent progress in the physics of neutrino cross sections, putting emphasis on the open questions that arise in the comparison with new experimental data. Following an overview of recent neutrino experiments and future plans, we present some details about the theoretical development in the description of (anti)neutrino-induced quasielastic (QE) scattering and the role of multi-nucleon QE-like mechanisms. We cover not only pion production in nucleons and nuclei but also other inelastic channels including strangeness production and photon emission. Coherent reaction channels on nuclear targets are also discussed. Finally, we briefly describe some of the Monte Carlo event generators, which are at the core of all neutrino oscillation and cross-section measurements.

Keywords: neutrino cross sections, oscillation experiments, electroweak hadronic form factors, nuclear effects

1. Introduction

Recent years have witnessed intense experimental and theoretical activity aimed at a better understanding of neutrino interactions with nucleons and nuclei. Although this activity has been stimulated mostly by the needs of neutrino oscillation experiments in their quest for a precise determination of neutrino properties, the relevance of neutrino interactions with matter extends over a large variety of topics in astrophysics, physics beyond the Standard Model, hadronic physics and nuclear physics.

Oscillation experiments: at present, the main motivation for neutrino cross-section studies comes from oscillation experiments. They aim at a precise determination of mass-squared differences and mixing angles in ν_μ disappearance and ν_e appearance measurements. The ability to reconstruct the neutrino energy is crucial for this program. Indeed, oscillation probabilities, such as

$$P\left(\nu_\mu \to \nu_\tau\right) = \sin^2 2\theta_{23} \sin^2 \frac{\Delta m^2_{32} L}{4E_\nu} \tag{1}$$

depend on the neutrino energy E_ν, which is not known for broad fluxes. A reliable determination of the neutrino energies in nuclear targets requires a good understanding of the reaction mechanisms and a precise simulation of final state interactions (FSI). There are also irreducible backgrounds, for example from neutral current (NC) π^0 or γ production when these particle produced showers are misidentified as electrons from $\nu_e\, n \to e^-\, p$.

Astrophysics: neutrinos play an important role in astrophysical phenomena and carry information about the emitting sources. In particular, the dynamics of core-collapse supernovae is controlled by neutrino interactions. The neutron rich environment of supernovae is a candidate site for r-process nucleosynthesis because radiated neutrinos convert neutrons into protons. To address these questions a good knowledge of low energy neutrino production and detection cross sections is required [1, 2].

Physics beyond the Standard Model: non-standard neutrino interactions leading, for example, to deviations from universality in the weak couplings or flavor violation in NC processes could affect neutrino production, propagation, and detection processes as subleading effects (see [3] for a recent review). Long and short baseline experiments allow one to set bounds on these interactions.

Hadronic physics: neutrino cross-section measurements allow us to investigate the axial structure of the nucleon and baryon resonances, enlarging our views of hadron structure beyond what is presently known from experiments with hadronic and electromagnetic probes, not forgetting about lattice QCD. Another fundamental and open question is the strangeness content of the nucleon spin which can be best unraveled in $\nu\, p(n) \to \nu\, p(n)$ studies.

Nuclear physics: modern neutrino experiments are performed with nuclear targets. For nuclear physics this represents a challenge and an opportunity. A challenge because precise knowledge of neutrino and baryon properties can only be achieved if nuclear effects are under control. An opportunity because neutrino cross sections incorporate richer information than electron-scattering ones, providing an excellent testing ground for nuclear structure, many-body mechanisms and reaction models.

We discuss the progress in the physics of neutrino interactions with nucleons and nuclei at intermediate energies, highlighting some of the open questions and challenges standing ahead.

We start with an overview of recent neutrino experiments and future prospects. The theory of neutrino interactions on nucleons is introduced placing emphasis on the symmetries, the sources of experimental information and major uncertainties. Pion production is covered, but also other no less interesting inelastic reactions with smaller cross sections. We present different descriptions of neutrino–nucleus scattering from a common perspective, indicating the different approximations and assumptions adopted. The role of multinucleon mechanisms is stressed as well as their impact on the neutrino energy reconstruction. Nuclear medium effects and FSI in particle production off nuclear targets are also addressed, paying special attention to the coherent reaction channels and their different theoretical approaches. The last part is devoted to the Monte Carlo (MC) models, which are applied to the simulation and analysis of neutrino experiments.

The present review complements other excellent articles of this kind that have recently appeared [4–7]. In [7] a very broad range of energies from the eV to EeV is covered, providing an impressive account of the existing experimental data. As we focus on the few-GeV region, we do not discuss the deep inelastic regime, nor questions like shadowing or duality, all of which can be found in [5, 6]. Instead, we address topics like superscaling, QE and inelastic strangeness production, photon emission or MC generators, which are at most mentioned in previous reviews.

2. Recent and future oscillation and cross-section experiments

The discovery of atmospheric neutrino oscillations [8] was made through the observed distribution of the outgoing charged leptons, produced by the interactions of atmospheric neutrinos with water in the Super-Kamiokande (SK) detector. The signature of the ν_μ disappearance was clearly seen as an up-down asymmetry in the zenith-angle distribution of muons, which is expected to be almost symmetric in the absence of neutrino oscillations. This result was quite robust against the uncertainties in the neutrino interactions considering the observed number of events at that time. By now, this experiment has accumulated a significant amount of atmospheric neutrino data which allowed more detailed analyses, establishing that these data are well explained by $\nu_\mu \leftrightarrow \nu_\tau$ oscillations and determining accurately the oscillation parameters [9, 10]. The generalization to the three flavor scenario, including matter effects, has also been performed [11].

In the mean time, several new accelerator-based long-baseline neutrino oscillation experiments, like K2K [12], MINOS [13], OPERA [14], and T2K [15] have started taking data to confirm the SK results and to measure more precisely the oscillation parameters. All these experiments use high purity ν_μ and/or $\bar{\nu}_\mu$ beams and search for the ν_μ ($\bar{\nu}_\mu$) oscillation into the other neutrino flavors.

The K2K experiment started operating in 1999 as the first accelerator-based long baseline neutrino experiment. The K2K experiment intended to confirm the neutrino oscillation phenomena observed in atmospheric neutrinos. It also aimed at the search for $\nu_\mu \to \nu_e$ appearance signals. The accelerator and the near detectors were located in KEK, Tsukuba, Japan. The average neutrino energy was 1.3 GeV, and the SK detector, situated 250 km away from KEK, was used as the far detector. K2K reported a deficit in the number of μ-like events observed at SK, and confirmed the ν_μ oscillation phenomenon. However, no indication of ν_e

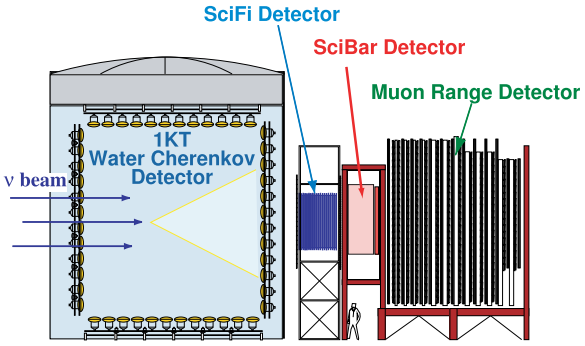

Figure 1. Near detector complex of the K2K experiment.

appearance events was observed. The near detector of the K2K experiment consisted of several components: a 1 kt water Cherenkov detector, a water target scintillator fiber tracker (SciFi), an iron target muon range and a lead glass (LG) detector. In the later stage of the experiment, the LG dectector was replaced with a fully active scintillator tracking detector (SciBar) (see figure 1). With these detectors, various neutrino interactions were studied. One of the interesting observations was a strong suppression of muons in the forward direction [16] and an enhancement of events for large scattering angles. This suppression was observed not only in SciFi but also in the water Cherenkov and the SciBar detectors. These measurements could be well described by increasing the axial vector masses (M_A) entering in the used models for the charged current quasi-elastic (CCQE) scattering and the charged current single pion production (CC1π). Moreover, to achieve a good agreement with data, corrections on the parton distribution functions (PDFs) [17] were also necessary. The CCQE interaction was extensively studied with the SciFi detector and as result an effective value of $M_A = 1.20 \pm 0.12$ GeV for the nucleon axial vector mass was extracted from the data [16]. The model dependence in the determination of M_A in experiments with nuclear targets, in the light of new theoretical developments, is discussed in section 3.

The NC π^0 production, which is one of the background sources in the search for ν_e appearance signatures, was also studied using the 1 kt water Cherenkov detector. The predicted number of interactions from the simulation agreed quite well with the data, but the π^0 momentum distribution turned out to be slightly shifted [18]. Another interesting result from the K2K experiment was the measurement of the charged current (CC) coherent pion production cross-section using the SciBar detector. The reported cross section was almost consistent with zero and much smaller than the predictions from simple partial conservation of the axial current (PCAC) models [19], which however successfully described old high energy experiments. This finding stimulated the theoretical work on coherent reactions induced by (anti)neutrinos described in section 5.

The MINOS experiment is also devoted to the study of ν_μ and $\bar{\nu}_\mu$ oscillations. The neutrino beam is produced at the Fermi National Laboratory (FNAL) in Illinois, US, using 120 GeV protons from the main injector. The mean energy of the neutrino beam is adjustable by changing the configurations of the target and the magnetic horns. Because the neutrino mass difference Δm^2_{32} turned out to be quite small, the nominal energy of the beam was set to 3 GeV. The produced neutrinos are studied in a near detector at FNAL and also in the far detector

located in the SOUDAN mine, 750 km away from the target. Both the near and far detectors are steel-scintillator sampling calorimeters with tracking and energy measurement capabilities. These detectors have a magnet field; thus, it is possible to measure the particle momentum and identify its charge. Owing to the intense neutrino beam, the most stringent limit was set on the squared mass difference Δm^2_{32} and the consistency of the oscillation parameters between ν_μ and $\bar{\nu}_\mu$ was also discussed [20]. They also studied CCQE scattering in the near detector and obtained a value for the effective axial nucleon mass of around 1.2 GeV [21], which is consistent with the result from K2K.

The OPERA experiment is slightly different from these two previous ones. It aimed to study the $\nu_\mu \to \nu_\tau$ oscillation in the appearance channel. The neutrino beam was produced using the 400 GeV SPS proton line in CERN. The far detector is located in the Gran Sasso Laboratory (LNGS) in Italy, which is 732 km away from the target. It consists of an emulsion detector and a high precision tracker, which are used to identify τ leptons by their decay products. The experiment identified 3 τ candidates and confirmed the appearance of τ's from ν_μ oscillation [22].

The MiniBooNE experiment [23] was constructed to study the neutrino oscillation pattern observed by the LSND experiment [24], which can not be explained with the standard three neutrino scenario. MiniBooNE used a line of 8 GeV kinetic-energy protons taken from the Booster at FNAL. The averaged energy of the produced neutrino beam was around 800 MeV and the detector is located 541 m away from the target. The MiniBooNE tank contains 800 tons of mineral oil which is used to detect Cherenkov and scintillation lights. Because the beam intensity was high and the mass of the detector was large, this experiment accumulated more than a hundred thousand neutrino and anti-neutrino events from 2002 to 2012. MiniBooNE measured CCQE [25, 26], CC1π differential cross sections [27, 28], and also the corresponding NC channels [29, 30]. Their results corroborated the muon forward suppression observed in K2K and MINOS, and a number of interactions significantly larger than expected from the theoretical predictions with the nominal theoretical parameters, i.e. $M_A = 1.0$ GeV, was also obtained. Besides, the pion momentum distribution of the CC single π^+ events is broader and larger than MC predictions, which might indicate that the effects of π^+ rescattering in the nucleus are much smaller than expected from the theoretical simulations. On the other hand, the momentum distribution of the NC π^0 production sample is more consistent with the theoretical predictions. More details in this respect can be found in section 4. MiniBooNE also observed a larger number of ν_e-like events than theoretically expected. This could not be explained by the known backgrounds. Various new models including possible 'non-standard' oscillation scenarios have been proposed, but no definitive conclusion has yet been reached [31, 32].

Another short baseline experiment, NOMAD [33], searched for the appearance of ν_τ neutrinos in the CERN SPS wideband neutrino beam with a 24 GeV neutrino energy. This study was motivated by the conjecture that ν_τ could have a mass of 1 eV or more. The NOMAD detector has a 2.7 ton active target made of drift chambers in a 0.4 T magnetic field. The target is followed by a transition radiation detector for electron identification, a preshower detector, a LG electromagnetic calorimeter, a hadron calorimeter and two stations of drift chambers for muon detection [33]. The analysis found no evidence of ν_τ appearance [34] but the good quality of event reconstruction and the large data set collected made detailed neutrino interaction studies possible. Such measurements at NOMAD include muon (anti)neutrino CCQE

cross section [35], NC coherent pion [36] and CC coherent ρ production [37], strangeness and charm production yields [38–40].

In 2007 and 2008, another experiment called SciBooNE took data in the Booster neutrino beam line, which was also used by MiniBooNE. This detector was located at a distance of about 100 m from the neutrino production target. The detector complex consists of a fully active scintillator tracking detector, called SciBar, and a muon tracker. The SciBar detector was used in KEK for the K2K experiment and transported to FNAL to study low energy neutrino and antineutrino interactions with much higher statistics. This detector was capable of finding low momentum protons and thus, it had power to select CCQE events exclusively [41]. The measured CCQE total cross section was found to be ∼10% smaller than in MiniBooNE [42]. The CC coherent pion production reaction was also studied and consistent results with the K2K findings were obtained [43]. This time, the NC coherent π^0 production cross section was also measured and found to be consistent with the predictions from PCAC based models [44]. The inclusive CC cross section was also measured in SciBooNE. In the energy region of, 0.5–1.5 GeV, it turned out to be significantly higher than NEUT and NUANCE MC predictions [45].

The ArgoNeuT experiment studies neutrino interactions using a liquid argon (LAr) time projection chamber (TPC) [46]. This LAr TPC has the capability of tracking low energy charged particles, which is difficult for other detectors. For this reason, ArgoNeuT is expected to provide more precise information on various neutrino cross sections. The detector is located just in front of the MINOS near detector, which is used as a muon spectrometer. Despite the small accumulated statistics, because of the limited run period, the inclusive ν_μ CC differential cross sections on argon have been measured [47]. Recently, ArgoNeuT succeeded in tracking a large number of protons after the neutrino interaction, and reported on the observed proton multiplicity. In particular, events with a final charged lepton and two back-to-back protons are quite interesting. These back-to-back protons might have been originated via neutrino interactions with two bound nucleons or from the absorption of a produced pion. This kind of data set will be useful in the future to improve the performance of the event generators used in neutrino experiments and as a new complement in the study of nuclear structure and the nucleon properties inside the nuclear medium.

The MINERνA experiment placed the detector after ArgoNeuT finished taking data. The setup consists of a fully active scintillator tracking detector, and electromagnetic and hadron calorimeters, together with various nuclear targets, including helium, carbon, water, iron and lead. This experiment also uses the MINOS near detector as a muon spectrometer. MINERνA can measure cross sections for several nuclei using the same neutrino beam, which will allow one to study the nuclear dependence of the different neutrino interactions with a minimized impact of systematic uncertainties. Charged current ν_μ and $\bar{\nu}_\mu$ quasi-elastic differential cross sections in carbon have been recently published. The interaction rates are consistent with a value of nucleon axial mass M_A ∼1.0 GeV [48, 49], in agreement with previous results from NOMAD [35], and in contradiction to the other recent experiments. On the other hand, deviations are found between the measured q^2 differential cross section and the expectations from a model of independent nucleons in a relativistic Fermi gas with a small M_A value [49].

After the K2K experiment was successfully finished in 2005, the T2K experiment started in 2009 as its natural upgrade. T2K aims to search for $\nu_\mu \to \nu_e$ oscillations and measure or set a

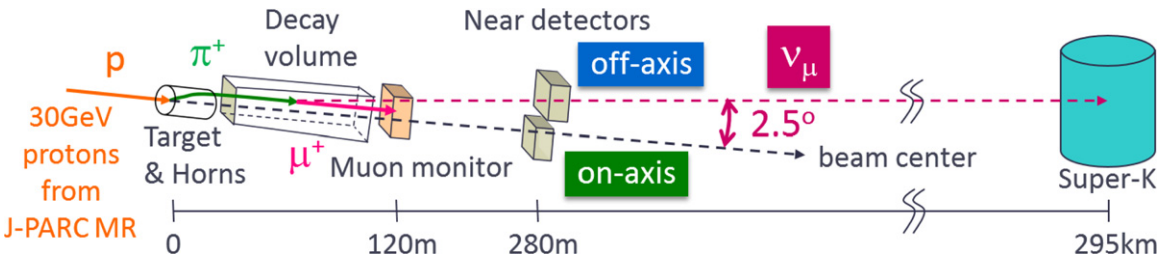

Figure 2. Schematic diagram of the T2K experiment.

limit for the θ_{13} mixing angle. This experiment also tries to improve by one order of magnitude the precision of the determination of Δm^2_{32} and θ_{23}. These parameters are essential to disentangle the pattern of CP violation in the lepton sector. The T2K experiment reported the first indication of a non-zero value for θ_{13} in 2011 at 2.5σ level [50] and the significance reached 7.5σ in 2013 [51]. After the first result from T2K, θ_{13} was also measured in nuclear reactor experiments in the anti-electron neutrino disappearance channel, and the precisions are being continuously improved [52–54]. The neutrino beam for the T2K experiment is produced by a 30 GeV proton line from the J-PARC proton synchrotron, located in Tokai, Ibaraki, Japan. The direction of the resulting neutrino beam is 2.5° shifted from the direction of the far detector, SK, located at 295 km from the target (figure 2). In this manner, the neutrino spectrum becomes narrower and peaks at lower energies. This configuration is called off-axis. With this method, the average energy of the neutrino beam is adjusted to peak around 700 MeV to match the oscillation maximum. There are several neutrino detectors, located at 280 m from the target, where the neutrino interactions before oscillations are measured. There are two sets of near detectors. The first one is aligned with the neutrino beam direction and consists of a steel-scintillator sampling tracker that allows one to monitor the direction and stability of the neutrino beam. The second set is aligned approximately in the direction of SK. This off-axis detector complex has full active scintillator tracking detectors, TPCs together with calorimeters. These detectors are located in a magnet that makes it possible to identify the charge and momentum of the produced particles. Various studies on neutrino interactions are been carried out using both on-axis and off-axis detectors. The inclusive CC and the CCQE cross sections have already been measured. Regarding CCQE, the distributions seem to favor a large M_A value. Total CC cross sections have been measured in carbon and iron, which turn out to be similar, once divided by the number of active nucleons, with small differences at the level of 3%.

In 2013, the NOνA experiment has started taking data. This experiment utilizes a fully active liquid scintillator tracking detector to accurately measure θ_{13}, and study CP violation and the neutrino mass hierarchy. The neutrino beam is produced at FNAL, and is formally used also for MINOS, but upgraded for this new experiment. The far detector is located in the Ash river, 810 km away from the target and 14 mrad off-axis to adjust the maximum neutrino energy. The construction of the far detector is still in process and shall be completed in 2014.

Until now, three mixing angles and two squared mass differences have been measured, but there is no information on whether CP is violated or not in the lepton sector. The mass hierarchy pattern is also unknown. In order to answer these questions, several high precision experiments with much higher statistics and precisions have been proposed. In Japan, a gigantic water Cherenkov detector, called Hyper-Kamiokande (HK), has been proposed. The fiducial volume

of HK is more than 20 times larger than SK. It is planned to be located in the Kamioka mine and thus it will be also possible to study atmospheric neutrinos with much higher precision. Furthermore, the existing neutrino beam line in J-PARC is expected to be upgraded. In the US, a project called LBNE has been launched. The proposed location of the far detector is the Sanford Laboratory, located at 1280 km from FNAL. Two LAr TPCs, with a total fiducial volume of 34 kton, have been proposed as far detectors. This type of detector allows one to measure low momentum particles; it is also expected to have a large electron–photon discriminating power. In spite of its relatively small mass compared to HK, the LBNE baseline is rather long, and thus this experiment would be quite sensitive to both the CP δ phase and the neutrino mass hierarchy. In Europe, the LBNO/Laguna project is being discussed. The proposal includes three types of the detectors: a 100 kton LAr TPC called GLACIER, a 500 kton water Cherenkov tank (MEMPHYS) and a 50 kton liquid scintillator detector (LENA). Several locations are under consideration including several detector configurations exploiting different advantages. Further study is underway.

This next generation of experiments would reduce the uncertainties of the neutrino interactions down to the few percent level from the around 10% affecting the current experiments. More precise theoretical models will be needed to understand and describe the future wealth of neutrino–nucleus data.

3. QE and QE-like scattering

3.1. QE scattering on the nucleon

Let us first consider the processes

$$\nu_l(k)\, n(p) \to l^-(k')\, p(p'), \qquad (\nu\text{CCQE}) \tag{2}$$

$$\nu_l(k)\, N(p) \to \nu_l(k')\, N(p') \quad N = n,\, p \quad (\nu\text{NCE}) \tag{3}$$

standing for charge-current (CC) quasielastic (CCQE) and neutral current (NC) elastic (NCE) scattering on nucleons induced by neutrinos. The corresponding reactions with antineutrinos are

$$\bar{\nu}_l(k)\, p(p) \to l^+(k')\, n(p') \qquad \left(\bar{\nu}\text{CCQE}\right) \tag{4}$$

$$\bar{\nu}_l(k)\, N(p) \to \bar{\nu}_l(k')\, N(p') \quad N = n,\, p \quad \left(\bar{\nu}\text{NCE}\right). \tag{5}$$

At energies low enough that the four-momentum squared transferred to the nucleon is much smaller than the intermediate vector boson mass squared [$q^2 = (k - k')^2 \ll M_{W,Z}^2$], their cross sections can be cast as

$$\frac{\mathrm{d}\sigma}{\mathrm{d}q^2} = \frac{1}{32\pi}\frac{1}{M^2E_\nu^2}G^2c_{\mathrm{EW}}^2L_{\alpha\beta}H^{\beta\alpha} \quad \mathrm{EW} = \mathrm{CC},\ \mathrm{NC}, \tag{6}$$

where $E_\nu \equiv k^0$ is the (anti)neutrino energy in the laboratory frame and M the nucleon mass (isospin symmetry is assumed); G is the Fermi constant while $c_{\mathrm{CC}} = \cos\theta_C$, in terms of the Cabibbo angle, and $c_{\mathrm{NC}} = 1/4$. The leptonic tensor is

$$L_{\alpha\beta} = k_\alpha k'_\beta + k'_\alpha k_\beta - g_{\alpha\beta}k\cdot k' \pm i\epsilon_{\alpha\beta\sigma\delta}k'^\sigma k^\delta, \tag{7}$$

where the +(−) sign is valid for $\nu(\bar{\nu})$ interactions ($\epsilon_{0123} = +1$). The hadronic part is contained in the hadronic tensor H which, in the case of CCQE and NCE processes, takes the form

$$H^{\alpha\beta} = \mathrm{Tr}\left[(\not{p}+M)\,\gamma^0\,(\Gamma^\alpha)^\dagger\,\gamma^0\,(\not{p}'+M)\Gamma^\beta\right]. \tag{8}$$

The amputated amplitudes J^α enter the weak charged and neutral currents. The latter ones can be written in the most general way consistent with the symmetries of the Standard Model, in terms of form factors that contain the information about nucleon properties

$$J^\alpha = \bar{u}(p')\Gamma^\alpha u(p) = V^\alpha - A^\alpha, \tag{9}$$

with the vector and axial currents given by

$$V^\alpha = \bar{u}(p')\left[\gamma^\alpha F_1\left(q^2\right) + \frac{i}{2\,M}\sigma^{\alpha\beta}q_\beta F_2\left(q^2\right)\right]u(p), \tag{10}$$

and

$$A^\alpha = \bar{u}(p')\left[\gamma^\alpha\gamma_5 F_A\left(q^2\right) + \gamma_5\frac{q^\alpha}{M}F_P\left(q^2\right)\right]u(p). \tag{11}$$

Vector-current conservation $q_\alpha V^\alpha = 0$ and isospin symmetry imply that vector form factors $F_{1,2}$ are given in terms of the electromagnetic form factors of protons and neutrons. On the other hand, the PCAC $q_\alpha A^\alpha = i\,(m_u + m_d)\,\bar{q}_u\gamma_5 q_d \to 0$ in the chiral limit of QCD ($m_q \to 0$), together with the approximation of the pion-pole dominance of the pseudoscalar form factor F_P, allows one to relate F_P to the axial form factor F_A. Explicit expressions for these relations among form factors can be found, for instance, in [55] for the CC case, and in [56] for the NC one.

With these ingredients, a compact expression of the cross section in equation (6) as a function of the form factors was obtained [57] and widely utilized [7]. Alternatively, it is instructive to write this cross section as an expansion in small variables[3] q^2, $m_l^2 \ll M^2$, E_ν^2. One has that

$$\frac{\mathrm{d}\sigma}{\mathrm{d}q^2} = \frac{1}{2\pi}G^2 c_{\mathrm{EW}}^2\left[R - \frac{m_l^2}{4E_\nu^2}S + \frac{q^2}{4E_\nu^2}T\right] + O\left(q^4,\, m_l^4,\, m_l^2 q^2\right). \tag{12}$$

For CC reactions, equations (2) and (4)

$$R_{\mathrm{CC}} = 1 + g_A^2, \tag{13}$$

$$S_{\mathrm{CC}} = \frac{2E_\nu + M}{M} + g_A^2\frac{2E_\nu - M}{M}, \tag{14}$$

$$T_{\mathrm{CC}} = 1 - g_A^2 + 2\frac{E_\nu}{M}\left(1 \mp g_A\right)^2 \mp 4\frac{E_\nu}{M}g_A\kappa^{\mathrm{V}} - \left(\frac{E_\nu}{M}\kappa^{\mathrm{V}}\right)^2,$$
$$+ 4E_\nu^2\left[\frac{1}{3}\left(\left\langle r_p^2\right\rangle - \left\langle r_n^2\right\rangle + g_A^2\left\langle r_A^2\right\rangle\right) - \frac{1}{2\,M^2}\kappa^{\mathrm{V}}\right], \tag{15}$$

where $\kappa^{\mathrm{V}} = \mu_p - \mu_n - 1$. The upper (lower) sign stands for $\nu(\bar{\nu})$CCQE. For NC reactions, equations (3) and (5), equation (12) remains valid when $m_l \to 0$ and the R, T functions are given by

[3] Close to threshold ($E_\nu \sim m_l$), and for CCQE with τ-neutrinos (due to the large m_τ value) the counting is different.

$$R_{\mathrm{NC}}^{(p)} = \alpha_{\mathrm{V}}^{2} + \left(g_A - \Delta s\right)^2, \tag{16}$$

$$\begin{aligned} T_{\mathrm{NC}}^{(p)} = {} & \alpha_{\mathrm{V}}^{2} - \left(g_A - \Delta s\right)^2 + 2\frac{E_\nu}{M}\left[\alpha_{\mathrm{V}} \mp \left(g_A - \Delta s\right)\right]^2 \mp 4\frac{E_\nu}{M}\left(g_A - \Delta s\right)\kappa_{\mathrm{NC}}^{(p)} - \left(\frac{E_\nu}{M}\kappa_{\mathrm{NC}}^{(p)}\right)^2 \\ & + 4E_\nu^2\left\{\alpha_{\mathrm{V}}\left[\frac{1}{3}\left(\alpha_{\mathrm{V}}\left\langle r_p^2\right\rangle - \left\langle r_n^2\right\rangle - \left\langle r_s^2\right\rangle\right) - \frac{1}{2M^2}\kappa_{\mathrm{NC}}^{(p)}\right]\right. \\ & \left. + \frac{1}{3}\left(g_A - \Delta s\right)\left(g_A\left\langle r_A^2\right\rangle - \Delta s\left\langle r_{As}^2\right\rangle\right)\right\}, \end{aligned} \tag{17}$$

on proton targets, with $\kappa_{\mathrm{NC}}^{(p)} = \alpha_{\mathrm{V}}\left(\mu_p - 1\right) - \mu_n - \mu_s$ and the (very small) quantity $\alpha_{\mathrm{V}} = 1 - 4\sin^2\theta_W$, where θ_W is the weak angle. On neutrons

$$R_{\mathrm{NC}}^{(n)} = 1 + \left(g_A + \Delta s\right)^2, \tag{18}$$

$$\begin{aligned} T_{\mathrm{NC}}^{(n)} = {} & 1 - \left(g_A + \Delta s\right)^2 + 2\frac{E_\nu}{M}\left[1 \mp \left(g_A + \Delta s\right)\right]^2 \pm 4\frac{E_\nu}{M}\left(g_A + \Delta s\right)\kappa_{\mathrm{NC}}^{(n)} - \left(\frac{E_\nu}{M}\kappa_{\mathrm{NC}}^{(n)}\right)^2 \\ & + 4E_\nu^2\left\{-\frac{1}{3}\left(\alpha_{\mathrm{V}}\left\langle r_n^2\right\rangle - \left\langle r_p^2\right\rangle - \left\langle r_s^2\right\rangle\right) + \frac{1}{2M^2}\kappa_{\mathrm{NC}}^{(n)}\right. \\ & \left. + \frac{1}{3}\left(g_A + \Delta s\right)\left(g_A\left\langle r_A^2\right\rangle + \Delta s\left\langle r_{As}^2\right\rangle\right)\right\}, \end{aligned} \tag{19}$$

with $\kappa_{\mathrm{NC}}^{(n)} = 1 - \mu_p + \alpha_{\mathrm{V}}\mu_n - \mu_s$.

In the q^2, $m_l^2 \ll M^2$, E_ν^2 limit, which is valid for most of the integrated cross section in the few-GeV region, the CCQE cross section is determined by a few experimentally well measured electromagnetic properties of the nucleon: charge, magnetic moments $\mu_{p,n}$ and mean squared charge radii

$$\left\langle r_p^2\right\rangle = \frac{6}{G_{\mathrm{E}}^{(p)}(0)}\frac{\mathrm{d}G_{\mathrm{E}}^{(p)}\left(q^2\right)}{\mathrm{d}q^2}\bigg|_{q^2=0} \qquad \left\langle r_n^2\right\rangle = 6\,\frac{\mathrm{d}G_{\mathrm{E}}^{(n)}\left(q^2\right)}{\mathrm{d}q^2}\bigg|_{q^2=0}, \tag{20}$$

where $G_{\mathrm{E}}^{(p,n)}$ are the electric form factors, and two axial quantities: coupling g_A, also well known from neutron β decay, and radius

$$\left\langle r_A^2\right\rangle = \frac{6}{F_A(0)}\frac{\mathrm{d}F_A\left(q^2\right)}{\mathrm{d}q^2}\bigg|_{q^2=0}. \tag{21}$$

It is remarkable that $\left\langle r_A^2\right\rangle$ can be extracted from single pion electroproduction data independently of neutrino experiments which could be distrusted due to low statistics, inaccuracies in the neutrino flux determinations or the influence of nuclear effects. It has been shown [58, 59] that up to $O\left(p^3\right)$ in a chiral expansion in small momenta and quark masses (chiral perturbation theory)

$$6\left.\frac{\mathrm{d}E_{0+}^{(-)}}{\mathrm{d}q^2}\right|_{q^2=0} = \left\langle r_A^2 \right\rangle + \frac{3}{M}\left(\kappa^{\mathrm{V}} + \frac{1}{2}\right) + \frac{3}{64 f_\pi^2}\left(1 - \frac{12}{\pi^2}\right), \tag{22}$$

where $E_{0+}^{(-)}$ is an s-wave electric dipole amplitude in a specific isospin combination (see [59] and references therein for more details). The derivative is taken over the virtual photon four-momentum squared, and f_π is the pion decay constant. Using an effective Lagrangian model to extrapolate pion electroproduction data to $q^2 = 0$ [60] and taking into account the hadronic corrections of equation (22) [58] one finds that

$$\left\langle r_A^2 \right\rangle = 0.455 \pm 0.012\ \mathrm{fm}^2. \tag{23}$$

At higher q^2, the relation between pion electroproduction amplitudes and the axial form factor becomes more uncertain and model dependent. Therefore, for information on the q^2 dependence of F_A one has to rely chiefly on (anti)neutrino experiments off hydrogen and deuterium targets. Although the contribution of the term proportional to F_A to the parity-violating asymmetry in electron–proton elastic scattering with polarized beams is typically orders of magnitude smaller than the dominant (magnetic) one, a detailed study at backward angles might also help constraining this form factor [61].

The axial form factor is usually parametrized with a dipole ansatz

$$F_A\left(q^2\right) = g_A\left(1 - \frac{q^2}{M_A^2}\right)^{-2}, \tag{24}$$

which corresponds to an exponential shape for the axial charge-density distribution. For such a one parameter function, the so-called axial mass M_A is directly related to the axial radius

$$\left\langle r_A^2 \right\rangle = \frac{12}{M_A^2}. \tag{25}$$

The value of M_A extracted from early CCQE measurements on deuterium and, to a lesser extent, hydrogen targets is $M_A = 1.016 \pm 0.026$ GeV [62]. It is in excellent agreement with the pion electroproduction result, $M_A = 1.014 \pm 0.016$ GeV, obtained from the axial radius, equation (22), using the relation of equation (24). In spite of the fact that deviations from the dipole form have not been observed so far, it is worth stressing that the dipole parametrization is not well justified from a theoretical point of view. In the case of the electromagnetic form factor, the dipole behavior arises from cancellations between monopole terms that appear naturally in the vector meson dominance picture [63]. The situation is more uncertain in the axial sector but a similar scenario might be in place from the interplay of two or more axial mesons [64]. The lack of knowledge about the q^2 dependence of F_A may result in large uncertainties in the CCQE cross section, especially at large energies as shown in [65], although the constraints in the axial radius from pion electroproduction would make the bands in figure 5 of that paper narrower.

In addition to the nucleon electromagnetic and axial properties that define the CCQE hadronic tensor at q^2, $m_l^2 \ll M^2$, E_ν^2, the NCE one depends on the strangeness content of the nucleon via the strange mean squared radius $\left\langle r_s^2 \right\rangle$, the magnetic moment μ_s, the strange axial coupling Δs, which is the strange quark contribution to the nucleon spin, and the corresponding

axial radius $\langle r_{As}^2 \rangle$. The impact of $\langle r_s^2 \rangle$, μ_s, $\langle r_{As}^2 \rangle$, which are not only small (see [66] for a recent global fit) but also appear in the subleading $T_{\rm NC}^{(p,n)}$ functions, is insignificant. This is not the case of Δs which, if different from zero, could change the NCE cross section appreciably. This becomes evident by looking at the ratio

$$\left.\frac{\mathrm{d}\sigma_{\rm NC}^{(p)}/\mathrm{d}q^2}{\mathrm{d}\sigma_{\rm NC}^{(n)}/\mathrm{d}q^2}\right|_{q^2=0} = \frac{\alpha_{\rm V}^2 + \left(g_A - \Delta s\right)^2}{1 + \left(g_A + \Delta s\right)^2} \approx \frac{\left(g_A - \Delta s\right)^2}{1 + \left(g_A + \Delta s\right)^2} \approx \begin{cases} 0.62 & \text{if } \Delta s = 0 \\ 1.27 & \text{if } \Delta s = -0.3 \end{cases}. \tag{26}$$

The MiniBooNE experiment performed a detailed study of NC nucleon knock-out on mineral oil (CH_2) but their measurement turned out to be rather insensitive to Δs because of difficulties distinguishing between protons and neutrons [29, 67]. The recently proposed MiniBooNE+ experiment with improved sensitivity to neutrons might allow a better determination of this important nucleon property [68]. The same is true about MicroBooNE [69], where a reliable identification of the low energy protons knocked out of argon should be possible. As a result, the error in the determination of Δs would be drastically reduced [66]. It should be recalled that for both MiniBooNE+ and MicroBooNE, running with nuclear targets, the presence of multinucleon contributions (discussed in section 3.3) and other inelastic mechanisms, together with FSI [56, 70], will certainly affect the extraction of Δs and should be carefully studied. In fact, we think that dedicated (anti)neutrino–nucleon experiments are needed in order to understand the axial structure of the nucleon in depth.

3.2. QE scattering on nuclei

For (anti)neutrinos interacting with nuclear targets,

$$\nu_l,\, \bar{\nu}_l(k)\, A_Z \to l^{\mp}(k')\, X, \tag{27}$$

$$\nu_l,\, \bar{\nu}_l(k)\, A_Z \to \nu_l,\, \bar{\nu}_l(k')\, X \tag{28}$$

the inclusive cross section per unit volume, which is the proper quantity for an extended system, is given by

$$\frac{\mathrm{d}}{\mathrm{d}^3 r}\left(\frac{\mathrm{d}\sigma}{\mathrm{d}\Omega(k')\mathrm{d}k'^0}\right) = \frac{G^2 c_{\rm EW}^2}{4\pi^2}\frac{|\vec{k}'|}{|\vec{k}|} L_{\alpha\beta} W^{\alpha\beta}. \tag{29}$$

This formula stands for both CC and NC processes, with $c_{\rm CC} = \cos\theta_C$ and $c_{\rm NC} = 1/4$. The lepton tensor is defined in equation (7), as in the nucleon case. By construction, the hadronic tensor can be decomposed as

$$W^{\alpha\beta} = W_s^{\alpha\beta} + iW_a^{\alpha\beta} \tag{30}$$

with W_s (W_a) being a real symmetric (antisymmetric) tensor. Furthermore, it can be expressed in terms of the polarization propagator (or tensor)

$$W_{(s,a)}^{\alpha\beta} = -\frac{1}{\pi}\,\mathrm{Im}\,\Pi_{(s,a)}^{\alpha\beta}. \tag{31}$$

This is a classic result, known for the response of many-body systems to external probes [71], that also holds for neutrino interactions. Some examples of different contributions to

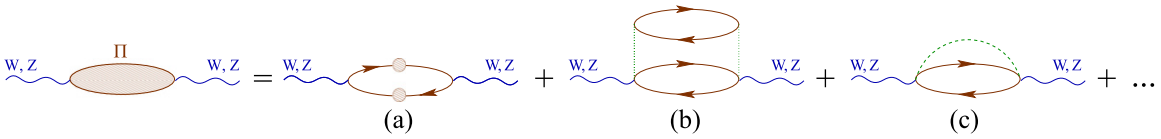

Figure 3. Diagrammatic representation of many-body contributions to the polarization propagator. Solid (dashed) lines correspond to free nucleon (pion) propagators; dotted lines stand for effective nucleon–nucleon interactions. The solid lines with a blob represent full (dressed) nucleon propagators. For nucleons, the lines pointing to the right (left) denote particle (hole) states.

the polarization propagator are diagrammatically represented in figure 3. Diagram (c) contributes mostly to pion production[4], discussed in section 4. Diagram (b) is an example of a meson exchange current (MEC) contribution to the interaction mechanisms involving two nucleons from the nucleus, also known as two-particle-two-hole (2p2h) terms. They play a very important role in neutrino scattering in the few-GeV region and will be covered in section 3.3.

Let us now consider diagram (a) of figure 3. This piece of the polarization tensor contributes mainly to the QE peak, where the interaction takes place on a single nucleon which is knocked out; these are one-particle-one-hole (1p1h) terms. Nevertheless, through the correlations in the initial or final state, this diagram also contains 2p2h, other multinucleon and even particle emission contributions. It can be shown that for the polarization propagator of diagram (a) in figure 3

$$\mathrm{Im}\,\Pi^{\alpha\beta}_{(s,a)} = -2\pi^2 \int \frac{\mathrm{d}^4 p}{(2\pi)^4} H^{\beta\alpha}_{(s,a)} \mathcal{A}_p(p+q)\,\mathcal{A}_h(p), \tag{32}$$

where $H^{\alpha\beta}_{(s,a)}$ are the symmetric and antisymmetric components of the QE hadronic tensor for nucleons introduced in equation (8). In this way, one disregards off-shell effects on the nucleon current and adopts the same form factors as for the free nucleon.

$$\mathcal{A}_{p,h}(p) = \mp \frac{1}{\pi} \frac{\mathrm{Im}\,\Sigma(p)}{\left[p^2 - M^2 - \mathrm{Re}\,\Sigma(p)\right]^2 + \left[\mathrm{Im}\,\Sigma(p)\right]^2} \tag{33}$$

are particle and hole spectral functions related to the scalar (averaged over spins) nucleon self-energy Σ present in the full (dressed) in-medium nucleon propagator as a result of nucleon–nucleon (NN) interactions. Here $p^0 \geqslant \mu$ and $p^0 \leqslant \mu$, with μ being the chemical potential, for $\mathcal{A}_p$ and $\mathcal{A}_h$, respectively. In the presence of the nuclear medium, nucleons have a modified dispersion relation and, in addition, become broad states.

Practically all approximations employed to calculate neutrino, but also electron, QE scattering with nuclei can be obtained from equation (31). The simplest description, present in most event generators used in the analysis of neutrino experiments, is the relativistic global Fermi gas (RgFG) [72]. In this model, the nuclear ground state is a Fermi gas of non-interacting nucleons characterized by a global Fermi momentum p_F and a constant binding energy E_B. Then, the hole spectral function is

[4] Mostly, because real pions produced inside the nuclei can be absorbed by two or more nucleons.

$$\mathcal{A}_h(p) = \frac{1}{2E(\vec{p})}\delta\left(p^0 - E(\vec{p})\right)\theta\left(p_F - |\vec{p}|\right), \tag{34}$$

where $E(\vec{p}) = \sqrt{M^2 + \vec{p}^{\,2}} - E_B$. The step function $\theta\left(p_F - |\vec{p}|\right)$, with p_F a constant Fermi momentum, accounts for the Fermi motion of the nucleons in the nucleus. For the particle

$$\mathcal{A}_p(p) = \frac{1}{2E(\vec{p})}\delta\left(p^0 - E(\vec{p})\right)\left[1 - \theta\left(p_F - |\vec{p}|\right)\right] \tag{35}$$

with $E(\vec{p})$ the on-shell energy. The factor $1 - \theta\left(p_F - |\vec{p}|\right)$ takes Pauli blocking into account. Such a simple picture with only two parameters $\left(p_F, E_B\right)$ explains qualitatively inclusive QE electron scattering data but fails in the details. A better description requires a more realistic treatment of nuclear dynamics.

An improvement over the RgFG is the so called relativistic local Fermi gas (RlFG) where the Fermi momentum is fixed according to the local density of protons and neutrons $\rho_{p,n}(r)$

$$p_F^{p,n}(r) = \left[3\pi^2\rho_{p,n}(r)\right]^{1/3}. \tag{36}$$

Equations (33) and (35) also hold after replacing the global Fermi momentum by the local one. The binding energy is often neglected but a minimal excitation energy required for the transition to the ground state of the final nucleus has been taken into account in the CCQE model of [55].

Nuclear spectral functions like the one of [73], obtained using empirical single particle wave functions and realistic calculations in nuclear matter (adapted for finite nuclei employing the local-density approximation (LDA)), from the convolution model [74] and from other (semi)phenomenological models [75, 76] have been applied to electron and neutrino scattering in the QE region [55, 77–82]. Sometimes, realistic spectral functions for holes are combined with the use of plane waves for nucleons in the final state, eventually including Pauli blocking with a global Fermi momentum like in equation (34). Examples of such an approach, known as plane wave impulse approximation (PWIA), for CCQE scattering can be found in [79, 80, 82, 83].

To put in perspective the RgFG, RlFG and realistic spectral function descriptions of the nuclear ground state, we consider the nucleon momentum distribution in nuclei, related to the hole spectral function by

$$n^{\mathrm{RgFG}}\left(|\vec{p}|\right) = \frac{4}{(2\pi)^3}\mathcal{V}\int \mathrm{d}p_0\left(2p_0\right)\mathcal{A}_h(p), \tag{37}$$

where $\mathcal{V}$ is the nuclear volume, and

$$n^{\mathrm{LDA}}\left(|\vec{p}|\right) = 4\int \frac{\mathrm{d}^3r}{(2\pi)^3}\mathrm{d}p_0\left(2p_0\right)\mathcal{A}_h(p) \tag{38}$$

within the LDA approximation. The momentum distribution is normalized as

$$(4\pi)\int \mathrm{d}|\vec{p}\,|\,\vec{p}^{\,2}n\left(|\vec{p}\,|\right) = A, \tag{39}$$

where A is the nuclear mass number. For simplicity, the same momentum distribution for protons and neutrons as in symmetric nuclei, has been assumed. In figure 4, $\vec{p}^{\,2}n\left(|\vec{p}\,|\right)$ on ^{12}C is plotted for RgFG (neglecting the binding energy), the RlFG (with density profiles taken from

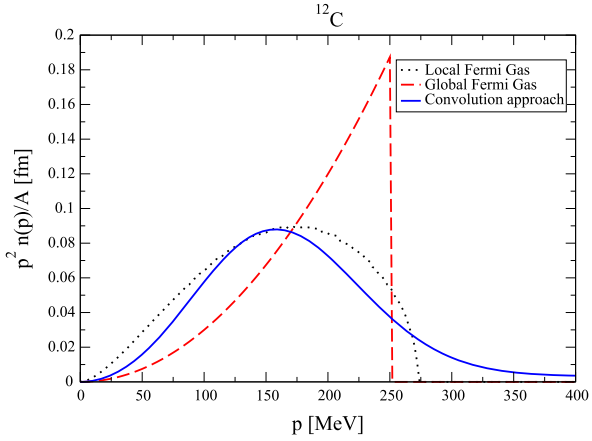

Figure 4. Comparison of the nucleon momentum distributions on ^{12}C for RlFG, RgFG and the convolution model of [74].

[84]) and the convolution approach of [74] that provides convenient parametrizations of these distributions. The plot shows the tail at high momenta of the realistic distribution due to short-range correlations, which is absent in the Fermi gas distributions. These correlations are investigated in two-nucleon knockout electron scattering experiments at specific kinematics where they are bound to be relevant [85]. In spite of its simplicity, the RlFG model introduces space–momentum correlations that translate into a considerably more realistic description of the momentum distribution than the RgFG.

Besides the short range correlations, the description of the nuclear ground state can be improved with more realistic treatments of the single particle content beyond the non-interacting Fermi-type picture. In the GiBUU model [86], the hole spectral function is modified with respect to that of the RlFG by the presence of a real position- and momentum-dependent mean-field potential generated by the spectator particles. The hole states remain narrow but the dispersion relation is modified: $p^2 = \left[M^*\left(\vec{r}, \vec{p}\right)\right]^2$, where $M^*\left(\vec{r}, \vec{p}\right)$ is the effective mass of the bound nucleon. The initial nucleons have also been treated as shell-model bound states with wave functions obtained as solutions of the Dirac equation in a $\sigma - \omega$ potential [87–89], or from a phenomenological energy and target dependent optical potential (OP) [90]. This is known as the relativistic mean field (RMF) approach.

Although the details of the particle spectral functions, and the FSI in general, do not affect the inclusive integrated cross section, they are important for the differential ones, particularly in the region of low-energy transfer, and are crucial to achieve a realistic description of the reaction final state. It is precisely through the detection of (some of the) final state particles that neutrinos can be detected and its energy, *a priori* not known in broad beams, identified. The role of final-state correlations is particularly important for NC processes because the outgoing neutrino cannot be detected. In an inclusive CC process of the type of diagram (a) in figure 3, the chief effects of the medium in the particle spectral function are an energy shift of the cross section caused by the mean field and a redistribution of the strength caused by *NN* interactions [79]. Particle spectral functions have been obtained in a variety of approaches: generalizing Glauber theory of multiple scattering [91], also using phenomenological potentials for the real part of the nucleon self-energy, and the low density limit to relate Im Σ to the *NN* cross section

[81, 92]. In [75], Im Σ is also expressed in terms of the free NN cross section in a LDA framework and taking polarization effects into account; Re Σ is obtained from the imaginary part using dispersion relations. All of them have been employed to study neutrino-induced QE reactions [55, 79, 81, 92].

The wave functions of the outgoing nucleons can be distorted with complex OP in an approach known as distorted-wave impulse approximation (DWIA) [82, 87–90, 93, 94] or with the Glauber multiple scattering approximation for knocked out nucleons with more than 1 GeV kinetic energy [93]. DWIA models are successful in describing a large amount of exclusive proton knockout $(e, e'p)$ data and are valid when the residual nucleus is left in a given state [95–97] but are not appropriate for inclusive scattering. Indeed, the imaginary part of the OP produces an absorption and a reduction of the cross section which accounts for the flux lost towards other channels. This is not correct for an inclusive reaction where all elastic and inelastic channels contribute and the total flux must be conserved. DWIA calculations using the same real potential (RMF) used to describe the initial state, or the real part of a phenomenological OP [88] are more suitable for inclusive processes although one should recall that OPs have to be complex owing to the presence of inelastic channels [98]. An alternative is the relativistic Green function (RGF) approach [99–102] which also starts from a phenomenological complex OP that describes proton–nucleus scattering data, but recovers the flux lost into non-elastic channels in the inclusive case. This in principle renders the model more appropriate for the study of CCQE scattering when nucleons are not detected in the final state, as in the MiniBooNE measurement (see the related discussion in section 3.3). NCQE[5] processes, instead, are identified by the detection of the knocked-out nucleon with no lepton in the final state. The RGF model may include channels which are not present in the measurement but, on the other hand, it contains contributions that are not present in DWIA calculations. DWIA, RMF and RGF approaches have been recently compared for different NCQE kinematics [103]. It is argued that RGF may provide an upper limit to the NCQE cross section while DWIA gives the lower one but one should keep in mind that other mechanisms like MEC not accounted for in these approaches can also contribute.

A detailed description of the FSI can be achieved using semiclassical MC methods. Moreover, at $E_\nu \gtrsim 500$ MeV, this is the only viable way to simulate the final hadronic state. These techniques allow one to take into account rescattering causing energy losses, charge exchange and multiple nucleon emissions [56, 70, 104]. Furthermore, there are QE-like processes in which a pion produced in the primary interaction and then absorbed, leads only to nucleons in the final state. These mechanisms, which can be very hard, if possible at all, to disentangle from those originated in an elastic or QE interaction on the nucleon, can be naturally incorporated into the framework. Other approaches to those discussed above have to rely on the subtraction of QE-like events performed by the different experiments, using event generators that do not necessarily incorporate state-of-the-art physics input.

3.2.1. Electron scattering and the superscaling approach. Electron scattering is a major source of information for neutrino interactions studies, providing not only the vector form factors of nucleons but also a testing ground for nuclear scattering models, which can be confronted with a large set of good quality data. As mentioned above, the RgFG model

[5] We prefer to call the $\nu, \bar{\nu}\ A \to \nu, \bar{\nu}\ N\ X$ reactions NCQE (or NCQE-like, depending on the primary mechanism) rather than NCE, which we keep for the corresponding reactions on nucleons, equations (3) and (5).

describes the main features of the inclusive (e, e') cross section at the QE peak. However, this model fails to reproduce simultaneously the longitudinal and transverse responses. In particular, the longitudinal response is overestimated (see for instance [105]). With the RGF approach, the longitudinal response is well reproduced, while the transverse is underestimated [106]. This disagreement can be attributed to the lack of MEC and resonance excitation in the model, which are much more important in the transverse than in the longitudinal channel. In microscopic calculations with realistic spectral functions, the longitudinal response, quenched with respect to the Fermi gas estimate, agrees with data, as well as the transverse one at energies low enough for inelastic processes to be negligible (see figure 32 of [107], showing the comparison of the theoretical results of [108] with data). The non-relativistic model of [78] incorporates a semiphenomenological particle spectral function, MEC and $\Delta(1232)$ degrees of freedom in a many-body framework for nuclear matter applied to final nuclei using the LDA. A good description of both responses is obtained as can be appreciated in figures 42 and 43 of [78]. Further details about different theoretical approaches to electron scattering and their comparison to data can be found in the review articles of [95, 107].

Inclusive electron scattering data exhibit interesting systematics that can be used to predict (anti)neutrino–nucleus cross sections. When the experimental (e, e') differential cross sections are divided by the corresponding single nucleon ones and multiplied by a global Fermi momentum, the resulting function

$$f = p_F \frac{\dfrac{\mathrm{d}\sigma}{\mathrm{d}\Omega' \mathrm{d}k'^0}}{Z\sigma_{ep} + N\sigma_{en}} \tag{40}$$

is found to depend on energy and three-momentum transfers $\left(q^0, |\vec{q}|\right)$ through a specific combination, the scaling variable ψ', and to be largely independent of the specific nucleus. This property is known as superscaling [109]. Scaling violations reside mainly in the transverse channel [110] and have their origin in the excitation of resonances and meson production in general, 2p2h mechanisms and even the tail of deep inelastic scattering (DIS). Therefore, an experimental scaling function $f(\psi')$ could be reliably extracted by fitting the data for the longitudinal response [111]. The experimental $f(\psi')$ has an asymmetric shape with a tail at positive ψ' (large q^0) as can be seen in figure 5. The requirement of a correct description of the scaling function is a constraint for nuclear models. The RgFG model fulfills superscaling exactly and has a very simple scaling function

$$f^{\mathrm{RgFG}} = \frac{3}{4}\left(1 - \psi'^2\right)\theta\left(1 - \psi'^2\right) \tag{41}$$

but with the wrong symmetric shape. It has been observed that models based on the impulse approximation are consistent with the superscaling. However, while PWIA and DWIA approaches with complex OP fail to reproduce the asymmetric shape and the tail of the scaling function, a very good description of it is achieved within the RMF model [113]. In addition, the RMF model predicts a larger scaling function in the transverse mode than in the longitudinal one ($f_T > f_L$) [114], which seems to be supported by data. Extensive studies with a wide class of models reveals the importance of a proper description of the interaction of knocked-out nucleons with the residual nucleus [115] to obtain the tail of the scaling function.

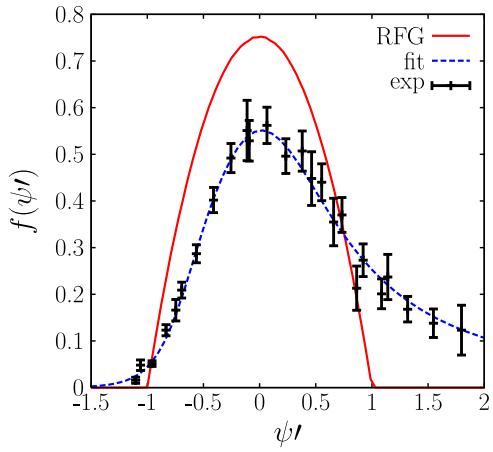

Figure 5. The QE scaling function obtained as a fit to the experimental data in the longitudinal channel [111] compared to the RgFG result. Data are from [112].

With the superscaling approximation (SuSA) a good representation of the nuclear response can be obtained by embedding nuclear effects in the scaling function: the observables can be calculated with the simple RgFG model followed by the replacement $f_{\mathrm{RgFG}} \to f_{\mathrm{exp}}$. The same strategy can be used to predict neutrino QE cross section, minimizing in this way the model dependence of the results. It has been found that the SuSA approach predicts a 15% smaller integrated CCQE cross section compared to the RgFG, close to the result obtained with the RMF model (figure 3 of [116]). Nevertheless, it should be remembered that scaling fails at $\omega < 40$ MeV and $|\vec{q}| < 400$ MeV due to collective effects.

3.2.2. Long-range RPA correlations. The theoretical models discussed so far assume the validity of the impulse approximation according to which the (anti)neutrino interacts with a single nucleon in the nucleus. The influence of the spectator nucleons is only present in the hole and particle spectral functions or in FSI. However, when the three-momentum transferred to the target $|\vec{q}|$ is small and $1/|\vec{q}|$ becomes comparable with the internucleon distance, one should not expect this approximation to hold. The comparison with inclusive electron scattering data shows that at $|\vec{q}| \lesssim 350-400$ MeV, systematic discrepancies associated with the breakdown of the impulse approximation start to show up [81, 92].

Collective effects can be handled within the random phase approximation (RPA) using the bare polarization propagators as input. For CCQE scattering this is illustrated in figure 6. These RPA correlations renormalize the different components of the hadronic tensor. One expects them to be relevant for neutrino interactions on the basis of the well established quenching of g_A in nuclear Gamow–Teller β decay. For CCQE scattering, these long-range correlations were taken into account in [117] using a RlFG model and an effective *NN* interaction in the nuclear medium (denoted *V* in figure 6) consisting of pion and rho-meson exchange plus a short range part effectively included in the phenomenological constant g', taken to be the same in the longitudinal and transverse channels. The contributions of the RPA sums to the tensor are expressed in an analytic form in terms of the 1p1h and Δh polarization propagators. Such a model has been subsequently applied to obtain inclusive and semi-inclusive cross sections in

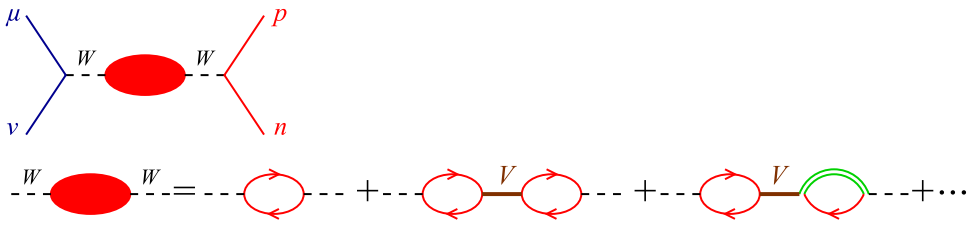

Figure 6. RPA correlations in CCQE scattering. Solid lines pointing to the right (left) denote particle (hole) states. The double line stands for the $\Delta(1232)$.

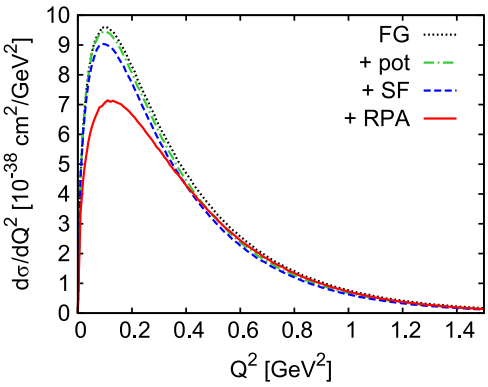

Figure 7. Differential cross sections for the CCQE reaction on ^{12}C averaged over the MiniBooNE flux [128] as a function of the 4-momentum transfer squared $Q^2 \equiv -q^2$. Dotted lines represent the RlFG model with Fermi motion and Pauli blocking. In the dash-dotted lines the nucleons are exposed to the mean field potential while the dashed ones also incorporate spectral functions for the outgoing nucleons [92, 104]. The full model with long range (RPA) correlations is denoted by solid lines [129].

different experimental situations [118–121]. This model was improved in [55, 56] by a more rigorous resummation of the RPA series in the vector–isovector channel, and the introduction of scalar–isoscalar, scalar–isovector and vector–isoscalar contact density dependent terms of the effective interaction (see equations (32)–(36) of [55] for details). The approach set up in [122–124] and that of [125] are quite similar. In this case the RPA equations are solved numerically. An algebraic solution of these equations was developed in [126] and applied to the study of τ polarizations in CC ν_τ, $\bar{\nu}_\tau$-nucleus scattering [127].

The impact of RPA correlations at MiniBooNE energies $\langle E_\nu \rangle \sim 750$ MeV is quite significant. This is shown in figure 7, where they have been calculated for CCQE on ^{12}C following [55]. At low $Q^2 \equiv -q^2 < 0.3$ GeV^2 these collective effects cause a sizable reduction of the cross section which, as will be discussed in the next section, is crucial to understand CCQE MiniBooNE data.

In the models outlined in this section, the effective *NN* interaction contains contact and energy independent interactions with strengths determined from low-energy collective excitations [130]. For this reason, the validity of *V*, like some of the non-relativistic approximations present in the models [55, 124], can be questioned at the rather high energy transferred of a few hundred MeV that can be encountered at MiniBooNE and other neutrino

experiments. However, it should be remembered that the inclusion of dynamical pion and rho propagators in the longitudinal and transverse interactions, as well as the presence of Δh excitations in addition to 1p1h ones, extend the validity of the framework towards higher energies. Furthermore, once $q^2 < 0$, high q^0 correspond to even higher $|\vec{q}|$; one then enters the realm of the impulse approximation, where collective RPA corrections are bound to be negligible. Therefore, even large corrections to the model should have a small impact on the cross sections. A similar situation takes place in inclusive electron scattering on nuclear targets.

Another point of concern is the validity of the RlFG description in the kinematic region of $q^0 \lesssim 50$ MeV, which can account for a large part of the cross section even at high neutrino energies [65]. It is indeed true that at such low q^0, details of the nuclear structure that are beyond reach for a non-interacting Fermi gas model become important, and continuum RPA [131–134] or even shell-model calculations [87, 89] should be more reliable. Nevertheless, there are indications [135] that the RlFG models with RPA corrections lead to realistic predictions for integrated quantities, for which the details of the excitation spectrum are not so relevant. The success of [55] describing simultaneously inclusive muon capture on ^{12}C and the low-energy LSND inclusive CCQE measurements reinforces this conclusion.

3.3. The role of 2p2h excitations

In May 2009, at NuInt09, the MiniBooNE Collaboration presented a new CCQE cross section measurement using a high-statistics sample of ν_μ interactions on ^{12}C [136]. The subsequent publication [23], describing the first measurement of the double differential CCQE cross section $\mathrm{d}^2\sigma/\left(\mathrm{d}k'^0\mathrm{d}\cos\theta'\right)$ as a function of the energy and angle of the outgoing muon, reaffirmed the surprising result reported earlier: a cross section per nucleon ~20% higher than expected from bubble chamber low-energy measurements. The size of the cross section was found to be well described with the RgFG model using the dipole parametrization of the axial form factor given in equation (23) with an axial mass of $M_A = 1.35 \pm 0.17$ GeV obtained with a shape-only fit to data [23]. Such a high value of M_A is in contradiction with the previous determinations discussed in section 3.1.

The origin of this *CCQE puzzle* has been extensively debated. It was conjectured that nuclear effects on ^{12}C were influencing the determination of M_A, which should be understood as *effective*. Such a pragmatic attitude that could bring short term benefits in the analysis of neutrino oscillations was dangerous in the long run because the underlying physics was not properly understood. The RgFG model used in the analysis of MiniBooNE data was too simple, but it turned out that more realistic models of the kind reviewed in the previous section also underestimated the data. This situation is illustrated in figure 8 for some of the calculations collected in [137]. Theoretical predictions with $M_A \sim 1$ GeV lie on a rather narrow band (narrower than the experimental errorbars) clearly below the data.

In a CCQE measurement on nuclear targets, there are CCQE-like events for which CC pion production is followed by pion absorption. The subtraction of this background relies partially on the MC simulation. In the case of the MiniBooNE CCQE measurement, the event generator has been adjusted to the CC π^+ data in order to reduce the uncertainty. In a rather light nucleus like ^{12}C absorption is not prominent and one should expect a rather small number of

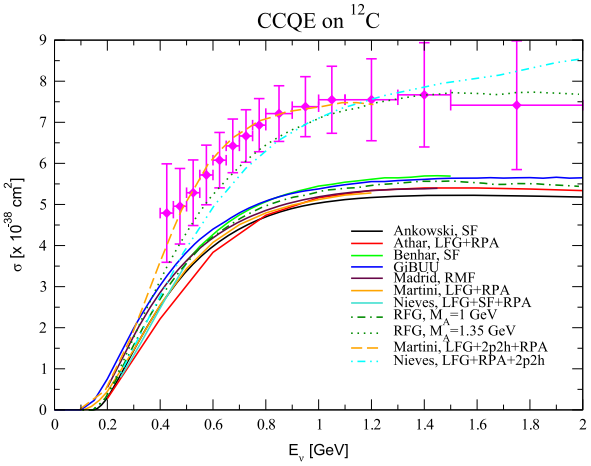

Figure 8. Summary of CCQE integrated cross sections as a function of the neutrino energy. Solid lines denote the models from [81], [138], [80], [104], [88], [124] and [55] in this order, as reported in [137]. The dash-dotted and dotted lines are RgFG calculations with $p_F = 220$ MeV, $E_B = 34$ MeV and $M_A = 1$ and 1.35 GeV respectively. The dashed and the dashed double-dotted lines are the result of [124] and [139] after adding the 2p2h contributions. The data points are from MiniBooNE [23] as a function of the reconstructed neutrino energy.

these CCQE-like events: it is unlikely that they were so badly underestimated to be responsible for the large CCQE cross section. Martini *et al* [124] pointed out that another so far unaccounted source of CCQE-like cross section arises from the contributions of two (or more) interacting nucleons (2p2h excitations), because ejected low energy nucleons are not detected at MiniBooNE.

One should recall that certain 2p2h mechanisms (diagrams (1) and (2) of figure 9) had been already taken into account in former CCQE calculations as part of the more general nucleon spectral functions for particles [55, 79, 81, 92] and holes [79, 81] and have a small effect on the integrated cross section, although they are known to play an important role in the description of the QE peak in inclusive electron scattering on nuclei [78, 79]. Diagram (7) in figure 9 has also been considered in calculations of the inclusive neutrino–nucleus cross sections as part of the in-medium $\Delta(1232)$ spectral function [79, 81, 92]. On the other hand, there are many 2p2h terms (for example MEC diagrams (3), (4) and interference diagram (8) in figure 9) that are not reduced to particle, hole or resonance spectral functions. They are required for a satisfactory description of the dip region between the QE and the $\Delta(1232)$ peaks in inclusive electron scattering [78]. Some of these 2p2h contributions have been taken approximately into account in [124] using two different parametrizations of the multinucleon terms, from pion absorption [140] and from electron scattering [141], extrapolated to the kinematic region of neutrino interactions. Once they were added to the *true* CCQE cross section, a very good agreement with the MiniBooNE data was obtained (see the dashed line in figure 8). A good description of the data, quite similar to the one obtained with the RgFG and $M_A = 1.35$ GeV, is also obtained with the microscopic model for 2p2h excitations developed in [142] (dashed double-dotted line in figure 8).

The importance of MEC has been further stressed in the recent *ab initio* calculation of the sum rules of the weak NC response functions on ^{12}C [143]. A significant enhancement (∼30%)

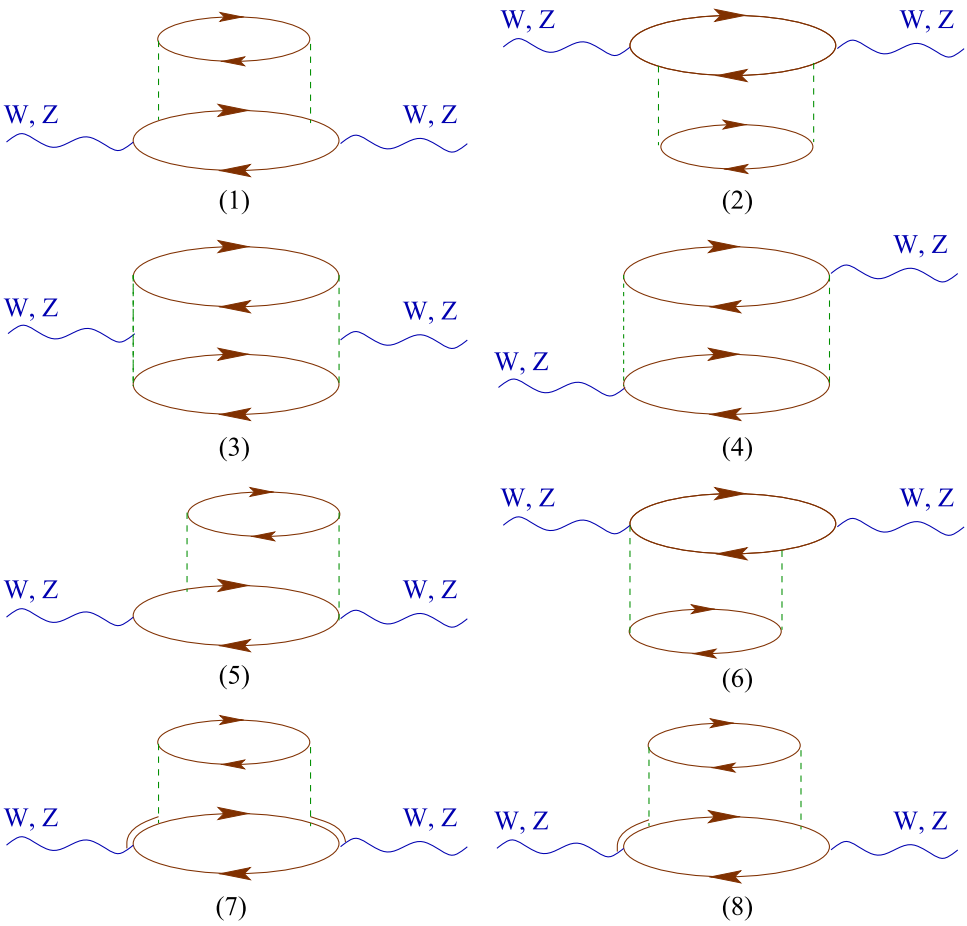

Figure 9. Some 2p2h contributions to the polarization propagators. Solid (dashed) lines denote nucleon (pion) propagators. Double lines represent $\Delta(1232)$ propagators. Solid lines pointing to the right (left) denote particle (hole) states.

of the weak response is due to two-nucleon currents. This approach implements non-relativistic currents and treats the Δ in the static limit but provides a state-of-the-art description of the nuclear ground state and the nuclear correlations. Therefore, it represents a benchmark for more phenomenological methods. Based on a recent calculation of sum rules for the electromagnetic response obtained in [144] within the *ab initio* Green function MC framework, it has been suggested [145] that 2p2h terms arising from the interference between one-body and two-body currents play a significant role in neutrino scattering. Indeed, the transverse sum rule on ^{12}C has a sizable contribution of this kind, as can be seen in figure 1 of [145]. Diagrams (5) and (6) of figure 9 are examples of these pieces in the polarization propagator: in the nomenclature of [145], diagram (5)[(6)] accounts for a MEC-final (initial) state correlation interference contribution to the 2p2h hadronic tensor. It should be stressed that, with the caveats discussed above about the kinematic extrapolations, the calculation of Martini *et al* [124] incorporates such interference terms, as can be seen in section 3.4 of [140] and in section 4 of [141]. In the model of [142], the final state correlation terms, and the interferences with MEC mechanisms, are included as part of the generic 2p2h diagram of figures 4 and 9 of that reference, while the initial state ones are neglected because they are of higher order in an expansion in powers of the

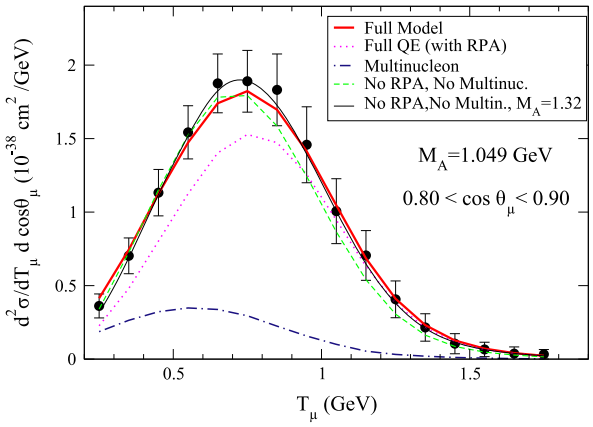

Figure 10. ν-^{12}C double differential cross section averaged over the MiniBooNE flux [128] as a function of the muon kinetic energy and for the $0.80 < \cos\theta_\mu < 0.90$ angular bin [139]. The thick solid line stands for the full model (RlFG+RPA+2p2h). The dashed, dotted and dash-dotted lines show partial results for only RlFG, RlFG+RPA and only 2p2h, respectively. All these curves are obtained with $M_A = 1.049$ GeV while the thin solid line is calculated with the RlFG and $M_A = 1.32$ GeV. The data of [23] have been rescaled by a factor 0.9 (compatible with flux uncertainties).

nuclear density (as diagram (2) of figure 9 is). Although the transverse sum rule is indicative, a systematic study of observable quantities at the kinematics encountered in neutrino experiments is required to establish the importance of these mechanisms for the QE-like cross section.

In neutrino experiments, the incident energy is not known *a priori* and its determination involves some model dependence (see the discussion in section 3.3.1). For this reason, theoretical models should be directly compared with the double differential cross section of [23] for neutrinos and [25] for antineutrinos. Such a comparison has been performed in [139, 146, 147] for neutrinos, and in [148–150] for antineutrinos. In [146, 148] the addition of the vector part of the MEC mechanisms to the result of the SuSa approach led to a better agreement with data. Within the model of [142] a very good agreement with the ν-^{12}C double differential cross section has been achieved with $M_A = 1.077 \pm 0.027$ GeV (see table I of [139]). This value is certainly much lower and closer to the determinations from CCQE on deuterium and pion electroproduction discussed in section 3.1 than the one obtained by the RgFG model.

The role of the different reaction mechanisms according to the model of [139, 142] can be appreciated in figure 10 where $\mathrm{d}^2\sigma/\left(\mathrm{d}k'^0\mathrm{d}\cos\theta'\right)$ is shown for a single muon-angle bin. Not only multinucleon mechanisms, but also RPA corrections are essential to understand the data. Indeed, RPA strongly decreases the cross section at low muon energies, where multinucleon contributions accumulate. Therefore, the final picture arises from a delicate balance between the dominant single nucleon scattering, corrected by collective effects, and mechanisms that involve two or more nucleons.

A good description of MiniBooNE data for both $\mathrm{d}^2\sigma/\left(\mathrm{d}k'^0\mathrm{d}\cos\theta'\right)$ and $\sigma\left(E_\nu\right)$ with an $M_A = 1.03$ GeV has also been found [100] with the RGF model with empirical OP briefly covered in the previous section. This has been achieved with a model that takes into account

those multinucleon contributions that can be ascribed to the particle spectral function (like, for example, diagram (1) in figure 9) but does not contain MEC mechanisms or in-medium Δ modifications. This finding, at odds with the picture outlined above, should be interpreted with care. First of all, the results depend rather strongly on the choice of OP: compare green and red lines in figures 1–3 of [100]. Second and most importantly, the imaginary part of the OP, which adds to the total cross section in the RGF model, is due to inelastic channels. These inelastic channels include pion emission and absorption, and have already been subtracted in the MiniBooNE analysis. Therefore, it would be very interesting to compare the RGF results with fully inclusive CC data.

Ultimately, it would be important to find a more direct experimental signature for the multinucleon processes. Possible observables have been considered in [151, 152]. It is found that 2p2h primary interactions do lead to an increase of multinucleon events. Such an enhancement may indeed be revealed in measurements by looking, for example, at proton pairs in the final state, or the total visible energy which would contain contributions from protons below reconstruction threshold. However, the primary distributions will be heavily distorted by FSI and, therefore, model discrimination would require a high precision and a considerable improvements in the MC simulations.

3.3.1. Multinucleon mechanisms and neutrino energy reconstruction. Neutrino beams are not monochromatic so that the energy of an interaction event is *a priori* not known. As the oscillation probability is energy dependent, the neutrino energy determination is important for oscillation analyses and also, needless to say, to measure the energy dependence of different cross sections, like the CCQE one from MiniBooNE [23] shown in figure 8. There are different strategies to reconstruct E_ν. In high energy experiments such as MINOS ($1 \lesssim E_\nu \lesssim 50$ GeV) it is reconstructed as the sum of the muon energy and the hadronic shower energy. As the detection of the final particles is never perfect, the procedure partially relies on the theoretical models contained in the simulation program [153].

At lower energies it is common to rely on a kinematic energy reconstruction based on the event identification as CCQE. In this case, the neutrino energy can be obtained from the measured angle and energy of the outgoing lepton using two-body kinematics

$$E_\nu^{\mathrm{rec}} = \frac{2M_n k'^0 - m_l^2 - M_n^2 + M_p^2}{2\left(M_n - k'^0 + \sqrt{\left(k'^0\right)^2 - m_l^2}\cos\theta'\right)}. \tag{42}$$

This formula, sometimes modified to incorporate the constant binding energy of the RgFG model, is only valid for a target neutron at rest. The Fermi motion of the nucleons in the nucleus causes a smearing of the reconstructed energy around the true value but the procedure remains accurate enough for oscillation analyses, and the energy dependence of the cross section is not affected. On the contrary, CCQE-like events from absorbed pions produce a systematic error in the neutrino energy determination, which is too large to be neglected. This was known and taken into account in the MiniBooNE analysis, by treating these events as a background that must be subtracted [23]. However, the same is true for multinucleon contributions. Once they are sizable, the effect on the E_ν determination is significant [154–156].

Figure 11 demonstrates the effect of the neutrino-energy reconstruction on the E_ν dependence of the CCQE-like (RlFG+RPA+2p2h) cross section according to the model of

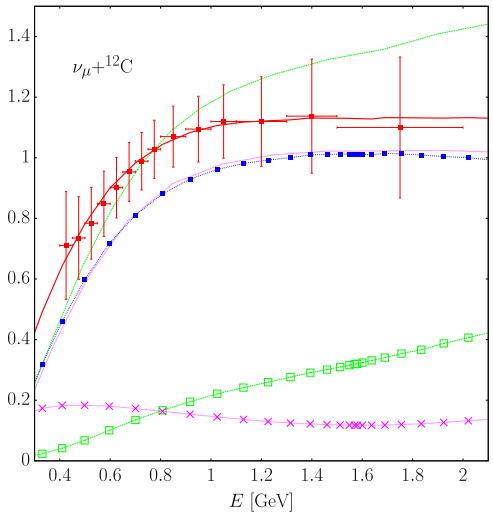

Figure 11. CCQE-like cross section as a function of the true and the reconstructed neutrino energies [155]. The RlFG+RPA cross section, given by the blue filled squares plotted as a function of $E_\nu^{\rm rec}$, is practically unaffected by the energy reconstruction as can be seen from the comparison with the solid magenta line. The 2p2h parts as a function of E_ν and $E_\nu^{\rm rec}$ are given by the open green squares and the magenta crosses respectively. The corresponding curves for the total RlFG+RPA+2p2h cross section are the green dotted and the red ones. MiniBooNE data [23] have been rescaled by a factor 0.9.

[139, 142]. The *true* CCQE (RlFG+RPA) cross section is unaffected by the energy reconstruction. The 2p2h contribution instead is a very different function of the true neutrino energy (green open squares) than as a function of $E_\nu^{\rm rec}$ (magenta crosses). In other words, $E_\nu^{\rm rec}$ is a poor estimate of the actual energy for multinucleon mechanisms. As a consequence, the total theoretical RlFG+RPA+2p2h cross section, when plotted in terms of $E_\nu^{\rm rec}$ shows a remarkably good agreement with the MiniBooNE data of [23] rescaled by a factor 0.9, which is consistent with the experimental normalization error of 10.7%. In conclusion, the actual energy dependence of the CCQE-like cross section is not given by the MiniBooNE data but would be steeper and closer to the dotted (green) line in figure 11. A similar finding has been made with the model of [124] as can be seen in figure 14 of [156].

The misreconstruction of QE events resulting from many-body dynamics is bound to have an impact on the oscillation analyses of experiments like MiniBooNE, T2K and LBNE [156–158]. The bias in the determination of oscillation parameters may remain even after the near detector has been taken into account [159, 160].

3.3.2. The high $E_\nu > 1$ GeV region. As the neutrino energy increases, so does the range of possible energies that can be transferred to the target. Large energy transfers make possible the excitation of baryon resonances heavier than the $\Delta(1232)$ not taken into account in the 2p2h models that have been developed so far. Based on the experience with weak resonance excitation and pion production (see section 4.2) one could expect the $D_{13}(1520)$ to play a role. The effective *NN* interaction used to compute RPA correlations are not realistic at high energies as discussed in section 3.2.2 although collective effects for this kinematics should be small. In addition, the MEC vertices present in the models come from effective low-energy interactions.

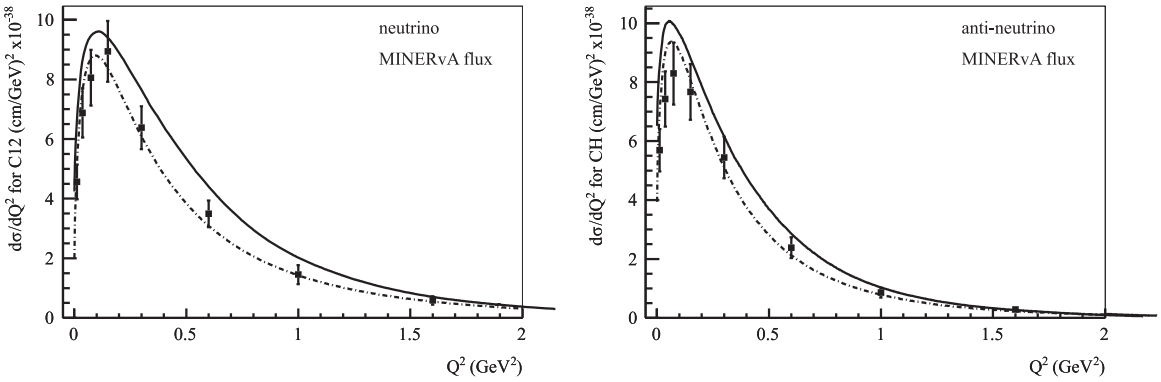

Figure 12. Differential Q^2 distribution averaged over the MINERvA ν_μ and $\bar{\nu}_\mu$ fluxes [48, 49] as a function of the reconstructed Q^2 for the RlFG (dash-dotted lines) and the RlFG+RPA+2p2h (solid lines) models. Data are from [48, 49].

Nevertheless, the model of [139, 142] has been applied to neutrino energies of up to 10 GeV, but limiting the 2p2h contribution to $|\vec{q}| < 1.2$ GeV [161]. The results obtained in this way, averaged over the neutrino and antineutrino fluxes at MINERvA, have been confronted with data [161] for the reconstructed q^2 distribution obtained using $E_\nu^{\rm rec}$. As can be seen in figure 12, the agreement is quite good, with a slight overestimation of the data. The impact of the reconstruction procedure in the case of MINERvA flux is small.

According to [161], as the neutrino energy increases, up to 10 GeV, the 2p2h contribution saturates to ∼30% of the QE cross section. *A priori*, there is no reason for this trend to change drastically at even higher energies. This brings us to a question that remains open: the compatibility of the MiniBooNE results with the NOMAD one of $M_A = 1.05 \pm 0.02\,(stat) \pm 0.06\,(syst)$ GeV [35]. The answer is not obvious and requires further investigations. The NOMAD measurement includes events with a muon track and one or no knocked out proton track. In principle the events without nucleon tracks should contain at least some 2p2h contributions producing unobservable low energy protons or neutrons but it is possible that, due to the high excitation energies involved, a fraction of the 2p2h events are observed as multi-track ones and removed from the CCQE sample.

3.4. QE production of hyperons

The existence of flavor changing CC converting u quarks into s quarks makes the QE production of hyperons induced by antineutrinos possible. One has the following $\Delta S = 1$, Cabibbo suppressed, reactions on nucleons

$$\bar{\nu}_l(k)\, p(p) \to l^+(k')\, Y^0(p'), \qquad Y^0 = \Lambda,\, \Sigma^0, \tag{43}$$

$$\bar{\nu}_l(k)\, n(p) \to l^+(k')\, \Sigma^-(p'), \tag{44}$$

which are related to the semileptonic decays of hyperons [162]. The theoretical study of these reactions has been undertaken in [163–165]. The framework outlined in section 3.1 for QE scattering on nucleons remains valid, now with $c_{\rm EW} = \sin\theta_C$ in equation (6),

$$H^{\alpha\beta} = \mathrm{Tr}\left[(\not{p} + M)\,\gamma^0 (\Gamma^\alpha)^\dagger \gamma^0 (\not{p}' + M_Y)\Gamma^\beta\right], \tag{45}$$

where M_Y is the hyperon mass and

$$J^\alpha = \bar{u}_Y(p')\Gamma^\alpha u(p) = V^\alpha - A^\alpha, \tag{46}$$

with the vector and axial currents given by

$$V^\alpha = \bar{u}_Y(p')\left[\gamma^\alpha f_1\left(q^2\right) + i\sigma^{\alpha\beta}\frac{q_\beta}{M + M_Y} f_2\left(q^2\right) + \frac{q^\alpha}{M_Y} f_3\left(q^2\right)\right] u(p) \tag{47}$$

and

$$A^\alpha = \bar{u}_Y(p')\left[\gamma^\alpha g_1\left(q^2\right) + i\sigma^{\alpha\beta}\frac{q_\beta}{M + M_Y} g_2\left(q^2\right) + \frac{q^\alpha}{M_Y} g_3\left(q^2\right)\right]\gamma_5 u(p). \tag{48}$$

Assuming SU(3) symmetry, the form factors can be related to the electromagnetic and axial form factors of nucleons (see for example table II of [163]). In this limit, $f_3 = g_2 = 0$. SU(3) breaking corrections, which can be systematically studied using chiral perturbation theory [166], are small for the accuracy presently achievable in neutrino experiments.

Weak hyperon emission off nuclear targets has been addressed in [163]. Apart from the Fermi motion of the initial nucleon and the mean field potential felt by the hyperons, estimated to be negligible [163], there are important FSI effects. The hyperons produced in the reactions of equations (42) and (43) undergo elastic and charge exchange scattering; Σ^0 can be converted into Λ via radiative decay $\Sigma^0 \to \Lambda\,\gamma$. These processes, which alter the composition and momentum distributions of the emitted hyperons, have been modeled in [163] by a MC cascade simulation using experimental information on hyperon–nucleon cross sections as input. Another consequence of FSI is that Σ^+ hyperons, not produced in the primary reactions, can emerge due to processes like $\Lambda p \to \Sigma^+ n$ or $\Sigma^0 p \to \Sigma^+ n$ although at a small rate (compare figure 9 of [163] with figures 4–6 of the same article).

An important issue brought up in [163] and elaborated further in [167] is that, owing to their weak decays $Y \to N\,\pi$, hyperons become a source of pions in experiments with antineutrino beams. As can be seen from figure 13, at low incident energies (550 MeV for π^- and 650 for π^0) the cross section for pion production from hyperons becomes larger than the one from $\Delta(1232)$ excitation, which is the dominant mechanism at higher energies (see section 4 for more details about weak pion production). Unlike Δ resonances, hyperons have a large mean life and decay predominantly outside the nucleus. Therefore, the resulting pions are not absorbed in the nucleus. This partially compensates the Cabibbo suppression, particularly for heavy nuclei where absorption is strong. In [167] it has been shown that for atmospheric and MiniBooNE $\bar{\nu}$ fluxes, a significant fraction of the π^- and π^0 originate indeed from hyperon decays.

4. Weak pion production and other inelastic channels

4.1. Introduction

Pion production cross section becomes quite relevant for neutrino energies above 400 or 500 MeV, and plays a central role for neutrino energies in the 1 GeV region, of the greatest

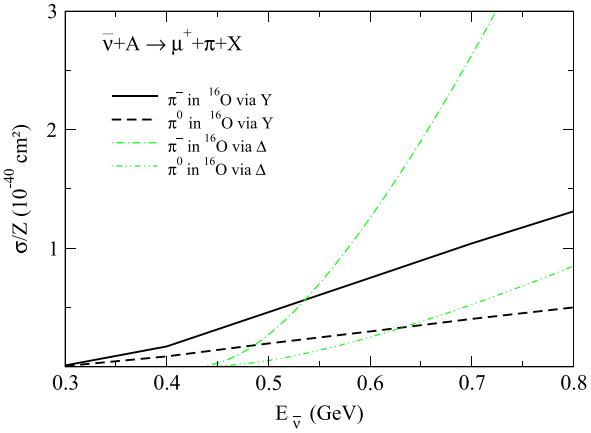

Figure 13. Integrated cross section for π production on ^{16}O induced by antineutrinos as a function of the antineutrino energy in the laboratory frame. Results for pions produced from Δ and hyperon (Y) decay are compared. Adapted from [163].

importance for neutrino oscillation experiments such as MiniBooNE or T2K. Recently, the MiniBooNE Collaboration has published one pion production cross sections on mineral oil by ν_μ and $\bar{\nu}_\mu$ neutrinos with energies below 2 GeV. The data include ν_μ and $\bar{\nu}_\mu$ NC single π^0 production [30], as well as ν_μ induced CC charged and neutral pion production [27, 28]. These are the first[6] pion production cross sections to be measured since the old deuterium bubble chamber experiments carried out at Argonne National Laboratory (ANL) [169, 170] and Brookhaven National Laboratory (BNL) [171].

These new data show interesting deviations from the predictions of present theoretical models that we will briefly discuss in what follows.

4.2. Pion production off nucleons

Pion production in weak interactions is a window to the poorly known axial properties of baryon resonances. In addition, the first requirement to put neutrino induced pion production on nuclear targets on a firm ground is to have a realistic model at the nucleon level. There have been several theoretical studies of the weak pion production off the nucleon at intermediate energies [57, 92, 172–189]. Most of them describe the pion production process by means of the weak excitation of the $\Delta(1232)$ resonance and its subsequent decay into $N\pi$, and do not incorporate any background terms. The models of [92, 173–175, 180, 181] include also the weak excitation of several resonance contributions as intermediate states. In these schemes, the vector form factors were fixed from helicity amplitudes extracted in the analysis of pion electroproduction data, while the axial couplings were obtained from PCAC. The most complete model in this respect is the one of [92], where all four-star resonances below 1.8 GeV have been included, with vector form factors taken directly over from the MAID analysis ([190] and [191]). The vector part of the background and its interference with the vector part of the

[6] There exist two other recent measurements of NC π^0 production (K2K [18] and SciBooNE [168]), which however do not provide absolutely normalized cross sections, but report only the ratios $\sigma\left(NC1\pi^0\right)/\sigma\left(CC\right)$, where $\sigma\left(CC\right)$ is the total CC cross section.

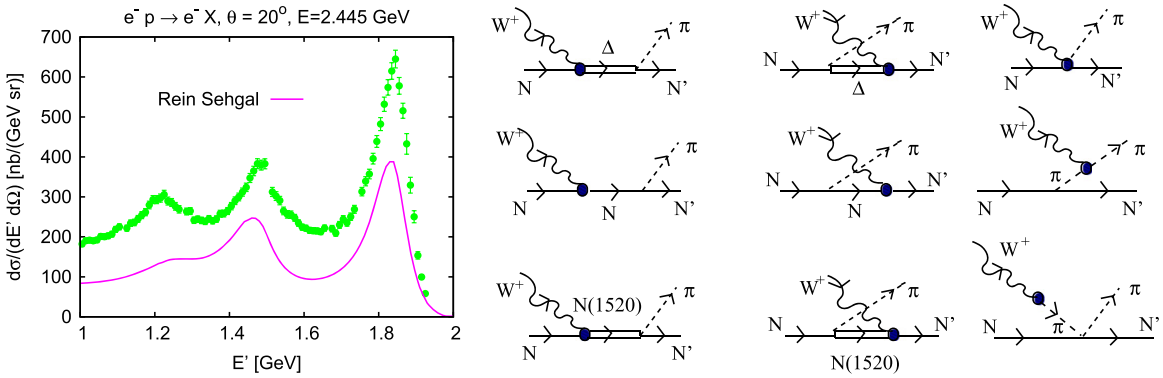

Figure 14. Left: double differential cross sections for scattering of electrons off protons. The predictions of the model of [175] are compared to data from JLAB [199] (see [195] for details). Right: model of [182–184] for the $W^+N \to N'\pi$ amplitude. It consists of direct and crossed $\Delta(1232)$, $N(1520)$ and nucleon pole terms, contact and pion pole contribution, and the pion-in-flight term.

resonant contributions was fixed using the empirical pion electroproduction amplitudes extracted in the MAID analysis [190]. The axial background part (including the vector-axial interference) was taken to be proportional to the vector one. The proportionality constant was adjusted to the old bubble chamber ANL and BNL data, neglecting deuteron effects. According to [92], the $D_{13}(1520)$ resonance, besides the $\Delta(1232)$, is the only one playing a significant role for neutrino energies below 1–1.5 GeV. However, at $E_\nu > 1$ GeV (MINERνA) higher N^* in general will become important.

We should pay special attention to the Rein–Sehgal model [175], because it is used by almost all MC generators. It was an attempt to describe all data available in 1980 on neutrino production of single pions in the resonance region up to πN invariant masses $W_{N\pi}$ of around 2 GeV. The basic assumption is that single pion production is mediated by all interfering resonances below 2 GeV, supplemented with a simple non-interfering, non-resonant phenomenological background of isospin 1/2. The needed transition matrix elements are calculated using the relativistic quark model of Feynman–Kislinger–Ravndal [192] (formulated in 1970) with SU(6) spin-flavor symmetry, and a total of 18 baryon resonances considered. The original work of [175] assumes massless leptons. Subsequently, the model for the CC reaction was extended in [193, 194] to include finite lepton mass effects in a manner consistent with PCAC. However, we should stress the Rein–Sehgal model provides a really poor description of the pion electroproduction data on protons [185, 195]. Actually, it underestimates significantly the electron data, as can be appreciated in the left panel of figure 14, and the more accurate predictions from the model of [92]. The model of Rein and Sehgal also reveals itself unsatisfactory in the axial sector at $q^2 = 0$, where the divergence of axial current can be related to the πN amplitude by PCAC [196]. This connexion was exploited in [197] to obtain the forward neutrino cross sections using a dynamical coupled channel model that successfully fits a large set of πN and γN data. The comparison with the Rein–Sehgal model, given in figure 3 of [198], shows a clear disagreement with the more realistic description, underestimating the Δ peak but overestimating the higher $W_{\pi N}$ region.

Background non-resonant terms, required and totally fixed at threshold by chiral symmetry, were evaluated in [182][7]. The background terms in [182] are the leading contributions of a SU(2) chiral Lagrangian supplemented with well known form factors in a way that respects both conservation of vector current (CVC) and PCAC. The interference between the Δ and the background terms produces parity-violating contributions to the pion angular differential cross section, which are intimately linked to T-odd correlations[8] which would be interesting to measure. The model of [182, 184] is diagrammatically shown in the right panel of figure 14 (note that the D_{13} contributions were not considered originally in [182]). Vector form factors are taken from fits to empirical helicity amplitudes [180]. The axial $N\Delta$ transition is parametrized in terms of four form factors $C^A_{3,4,5,6}\left(q^2\right)$, as in [57]. Among the axial form factors the most important contribution comes from C^A_5, whose numerical value is related to the pseudoscalar form factor C^A_6 by PCAC. Moreover, in the massless lepton limit, the direct Δ pole term gives

$$\frac{\mathrm{d}\sigma}{\mathrm{d}q^2} \propto \left\{ \left[C^A_5(0) \right]^2 + q^2 a\left(q^2\right) \right\}, \tag{49}$$

with $C^A_{3,4}(0)$ contributing to $a\left(q^2\right)$, i.e. to $O\left(q^2\right)$, which also gets contributions from vector form factors and terms proportional to $\mathrm{d}C^A_5/\mathrm{d}q^2\ |_{q^2=0}$. For the subleading $C^A_{3,4}$ form factors, the Adler's parametrizations [200, 201] were adopted ($C^A_3 = 0$, $C^A_4 = -C^A_5/5$), while the dominant axial ($C^A_5\left(q^2\right)$) form-factor was fitted to the flux averaged $\nu_\mu p \to \mu^- p \pi^+$ ANL q^2-differential cross section data [170], finding a correction of the order of 30% to the off diagonal Goldberger–Treiman relation (GTR) prediction $C^A_5(0) \sim 1.15$. Considering electroproduction experiments as benchmark, the model provides an accurate description of the data up to pion–nucleon invariant masses of the order of $W_{\pi N} < 1.4$ GeV [202].

Deuterium effects and BNL data were not taken into account in the analysis carried out in [182]. It is well known that there exists some tension between ANL and BNL $p\pi^+$ data samples. It has become a relevant issue that the more than 30-year-old ANL and BNL low statistics deuterium pion production data are still the best source of information about the $N\Delta$ transition matrix element. The authors of [186] made a simultaneous fit, considering only the Δ-mechanism, to both ANL and BNL data including separate overall flux normalization uncertainties for each experiment. The main conclusion was that ANL and BNL data are in fact consistent only when these systematic uncertainties are taken into account. This strategy was followed in [183], where the $N\Delta$ axial transition form-factors within the model derived in [182] were simultaneously fitted to both bubble chamber data sets. Deuterium effects were also taken

[7] Some background terms were also considered in [173, 174, 178]. In the latter reference, the chiral counting was broken to account explicitly for ρ and ω exchanges in the t-channel, while the first two works are not fully consistent with the chiral counting either, since contact terms were not included, and use a rather small axial mass (∼650 MeV) for the $N\Delta$ transition form factor.

[8] However, these correlations do not imply a genuine violation of time-reversal invariance because of the existence of strong final re-scattering effects.

into account. As a result of this improved analysis, a value of 1.00 ± 0.11 for $C_5^A(0)$, 2σ away from the GTR estimate[9], was found [183]. This model, which includes a non-resonant chiral background, was further refined in [184] by adding a new resonance ($D_{13}(1520)$) aiming to extend the model to higher energies above the Δ resonance region for which it was originally developed. Thus, this scheme emerges as one of the most adequate ones, from a theoretical perspective, to analyze pion production data and neutrino energies up to 1 or 1.2 GeV.

Another theoretical description is based on a dynamical model of photo-, electro- and weak pion production [178]. Starting from an effective Hamiltonian with $N\Delta$ couplings obtained with the constituent quark model (30% below the measured ones), the T matrix is obtained by solving the Lippmann–Schwinger equation in coupled channels. In this way the bare couplings get renormalized by meson clouds. The predicted cross sections are in good agreement with data (figures 5–8 of [178]).

More recently, a Lorentz-covariant effective field theory scheme that contains nucleons, pions, Δ, isoscalar scalar (σ) and vector (ω) fields, and isovector vector (ρ) fields consistent with chiral symmetry has been also employed to study the neutrino-production of pions from nucleons [189]. At low neutrino energies, below 500 MeV, the convergence of the power-counting scheme used in [189] is fast and next-to-leading-order tree-level corrections are found to be small. To go beyond this energy regime, the authors of [189] use phenomenological form factors. Nevertheless, they are mostly concerned with the $E_\nu < 0.5$ GeV region, where a satisfactory agreement with ANL data is obtained.

Finally, we just mention the approach of [196] entirely based on PCAC and valid only at low energies and in the small q^2 region.

4.3. Pion cross sections in nuclei and the MiniBooNE puzzle

The main contribution to MiniBooNE data comes from ^{12}C and this poses an extra problem to theoretical calculations because the in-medium modifications of the production mechanisms, and the FSI effects on the produced pions are important. As in QE scattering, pion production in nuclei is affected by the description of the initial nucleus. Although the most common approximation adopted for resonance production, and inelastic scattering in general, on nuclear targets is the Fermi gas in its global [203] and local [204] versions, more precise descriptions based on realistic spectral functions [79] or bound-sate wave functions [205] have been developed. The integrated cross sections obtained with Fermi gas models are very similar to those from sophisticated approaches (see for instance figure 7 of [205]). This reflects the fact that at the higher energy transfers present in inelastic processes, the details of nuclear structure are less relevant. Given the prevalent role of the $\Delta(1232)$ excitation in pion production, it is not surprising that the in-medium modification of its properties represents the most important nuclear effect, as already stressed in the early work of [203, 204] and illustrated below.

On the other hand, FSI takes into account that pions can be absorbed on their way out of the nucleus, and can also suffer different QE collisions that modify their energy, angle, and charge when they come off the nucleus. For instance, in the case of NC π^0 production, signal events originate mostly from a NC1π^0 primary interaction with a π^0 not being affected by FSI,

[9] The approach does not satisfy the Watson theorem; the inclusion of constraints derived from this latter requirement could diminish the discrepancies with the GTR prediction.

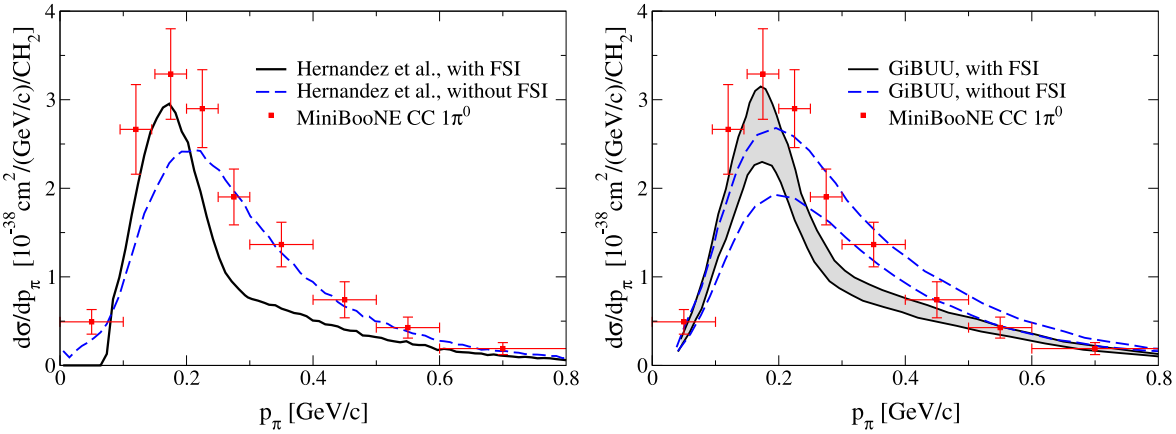

Figure 15. MiniBooNE flux-folded differential $d\sigma/dp_\pi$ cross section for CC1π^0 production by ν_μ in mineral oil. Data are from [27]. Left: predictions from the cascade approach of [184]. The solid curve corresponds to the full model and the dashed one stands for the results obtained neglecting FSI effects. Right: predictions from the GiBUU transport model of [207]. The dashed curves give the results before FSI, the solid curves those with all FSI effects included. Two different form factors $C_5^A\left(q^2\right)$, tuned to the ANL and BNL data-sets have been employed and give rise to the systematic uncertainty bands displayed in the figure.

but also from a NC1π^+ primary interaction with the π^+ being transformed into π^0 in a charge exchange FSI reaction. In this particular case, an additional difficulty in interpreting the NC π^0 production comes from the presence of a coherent contribution. FSI definitely alters the signature of the event and thus the correct simulation of pion production requires a model not only able to describe the elementary reactions (discussed in the previous subsection), but also the FSI.

MiniBooNE presented their results as measurements of final states with only one pion, with the appropriate charge, and no other mesons. A variety of flux integrated differential cross sections were reported in final pion momentum or scattering angle. For the case of CC reactions, total cross sections as a function of the reconstructed neutrino energy were provided as well. MiniBooNE data show substantial discrepancies (enhancement) with respect to the Rein–Sehgal interaction [175] prediction with FSI effects as implemented in the NUANCE event generator [206]. Some important discrepancies still remain when these measurements are compared with the most comprehensive approaches [184, 207] available in the literature until now, as highlighted in the case of CC1π^0 in figure 15. Both theoretical approaches start from a quite complete microscopic description of the pion production on the nucleon at MiniBooNE energies ([182–184] and [92], respectively) and incorporate a number of standard nuclear medium effects in the initial interaction model (Pauli blocking, $\Delta(1232)$-spreading potential, etc).

The work of [207] uses the Giessen Boltzmann–Uehling–Uhlenbeck (GiBUU) model to account for FSI effects. It is a transport model where FSI are implemented by solving the semi-classical Boltzmann–Uehling–Uhlenbeck equation. It describes the dynamical evolution of the phase space density for each particle species under the influence of the mean field potential,

introduced in the description of the initial nucleus state. Equations for various particle species are coupled through this mean field and also through the collision term. GiBUU provides a unified framework for nucleon–, nucleus–, pion–, electron– and neutrino interactions with nuclei, from around 100 MeV to tens of GeV. It has been extensively and successfully used [86] in the last years, with special attention to pion- and photo-nuclear reactions. The study of [207] is limited only to the incoherent part of the CC induced reaction. The comparison with the MiniBooNE NCπ data was presented and discussed at the NUFACT and NUINT conferences [208, 209]. Previous work of the group can be found in [92, 210].

Coherent contributions, when relevant, are included in the work of [184] from the microscopic approach of [211, 212]. This is based on the same pion production model on nucleons [182, 183] employed in [184]. On the other hand [184] makes use of the LDA to evaluate the incoherent production on finite nuclei. This approximation, also part of the GiBUU model, turns out to be quite convenient when using a cascade algorithm, as we will see. The work of [184] is based on the many body scheme set up in [55, 142] to study inclusive neutrino–nucleus reactions. It establishes a systematic many body expansion of the gauge boson absorption modes that includes one, two and even three body mechanisms, as well as the excitation of Δ resonances and pion production.

To compute the incoherent pion production on a nucleus, one should sum the nucleon cross section over all nucleons in the nucleus. For a neutrino CC process (for antineutrino or NC induced reactions the discussion is similar) within the LDA one gets for initial pion production (prior to any pion FSI) [184]

$$\frac{\mathrm{d}\sigma}{\mathrm{d}|\vec{k}|4\pi r^2\,\mathrm{d}r\,\mathrm{d}\cos\theta_\pi\,\mathrm{d}E_\pi} = \Phi\left(|\vec{k}|\right)\sum_{N=n,p} 2\int \frac{\mathrm{d}^3p_N}{(2\pi)^3}\theta\left(E_F^N(r)-E_N\right)$$
$$\times\,\theta\left(E_N+q^0-E_\pi-E_F^{N'}(r)\right)\frac{\mathrm{d}\hat{\sigma}\left(\nu N\to l^- N'\pi\right)}{\mathrm{d}\cos\theta_\pi\,\mathrm{d}E_\pi} \tag{50}$$

with $E_F^N(r)=\sqrt{M^2+\left(p_F^N(r)\right)^2}$, given in terms of the local Fermi momentum $p_F^N(r)$ defined in equation (35). The step functions implement Fermi motion and Pauli blocking. Besides, $\Phi\left(|\vec{k}|\right)$ is the neutrino flux as a function of the incoming-neutrino energy $E_\nu\equiv|\vec{k}|$; $\hat{\sigma}\left(\nu N\to l^- N'\pi\right)$ is the cross section at the nucleon level modified by medium effects, which in this case consist in the modification of the $\Delta(1232)$ spectral function. The Δ properties are strongly modified in the nuclear medium [213], and since the direct Δ-mechanism is dominant, a correct treatment is needed for π production inside a nucleus. This is accounted for, both in the works of [184] and [207], using a realistic spreading potential (Δ-self-energy). In the nuclear medium, on one hand, the width is reduced due to Pauli blocking, but on the other hand, it is increased by the collisions inside the nucleus. For example, via the processes $\Delta N\to NN$ and $\Delta NN\to NNN$, the Δ can disappear without producing a pion. Secondary pion production is also possible, namely via the process $\Delta N\to\pi NN$. These processes contribute to the in medium Δ width that generally becomes larger than in the free space.

The in medium differential cross section of equation (48) is used in a simulation code to generate, at a given point $\vec{r}$ inside the nucleus and by neutrinos of a given energy, on-shell pions with a certain momentum. These pions are followed through their path across the nucleus. To

evaluate these FSI effects, the authors of [184] follow the approach of [214], where a computer simulation code was developed to describe inclusive pion nucleus reactions (QE, single charge exchange, double charge exchange, and absorption). The πN interaction is dominated by the Δ resonance excitation, modified in the nuclear medium in the same way as it was modified in $\hat{\sigma}\left(\nu N \to l^{-} N' \pi\right)$. The different contributions to the imaginary part of its self-energy account for pion, two- and three-nucleon absorption and QE processes. The probabilities for the different processes are evaluated in nuclear matter as a function of the density, then the LDA prescription is used to obtain results in finite nuclei. After a QE event, pions change momentum and may change electric charge. The probability for charge exchange and the final momentum distribution after a QE interaction were computed in [214]. That information is used in the simulation program to generate the pion resulting from such a collision.

The model of [184] provides an overall acceptable description of MiniBooNE data, better for NC than for CC channels, although the theoretical predictions are systematically below data. Differential cross sections, folded with the full neutrino flux, show that most of the missing pions lie in the forward direction and at high energies. An example of this is shown in figure 15 for CC $1\pi^0$. FSI effects are clearly visible in the distribution. Because of the FSI some pions are absorbed, but other ones are scattered and lose to nucleons part of their energy. FSI is essential to fill the low momentum part of the distribution. On the other hand, the combined effect of QE scattering and pion absorption through Δ excitation, depletes the $p_\pi = 250 \sim 450$ MeV region producing a distortion of the differential cross section shape that significantly worsens the description of the data. The artificial exclusion of the FSI effects leads to a better description of the high momentum tail of the $\mathrm{d}\sigma/\mathrm{d}p_\pi$ distribution.

These findings are fully supported by the results obtained within the GiBUU scheme of [207]. Actually both approaches produce quite similar results, as can be seen in figure 15 for the particular case of CC $1\pi^0$. The authors of [207] also pointed out that MiniBooNE seems to suggest that the higher elementary BNL data for pion production are correct and that the ANL data underestimate the elementary production cross section. Nevertheless, the discrepancy with theory is not only due to an overall normalization factor, but as stressed above, the experimental shape of the pion momentum distributions considerably differ from those predicted by both approaches. However the theoretical model calculations [207, 215] turn out to be in agreement with experimental results for the photo-production of pions on nuclei, predicting a suppression in the pion spectra around the Δ resonance region which is not seen in the MiniBooNE neutrino data.

FSI effects could be reduced by considering the so called 'formation zone', that among other effects includes the propagation of the Δ before decaying into a πN pair. The NuWro MC event generator [216, 217] includes the concept of formation zone, and its predictions for NC $1\pi^0$ have been compared in [218] to MiniBooNE data [30]. The overall agreement is quite satisfactory[10], better for neutrino induced reactions than for antineutrino ones. Shapes of the distributions of final state π^0's are affected by an interplay between pion FSI such as absorption and formation time effects, and turn out to agree significantly better with the data than those found in [184, 207–209].

[10] To describe the pion production on the nucleon, a simple theoretical model, that does not consider background terms, is used in [218]. Moreover, the coherent pion production is calculated using the Rein–Sehgal model [219], which is not appropriate at low energies (this will be discussed in detail in section 5.2).

Of course, the 'formation zone' could be adjusted to reproduce data. However, these kind of modifications of the FSI could be difficult to justify, as they might be in conflict with much other phenomenology; it might hide our ignorance on the relevant dynamics. Even when they could help in reproducing some observables, if we lack a correct understanding of the physical mechanisms responsible for them, they might lead to wrong predictions for other observables sensible to other kinematics, dynamical mechanisms or nuclear corrections.

In this respect, the DUET experiment at TRIUMF, that uses the PIAνO detector [220], will provide quite valuable information in the future. Pion FSI models were tuned to available pion–nucleus data measured in the 1980s and affected by large uncertainties. The objective of the experiment is to measure π absorption and π charge exchange cross section with $\sim$10% and $\sim$20% accuracy, respectively.

Another useful MiniBooNE measurement was the ratio of CC1π^+-like (one pion in the final state) to CCQE-like (no pions in the final state) cross sections on CH_2 , as a function of the neutrino energy. This ratio was reported in [221] with an accuracy of around 10% (The K2K Collaboration has also measured this ratio [222], but the reported errors are much larger than those in the MiniBooNE data). This ratio becomes quite interesting because of the apparent data/MC normalization discrepancy for the CC1π^+ production channel at MiniBooNE [28], since it would be free from the overall flux normalization uncertainty. However, it is not a directly observable quantity, because in the experimental analysis it is necessary to reconstruct the neutrino energy. This measurement puts constraints on the theoretical models which include QE, Δ excitation and MEC/2p2h dynamics. In addition, the theoretical approaches need to include FSI effects as well. There exist three theoretical estimates of this ratio: (i) The GiBUU group found a significant discrepancy between the model and the MiniBooNE data, its prediction being smaller than the experimental ratio [210], (ii) NuWro MC results [186] are slightly below the MiniBooNE data for larger neutrino energies and (iii) the Aligarh group [223] predictions[11] agree with MiniBooNE measurement for $E_\nu < 1$ GeV and are below MiniBooNE data for larger neutrino energies.

However, one cannot extract any robust conclusion from these comparisons, since none of the theoretical estimates for the CCQE-like cross section include multinucleon mechanisms (2p2h) or properly compute RPA corrections. Moreover, as discussed in section 3.3.1, because of the 2p2h effects, the algorithm used to reconstruct the neutrino energy is not adequate when dealing with QE-like events, and a distortion of the total flux-unfolded cross section shape is produced (redistribution of strength from high to low energies, which gives rise to a sizable excess (deficit) of low (high) energy neutrinos in QE-like distributions) [155].

Forthcoming T2K and MINERνA pion production data will hopefully shed light on the existing puzzle originated by the large discrepancy between MiniBooNE pion production measurements and theoretical model predictions. It is worth noting that the GiBUU group has already studied pion production at the T2K and MINERνA experiments within its model [224, 225]. It is found that pion absorption is less pronounced at the MINERνA energies than

[11] In what concerns the initial interaction, this approach treats the Δ inside of the nucleus in a way that has many resemblances to the scheme of [184] and also accounts for FSI effects by means of a cascade algorithm. However, the cascade uses free space $\pi N \to \pi' N'$ cross sections instead of cross sections appropriately modified in the nuclear medium. Moreover, the model did not include contributions from the non-resonant background and from higher resonances, and includes an unexpectedly large π^+ coherent production cross section.

for MiniBooNE/T2K experiments. This is attributed in [225] to a minimum in the πN cross section at around 0.7 GeV pion kinetic energy.

4.4. Other inelastic processes

4.4.1. Weak K and $\bar{K}$ production. Although in the few-GeV region, the attention has been focused on pion production because it is the inelastic process with the largest cross section, (anti)kaon, and strangeness production in general, are also relevant. In particular, kaon production induced by atmospheric neutrinos is a potential background for the proton decay mode with a kaon in the final state ($p \to \bar{\nu}\, K^+$), which has large branching ratios in different theories beyond the Standard Model. Several neutrino oscillation experiments like MINOS, NOνA, T2K or LBNE have or will have fluxes that extend to energies where strange particles can be produced. Therefore, a better understanding of these reactions is important to reduce systematic errors, which will be the dominant ones in the era of precise neutrino oscillation measurements. Such a progress is even more desirable for experiments running in the $\bar{\nu}$ mode as no measurements of strange-particle production cross sections exist with $\bar{\nu}$ fluxes.

The main reaction channels at these energies are single K production ($\Delta S = 1$)

$$\nu_l\, p \to l^-\, K^+\, p, \tag{51}$$

$$\nu_l\, n \to l^-\, K^+\, n, \tag{52}$$

$$\nu_l\, n \to l^-\, K^0\, p, \tag{53}$$

single $\bar{K}$ production ($\Delta S = -1$)

$$\bar{\nu}_l\, p \to l^+\, K^-\, p, \tag{54}$$

$$\bar{\nu}_l\, n \to l^+\, K^-\, n, \tag{55}$$

$$\bar{\nu}_l\, p \to l^+\, \bar{K}^0\, n, \tag{56}$$

and associated strangeness production ($\Delta S = 0$)

$$\nu_l\, n \to l^-\, K^+ \left(\Lambda,\, \Sigma^0\right), \tag{57}$$

$$\nu_l\, n \to l^-\, K^0\, \Sigma^+, \tag{58}$$

$$\nu_l\, p \to l^-\, K^+\, \Sigma^+, \tag{59}$$

$$\bar{\nu}_l\, p \to l^+\, K^+\, \Sigma^-, \tag{60}$$

$$\bar{\nu}_l\, p \to l^+\, K^0 \left(\Lambda,\, \Sigma^0\right), \tag{61}$$

$$\bar{\nu}_l\, n \to l^+\, K^0\, \Sigma^-, \tag{62}$$

$$(\nu_l,\, \bar{\nu}_l)\, p \to (\nu_l,\, \bar{\nu}_l)\, K^+ \left(\Lambda,\, \Sigma^0\right), \tag{63}$$

$$(\nu_l,\, \bar{\nu}_l)\, n \to (\nu_l,\, \bar{\nu}_l)\, K^+\, \Sigma^-, \tag{64}$$

$$(\nu_l \bar{\nu}_l) n \to (\nu_l,\, \bar{\nu}_l)\, K^0 \left(\Lambda,\, \Sigma^0\right), \tag{65}$$

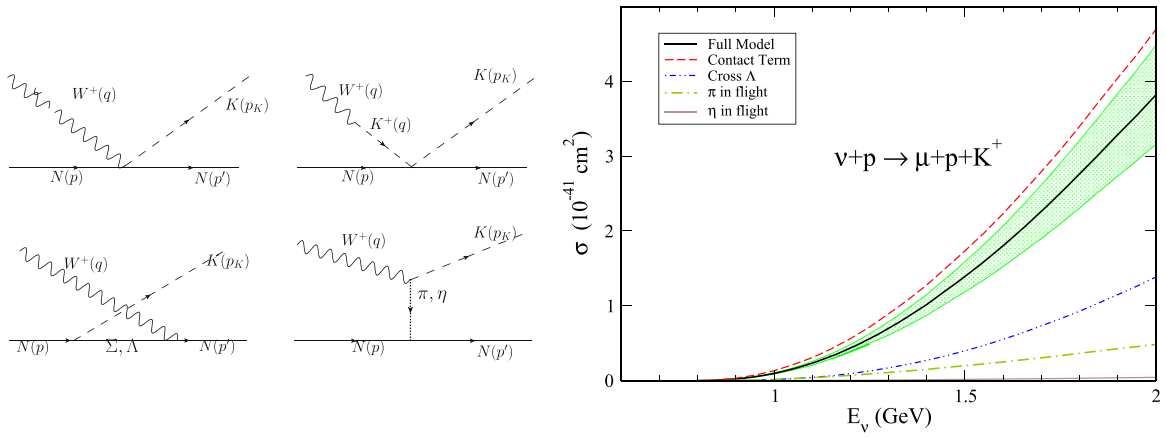

Figure 16. Left panel: Feynman diagrams for $W^+N \to NK$ [227]. From the upper left corner in clockwise order: contact term (CT), kaon pole (KP), π and η in flight (πP, ηP) and u-channel hyperon exchange (CrΣ, CrΛ) terms. Right panel: integrated cross-section for the reaction of equation (51) with $l = \mu$ and the contribution of different terms singled out. The band corresponds to a 10% error in M_F [227].

$$(\nu_l, \bar{\nu}_l)\, p \to (\nu_l, \bar{\nu}_l)\, K^0\, \Sigma^+. \tag{66}$$

Associated strangeness production is the dominant process but it has a high threshold because both a kaon and a hyperon are produced. This leaves single kaon production as the main source of kaons at low energies, in spite of being Cabibbo suppressed. Owing to the absence of flavor-changing NC in the Standard Model, $\Delta S = \pm 1$ reactions proceed via CC interactions. Channels (49), (50), (52) and (53) make coherent K ($\bar{K}$) production in nuclei induced by $\nu(\bar{\nu})$ possible. These are discussed in section 5.3.

After the early work of [226], new theoretical developments on $\Delta S = 1$ reactions (49)–(51) have become available only recently [227]. In the description of [227], the reaction mechanisms are derived from a Lagrangian that implements the QCD chiral symmetry breaking pattern. Although the vertices are SU(3) symmetric, this flavor symmetry is broken in the amplitudes by the physical hadron masses. The resulting set of diagrams for the hadronic currents are shown in figure 16 and are referred to as contact (CT), kaon pole (KP), u-channel crossed Σ (Cr Σ) and Λ (CrΛ), pion in flight (πP) and eta in flight (ηP) terms. The absence of $S = 1$ baryons implies that there are no s-channel amplitudes. The structure of these currents and the corresponding cross sections at threshold are fully determined by chiral symmetry, with couplings fixed from nucleon and hyperon semileptonic decays and pion decay. Some corrections of next order, whose couplings are constrained by measured values of nucleon magnetic moments, have also been included. PCAC is implemented for the axial part of the currents. As the dependence of the different terms of the hadronic current on the momentum transferred to the nucleon is poorly known, if at all, the authors of [227] adopt a global dipole form factor

$$F\left(q^2\right) = \left(1 - \frac{q^2}{M_F^2}\right)^{-2}, \tag{67}$$

assuming $M_F = 1$ GeV.

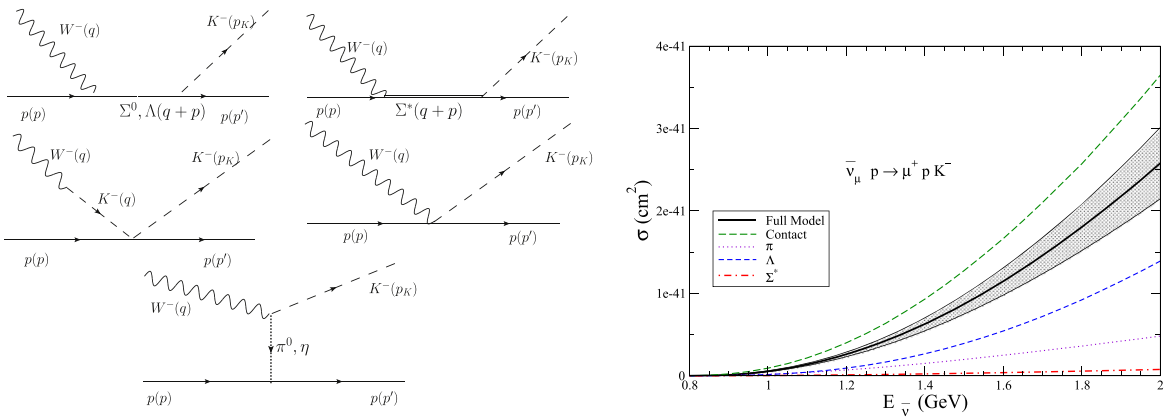

Figure 17. In the left panel the Feynman diagrams for $W^-N \to N\bar{K}$ [228] are shown. First row: s-channel Σ, Λ and Σ^* exchange terms; second row: contact (CT) and kaon pole (KP) terms; last row: π and η in flight (πP, ηP) terms. The right panel shows the cross section for the reaction of equation (54) with $l = \mu$ as a function of the neutrino energy together with the isolated contributions from different mechanisms. The band corresponds to a 10% error around $M_F = 1$ GeV [228].

The results obtained in [227] for the integrated cross sections are shown in figure 16 for the reaction of equation (49). In the validity region assumed for the model ($E_\nu \leqslant 2$ GeV), the CT amplitude, not included in [226], is dominant and interferes destructively with the rest. The KP term is negligible, while the CrΣ contribution is much smaller than the CrΛ one because of the much smaller coupling in the strong vertex. The cross section of the reaction of equation (51) has similar size and exhibits much the same features. Instead, the reaction of equation (50) has a 4–5 times smaller cross section almost completely determined by the CT.

For the $\Delta S = -1$ reactions (52)–(54) close to threshold, the relevant mechanisms can also be obtained from chiral SU(3) Lagrangians (see figure 17). The CT, KP, πP and ηP contributions to the hadronic current are present but now the Λ and Σ hyperons appear in the s-channel. As for K^+ production, the structure of these amplitudes close to threshold is fully defined by chiral symmetry, with the couplings determined from semileptonic decays. In [228], the q^2 dependence of equation (65) was also adopted. In pion production reactions, the excitation of the spin-3/2 $\Delta(1232)$ plays a dominant role at relatively low excitation energies (∼200 MeV). Therefore, the corresponding state of the baryon decuplet $\Sigma^*(1385)$ that couples to $N\bar{K}$ should be considered here. The vector and axial $N - \Sigma^*$ form factors, which are not known, were related to the better known $N - \Delta(1232)$ ones using SU(3) rotations [228].

As can be seen in figure 17, the CT provides the largest contribution to the cross section. The small impact of the Σ^* resonance, contrasting with the dominance of the Δ in the pion case, can be explained by the fact that the Σ^* is below the kaon production threshold [228]. The other two channels (53) and (54) have similar cross sections [228]. It should be mentioned that while the weak K production model described above represents a theoretically solid prediction at threshold, the situation is different for the $\bar{K}$ channels. The presence of a baryon resonance, $\Lambda(1405)$, just below the $\bar{K}N$ threshold might have a non-negligible influence on the weak $\bar{K}$ production cross sections that needs to be investigated.

The same formalism has been applied to the study of CC associated strangeness production reactions, equations (55)–(60), at low (anti)neutrino energies. Again, it is found that the CT vertices, present in the leading order chiral Lagrangian and ignored in previous calculations [229, 230], are responsible for most of the cross section [231, 232]. Channels (56) and (58) where CTs are not allowed (at leading order) show relatively smaller cross sections. However, we must point out there may be important resonant contributions to the $\Delta S = 0$ processes, such as the $N^*(1535)$ below the $K\Lambda$ threshold, which have not been considered. This is known to be the case for associated strangeness photoproduction. Recently, a model that describes associated strangeness production induced by pions and photons has been used to predict the corresponding reactions induced by neutrinos in the forward direction by applying PCAC [197].

The dynamics of strange-particle production in nuclear targets is considerably more involved. The interaction of kaons with the nuclear medium is not so strong due to the absence of baryon resonances but QE and charge-exchange scattering are present. Furthermore, as the energy increases, inelastic processes like secondary kaon production $K\,N \to K'\,N'\pi$ become sizable. Instead, the $\bar{K}$ interaction with the nucleons is strong starting from very low energies due to the presence of the $\Lambda(1405)$; $\bar{K}$ can disappear leading to hyperons via $\bar{K}\,N \to \pi\,Y, \eta\,Y$ with $Y = \Lambda,\ \Sigma$. Due to FSI, (anti)kaons can be produced in secondary collisions such as $\pi\,N \to Y\,K$, $K\,\bar{K}\,N'$ and $N\,N \to N\,Y\,K$. Indeed, the number of low-energy K produced in neutrino–nucleus collisions is actually enhanced by FSI; in the case of $\bar{K}$, secondary interactions tend to compensate their absorption [233]. For this reason, from the ongoing exclusive strangeness production measurements on nuclear targets at MINERνA, it will be very hard to extract the corresponding reactions on the nucleon, unless a very reliable modeling of the nuclear dynamics is implemented [233].

4.4.2. NC photon emission. One of the possible inelastic reaction channels is photon emission induced by NC interactions (NCγ), which can take place on single nucleons

$$\nu(\bar{\nu})N \to \nu(\bar{\nu})\gamma\,N, \tag{68}$$

or on nuclear targets

$$\nu(\bar{\nu})A \to \nu(\bar{\nu})\gamma\,X, \tag{69}$$

$$\nu(\bar{\nu})A \to \nu(\bar{\nu})\gamma\,A, \tag{70}$$

$$\nu(\bar{\nu})A \to \nu(\bar{\nu})A'^{*}N \to \nu(\bar{\nu})\,\gamma\,A'N \tag{71}$$

via incoherent (equation (67)) or coherent (equation (68)) scattering. It is also possible that, after nucleon knockout, the residual excited nucleus decays emitting γ rays (equation (69)). This mechanism has been identified as an important source of low ($\sim$10 MeV) photons for neutrinos of intermediate energies, whose main reaction mechanism is QE scattering [234].

Weak photon emission has a small cross section compared, for example, with pion production. Indeed, while pion production involves predominantly two weak vertices followed by a strong (resonant) decay, in NCγ one has a much weaker electromagnetic vertex instead of the strong one. In spite of this, NCγ turns out to be one of the largest backgrounds in appearance $\nu_\mu \to \nu_e(\bar{\nu}_\mu \to \bar{\nu}_e)$ experiments when photons with hundreds of MeV energies are

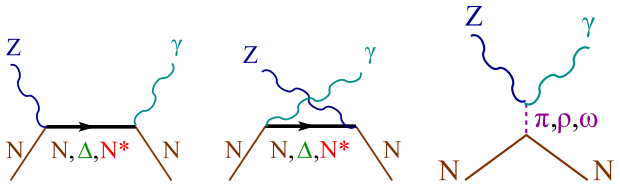

Figure 18. Feynman diagrams for NC photon emission considered in the literature. The first two diagrams stand for direct and crossed baryon pole terms with nucleons and resonances in the intermediate state: *BP* and *CBP* with $B = N$, $\Delta(1232)$, $N^*(1440)$, $N^*(1520)$, $N^*(1535)$. The third diagram represents t-channel meson exchange contributions mEx with $m = \pi, \rho, \omega$.

misidentified as $e^{\mp}$ from CCQE scattering of $\nu_e\,(\bar{\nu}_e)$ in the detector. This was the case at MiniBooNE, where the photon background is estimated from the measured NCπ^0 rate assuming that it comes from radiative decay of weakly produced resonances, mainly $\Delta \to N\,\gamma$. The experiment has found an excess of events with respect to the predicted background in both ν and $\bar{\nu}$ modes. In the $\bar{\nu}$ mode, the data are consistent with $\bar{\nu}_\mu \to \bar{\nu}_e$ oscillations and have some overlap with a previous LSND result [32]. In contrast, the reconstructed neutrino-energy distribution (E_ν^{QE}) of e-like events in the ν mode is only marginally compatible with a two-neutrino oscillation model, showing an unexplained excess of events for $200 < E_\nu^{QE} < 475$ MeV [32, 235]. This puzzle triggered a theoretical interest in the NCγ processes as an important background to the MiniBooNE measurement, which was not directly constrained by data.

Theoretical models for the reaction of equation (66) in the few-GeV region have been developed in [236–238]. These calculations incorporate s- and u-channel amplitudes with nucleons and $\Delta(1232)$ in the intermediate state (see figure 18). The structure of nucleon pole terms, *NP* and *CNP*, at threshold is fully determined by the symmetries of the Standard Model. They are infrared divergent when the photon energy $E_\gamma \to 0$ but this becomes irrelevant when the experimental detection threshold ($E_\gamma > 140$ MeV in the case of MiniBooNE) is taken into account. The extension towards higher energy transfers required to make predictions for the neutrino cross sections is performed by the introduction of phenomenological parametrization of the weak and electromagnetic form factors. The same strategy has been followed for the ΔP and $C\Delta P$ terms. As can be seen in figure 19, where the NCγ cross sections for the different mechanisms according to the model of [238] are displayed, the $\Delta(1232)$ excitation followed by its radiative decay is the dominant mechanism. Heavier N^* resonances, $P_{11}(1440)$, $D_{13}(1520)$ and $S_{11}(1535)$, were included as intermediate states in [238]. The contribution from the $D_{13}(1520)$ on proton targets is sizable above $E_\nu \sim 1.5$ GeV. Instead, the other two N^* are negligible (see figure 19).

The pion pole (πEx) mechanism originates from the $Z^0\gamma\pi$ vertex, which is fixed by the axial anomaly of QCD. It is nominally of higher order [189] and, indeed, gives a very small contribution to the cross section as shown in the lower panels of figure 19. Other t-channel mechanisms from the exchange of vector (ρEx) and pseudoscalar (ωEx) mesons [236] arise from the anomaly-mediated $Z^0\gamma\rho$ and $Z^0\gamma\omega$ interactions [239]. Among them, the ωEx contribution is favored by the size of the couplings. In addition, the isoscalar nature of the ω

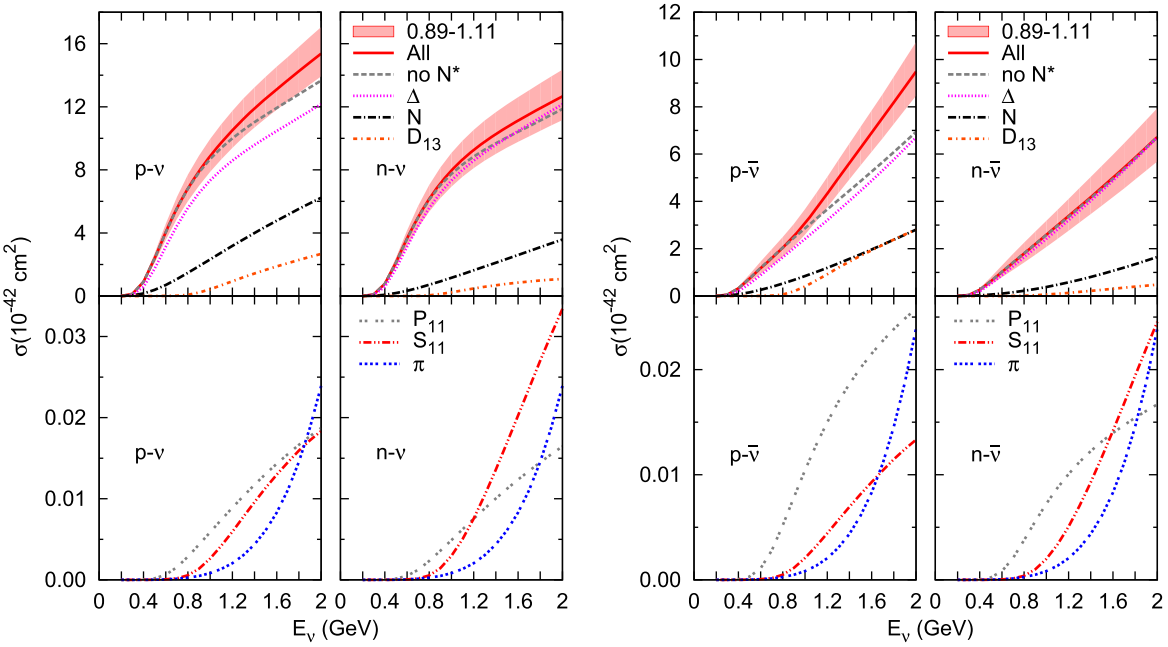

Figure 19. $\nu N \to \nu N\gamma$ (left) and $\bar{\nu}N \to \bar{\nu}N\gamma$ (right) cross sections on protons and neutrons as a function of the (anti)neutrino energy, obtained with the model of [238]. A cut of $E_\gamma \geqslant 140$ MeV in the phase space integrals has been applied. The error bands in the full-model results (solid lines) represent the uncertainty in the axial $N\Delta$ coupling $C_5^A(0) = 1.00 \pm 0.11$ according to the determination of [183]. The curves labeled N, Δ, D_{13}, P_{11} and S_{11} stand for the partial contributions of the *BP* and *CBP* mechanisms of figure 18; the label π corresponds to the πEx one. The lines labeled as 'no N^*' display the predictions without the N^* contributions.

meson makes the ωEx mechanism potentially interesting for the coherent scattering reaction of equation (68). This is discussed in section 5.4. The $Z^0\gamma\omega$ vertex has been revisited using a framework which incorporates vector mesons as composite gauge bosons of the spontaneously broken hidden local symmetry [240]. It is shown that this vertex arises from the homogeneous part of the general solution to the anomaly equation and is not fully determined by the anomaly; the corresponding free parameters are related to the $\omega \to \pi^0\,\gamma$ decay. Reference [189] assumes that the ρEx and ωEx mechanisms, taken from [236], saturate the low-energy constants in the contact terms, although it is emphasized that other sources are possible. The contribution of these contact terms, and of the ωEx in particular, to the NCγ cross section on the nucleon is very small at $E_\nu \leqslant 550$ MeV [189, 236], as expected from power counting arguments. The extension to higher energies requires the introduction of poorly understood form factors [236, 237]. The cross section from these mechanisms increases fast with energy. This rapid growth might be a concern for experiments at higher energies, or with a high-energy tail in the neutrino flux (like T2K), as a source of NCγ events and, therefore, unconstrained background. However, one should recall that this trend will be limited by unitarity bounds: in a realistic framework, these amplitudes will be modified by loop contributions and partially canceled by contact terms of even higher orders.

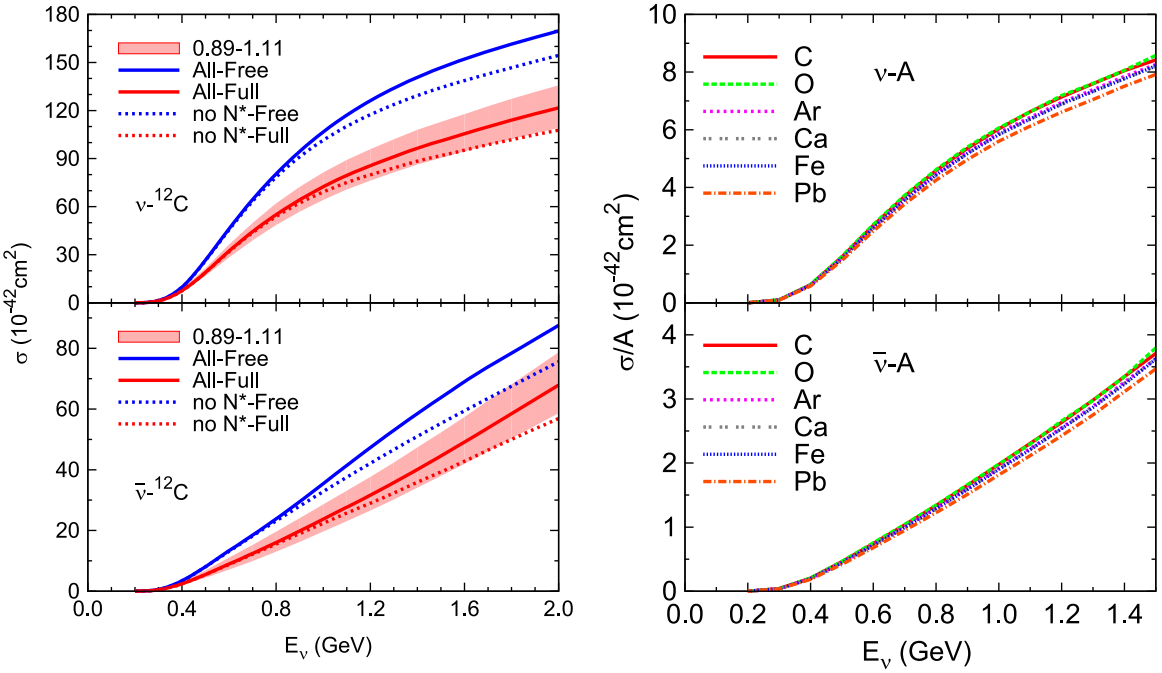

Figure 20. Left panel: neutrino (top) and antineutrino (bottom) incoherent NCγ cross sections on ^{12}C according to the model of [238]. All curves have been obtained with an $E_\gamma \geqslant 140$ MeV cut in the phase space. Solid lines stand for results from the complete model at the nucleon level, while the dotted lines display the predicted cross sections without the N^* contributions. Curves denoted as 'Free' (upper blue curves) do not include any nuclear correction: ($\sigma_A = Z\sigma_p + N\sigma_n$). Curves labeled as 'Full' (lower red curves) take into account Pauli blocking, Fermi motion and the in medium Δ resonance broadening. The error bands on the full model result show the uncertainty from the axial $N\Delta$ coupling ($C_5^A(0) = 1.00 \pm 0.11$). Right panel: results for different nuclei (^{12}C,^{16}O,^{40}Ar, ^{40}Ca,^{56}Fe and ^{208}Pb) divided by the number of nucleons [238].

The incoherent NCγ reaction, equation (67), on nuclear targets has been studied in [238, 241] using the R1FG approximation. The broadening of the Δ resonance in the medium has also been incorporated into the models using a spreading potential in [237, 241], while [238] uses the parametrization of the imaginary part of the in-medium Δ self-energy as a function of the local nuclear density derived in [213]. In the left panel of figure 20, the cross sections on ^{12}C obtained with the model of [238] are shown. It is clear that the neglect of nuclear medium corrections is a poor approximation. By taking into account Fermi motion and Pauli blocking, the cross section already goes down by more than 10%. With the full model the reduction is of the order of 30%. A similar net effect is obtained in [237]. However, the reduction quoted for the direct Δ mechanism is substantially larger for neutrinos (∼50%) but not for antineutrinos, which is hard to understand (see the comparison in figure (9) of [238] and the related discussion). The cross section shows an approximate scaling with the target mass (A), as can be seen in the right panel of figure 20. Nevertheless, the cross section is smaller for heavier nuclei, particularly ^{208}Pb.

The theoretical models outlined above have been used to calculate the NCγ events at MiniBooNE (including the coherent contribution described in section 5.4). With the model of [236] the number of these events were calculated to be twice as many as expected from the MiniBooNE *in situ* estimate [242]. The conclusion was that NCγ events give a significant contribution to the low-energy excess of e-like events. However, in [242] the nuclear target (^{12}C) was treated as an ensemble of nucleons, neglecting the important nuclear-medium corrections. Furthermore, an energy independent and rather high efficiency correction compared with the presently available figures [243] was assumed in the analysis. In contrast, the predictions based on the models of [237, 238] are compatible with the MiniBooNE determination in spite of the quantitative differences in these approaches [237, 244, 245]. One would then conclude that the NCγ reactions cannot explain the excess of e-like events at low E_ν^{QE} observed at MiniBooNE, which remains an open question.

5. Weak coherent processes at intermediate energies

5.1. Introduction

As discussed in section 4, neutrino-induced pion, photon and (anti)kaon production off nucleons and nuclei in the intermediate energy region is not only important for neutrino oscillation experiments but is also a source of relevant data on the structure of hadrons and especially of their axial properties. At intermediate energies, pions, antikaons or photons are mainly produced through resonance excitation and these reactions can be used to extract information on nucleon-to-resonance axial transition form factors. In reactions on nuclei, these outgoing particles can be produced incoherently or coherently. In the latter case the nucleus is left in its ground state in contrast with the incoherent case where it is either broken or left in some excited state. For instance, the CC coherent pion production (COHπ) reaction reads

$$\nu_l(k) + A_Z\big|_{gs}(p_A) \to l^-(k') + A_Z\big|_{gs}(p'_A) + \pi^+(k_\pi). \tag{72}$$

The same is true for the rest of the neutrino induced coherent channels reviewed in this section.

A proper understanding of the coherent processes is very important in the analysis of neutrino oscillation experiments. For instance, coherent π^0 or γ production by NC is among the most important ν_μ-induced backgrounds to experiments that measure $\nu_\mu \to \nu_e$ oscillations in the neutrino energy range around 1 GeV [235]. This is because NC γ or π^0 events can mimic ν_e signal events, since the electromagnetic showers instigated by electrons or positrons and photons are not distinguishable in the large Cherenkov tanks used as far detectors[12]. Similarly, coherent CC π^+ production is a background in ν_μ disappearance searches [246].

[12] In the case of π^0 production, the misidentification can occur when one of the two photons from the $\pi^0 \to \gamma\gamma$ decay is not detected. This might happen when the photon exits the detector before showering or does not have enough energy to initiate a shower.

Coherent reactions have smaller cross sections and are clearly more forward peaked than incoherent ones. Indeed, large momentum transfers to the nucleus are suppressed by the nuclear form factor (Fourier transform of the nuclear density), which takes its largest values when the lepton transferred ($\vec{q}$) and produced particle ($\vec{k}_{\rm coh} = \vec{k}_\pi, \vec{k}_\gamma, \vec{k}_K \cdots$) momenta are similar. Because the kinetic energy of the final nucleus is negligible, the energy of the outgoing particle, $k^0_{\rm coh}$, coincides, in a very good approximation, with the lepton transferred energy q^0. The limiting case $\vec{q} = \vec{k}_{\rm coh}$ would correspond to $q^2 = m^2$, being m the mass of the produced particle (photon, pion, kaon,...), which is not kinematically accessible (except for photon emission). Instead, $q^2 = 0$ can be reached for massless leptons in the strictly forward kinematics. In this case, the lepton tensor is such that

$$L^{(\nu,\bar{\nu})}_{\mu\sigma} \sim q_\mu q_\sigma, \tag{73}$$

and, because of CVC, its contraction with the vector part of the hadron tensor vanishes. This is the reason why the COHπ part of electron and photon induced reactions turned out to be a quite small fraction of the total inclusive nuclear absorption cross section [247, 248]. The largest differential cross sections in coherent particle production with electromagnetic probes arise in kinematics that optimize the product of the amplitude squared of the elementary process times the nuclear form factor. However, in weak processes, there is an axial part which is not suppressed for kinematics where $\vec{q}$ and $\vec{k}_{\rm coh}$ are almost equal (the exception being coherent photon emission, as discussed in section 5.4). Thus, the reduction induced by the nuclear form factor is less significant, and the relative contribution of the coherent production channel to the total cross section, larger. A similar scenario is encountered in some hadronic reactions such as $\left({}^3{\rm He}, {}^3{\rm H}\pi^+\right)$ in nuclei [249].

It is worth stressing the important role played by nuclear effects. The Δ (1232) resonance, which is the dominant intermediate state in coherent photon and pion production, is strongly modified in the nuclear medium. In addition, the pion and (anti)kaon outgoing wave functions are distorted inside the nuclei. This distortion is particularly strong in the case of pions, owing to the presence of the Δ (1232) resonance in the pion–nucleus OP and rather mild for kaons due to the absence of KN resonances. Thus, these processes are quite sensitive to the pion or (anti) kaon dynamics in nuclei. We should also mention the non-locality in the Δ propagation which is often neglected in the microscopic models. The effects of this approximation were discussed in [250] in the context of COHπ reactions, without considering the modification of Δ properties in the nucleus and the distortion of the outgoing pion. Sizable effects (reductions as large as a factor of two at $E_\nu \sim 500$ MeV) were claimed in [250], which might question the validity of the local Δ propagation. In the more realistic description of [251], the non-locality is preserved for the Δ kinetic term in a linearized version of the Δ propagator but, at the same time, a local approximation for vertices and Δ self-energy have been adopted. Nevertheless, the mismatch between the non-local recoil effects and the local approximation is likely to be minimized by the fact that the parameters in the Δ self-energy are adjusted to describe pion–nucleus scattering data with the same model. The problem of non-locality should be further investigated, performing a realistic calculation including full nuclear effects, and disentangling up to what extent some of the non-local effects are effectively accounted for in the empirical Δ-nucleus OP,

usually tested/fitted in pion–nucleus reactions, employed to describe the dynamics of the Δ resonance in the nuclear environment.

5.2. CC and NC coherent π production reactions

Models for COHπ can be classified as PCAC or microscopic. The dominance of the axial contributions at $q^2 = 0$ has been extensively exploited, through PCAC, to relate[13] the neutrino COHπ cross sections [$\sigma_{\rm COH}\left(\nu + A_Z|_{gs} \to \nu + A_Z|_{gs} + \pi^0\right)$, $\sigma_{\rm COH}\left(\nu + A_Z|_{gs} \to \ell^- + A_Z|_{gs} + \pi^+\right)$] with the pion–nucleus elastic ones [$\sigma\left(\pi^0 + A_Z|_{gs} \to \pi^0 + A_Z|_{gs}\right)$, $\sigma\left(\pi^+ + A_Z|_{gs} \to \pi^+ + A_Z|_{gs}\right)$] [193, 219, 252–254], and similarly for antineutrino induced reactions. On the other hand, microscopic approaches [124, 211, 212, 251, 255–258] start from a model for weak pion production on the nucleon, and perform a coherent sum over all nucleon contributions, taking into account modifications of the elementary amplitudes in the nuclear medium. Since the nucleus remains in its ground state, a quantum treatment of pion distortion becomes possible. In microscopic COHπ models, the hadronic and nuclear physics input is the same employed to describe the related incoherent pion production process. The main drawbacks of this kind of approach are: (i) the available descriptions are restricted to the kinematic region where pion production is dominated by the excitation of the $\Delta\,(1232)$ resonance and cannot be easily extended to higher energies, and (ii) these models are also technically more involved than PCAC ones and difficult to implement in MC simulations.

High neutrino energy ($E_\nu \gtrsim 2$ GeV) COHπ production data (including the recent NOMAD measurement of the NC COHπ^0 cross section [36]) were successfully explained with the PCAC based model of [219]. The experimental investigation at $E_\nu \sim 1$ GeV started only recently. Contrary to PCAC based models expectations, the K2K Collaboration obtained only an upper bound for CC COHπ at $\left\langle E_\nu \right\rangle = 1.2$ GeV [19]. This unexpected result triggered a renewed theoretical interest in this process. The present experimental situation is puzzling because the upper limits obtained by K2K [19] and SciBooNE [43] coexist with measurements of NC COHπ^0 (MiniBooNE [30] and SciBooNE [44]) with a presumably larger cross section. Indeed, SciBooNE reported [44] a value

$$\frac{\sigma_{\rm CC-COH\pi^+}}{\sigma_{\rm NC-COH\pi^0}} = 0.14^{+0.30}_{-0.28} \tag{75}$$

[13] At $q^2 = 0$ only the axial current survives, being its contribution proportional to its divergence $\left(q_\mu A^\mu\right)$. The relation with the pion–nucleus elastic differential cross section follows from PCAC

$$\partial_\mu A^\mu(x) \sim f_\pi m_\pi^2 \pi(x) \tag{74}$$

with f_π the pion decay constant and $\pi(x)$ a pion field. In addition, one should assume dominance of the $\vec{q} = \vec{k}_\pi$ kinematics (thanks to the nuclear form factor) and neglect some off-shell effects since $q^2 = 0 \neq m_\pi^2$.

for carbon and an average neutrino energy in the 0.8 GeV region. This result is difficult to accommodate with the relation $\sigma_{\mathrm{CC-COH}\pi^+}/\sigma_{\mathrm{NC-COH}\pi^0} = 2$ which, up to kinematic corrections, follows from PCAC and isospin invariance in the case of isoscalar nuclei. There exists a general consensus within the theory community, that though this ratio in carbon at these energies could deviate from 2, it is in any case expected to be close to 1.5. This is more than 4 σ far from the SciBooNE measurement.

PCAC was used by Rein and Sehgal [219] to study the COHπ^0 reaction, extending it to $q^2 \neq 0$ by means of a phenomenological form factor. Subsequently, the model for the CC reaction has been upgraded [193] to include lepton mass effects important for low E_ν studies. This simple model is a reference in the field of neutrino interactions and has been adopted by the MC simulations employed in neutrino experiments[14]. However in the $E_\nu < 2$ GeV region, and for light nuclei, there are drawbacks that render the model inaccurate [211, 259]. Far from the $q^2 = 0$ kinematic point, PCAC models cannot be safely used to determine the angular distribution of the outgoing pions. Terms that vanish at $q^2 = 0$, and that are not considered in PCAC based models, provide much more forward peaked pion angular distributions [259]. (We will discuss this in detail below, see figure 21). For neutrino energies above 2 GeV, the involved momenta, in most of the available phase space, are sufficiently large to guarantee that only kinematics close to the $\vec{q} = \vec{k}_{\mathrm{coh}}$ configuration lead to non totally-negligible values of the nuclear form factor, making the $q^2 = 0$ approximation quite appropriate. Hence, PCAC models provide accurate predictions of neutrino COH π cross sections for high neutrino energies. However, for lower neutrino energies, these models overestimate both the CC and NC total coherent cross sections as compared to the results obtained in more realistic microscopical models.

Within microscopic models there are still, in principle, various approaches e.g. due to differences in the treatment of the non-resonant background. A common assumption is that the reaction proceeds solely via the Δ excitation [124, 255–256]. Non-resonant contributions required by chiral symmetry at threshold have been also included in [211, 212, 257] using the model for the weak pion production off the nucleon of [182, 183], though they turn out to be very small because of large cancellations, some of them exact for isospin symmetric nuclei. The absolute normalization of the predicted cross section depends on the adopted value of the dominant axial $N \to \Delta$ form factor $C_5^A(0)$, as the process is dominated in large extent by the axial part of the weak current (central values for the total cross sections may suffer by some

[14] An important improvement [259–261] in these models is the use of a better input for the elastic $\pi + A_Z|_{gs} \to \pi + A_Z|_{gs}$ angular differential cross section than that employed in the Rein and Sehgal model [219]. There, this distribution was approximated by the forward cross section modulated by the nuclear form factor and an angular-independent attenuation factor that should take into account effects of the outgoing pion absorption in the nucleus. As a result in [260, 261], and using experimental information on the angular dependence of the elastic pion–nucleus cross section, the predicted COHπ cross section became reduced by a factor of 2–3 for neutrino energies around 1 GeV and for light nuclei in the carbon region. Apart from the obvious limitation coming from the lack of experimental data for many pion energies and nuclei, it could be also argued that because of the strong distortion of the incoming pion in the on-shell elastic pion–nucleus process, one cannot directly relate the amplitude of the latter reaction to that of pion production induced by a weak current (more details can be found in [259]).

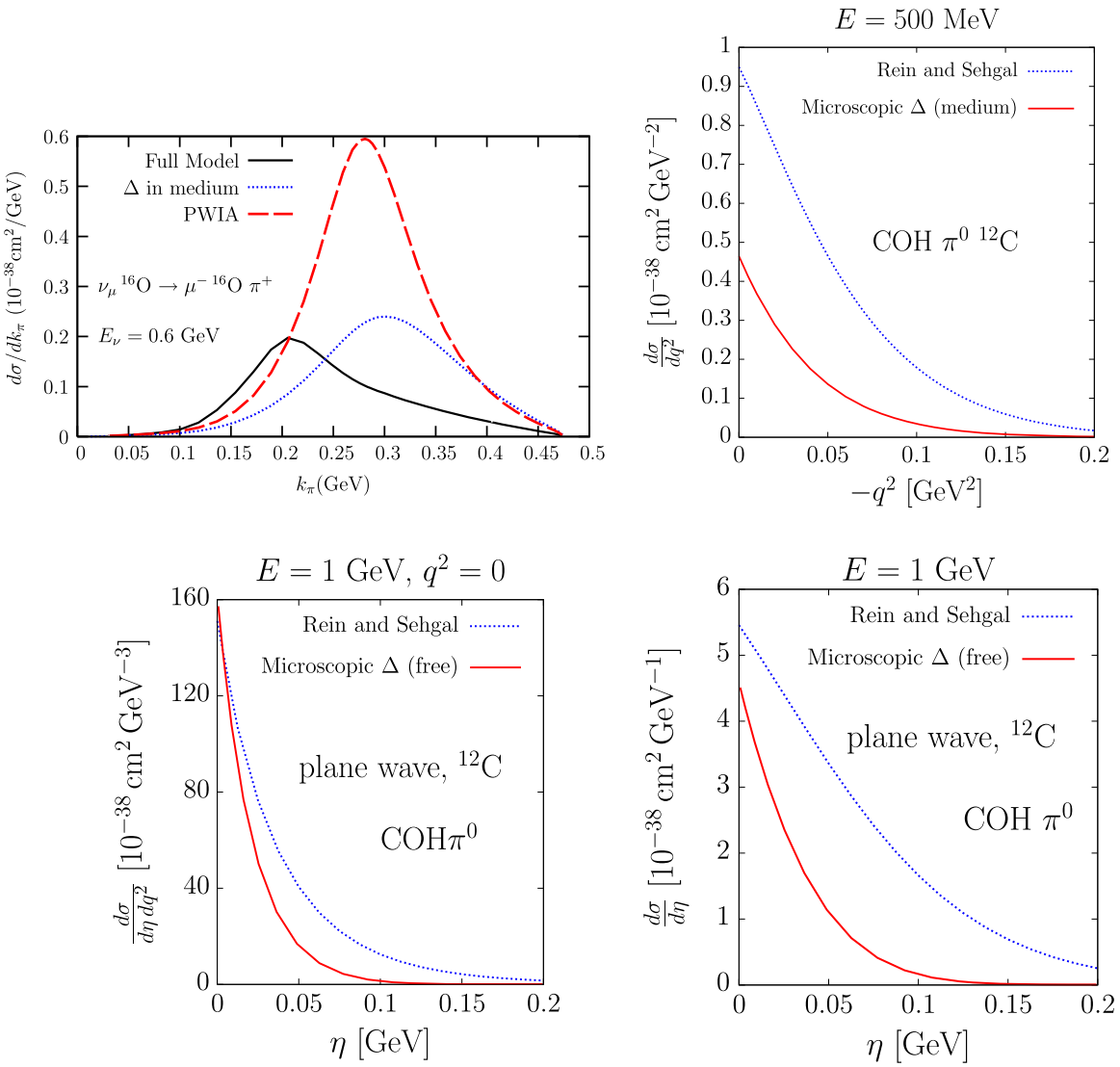

Figure 21. Laboratory frame COHπ differential cross section results from the microscopic Δ and the PCAC Rein and Sehgal models of [211] and [219], respectively. The variable η is defined as $E_\pi\left(1 - \cos\theta_\pi\right)$, with the pion angle defined with respect the incoming neutrino momentum. In the right top panel and in the bottom panels, the microscopic Δ contribution is calculated following [211], but using $C_5^A\,(0) = 1.2$.

20–30% uncertainty), while differential cross sections do not appreciably change their shape [212].

In figure 21, we show some results at low and intermediate neutrino energies from the microscopic Δ-hole and the PCAC Rein and Sehgal models of [211] and [219], respectively. The scheme of [256, 257] is quite similar to that employed in [211] and leads to qualitatively similar results, while the approach of [255], although less sophisticated in the treatment of the distortion of the outgoing pion waves, makes use of the same model to account for the Δ properties in the nuclear medium. The importance of the nuclear medium effects is stressed in the top left panel of figure 21. To this end, different predictions for the pion momentum

differential cross section are displayed [211]. The long-dashed line (in red) has been calculated using planes waves for the outgoing pion and without including any in-medium correction for the Δ. Results with Δ nuclear medium effects are shown by the dotted line (in blue). The full model calculation of [211] including medium effects on the Δ and the distortion of the outgoing pion wave function[15] is shown by the solid line (in black). We can see the in-medium modifications of the Δ properties produce a strong reduction and broadening of the peak. Pion distortion further decreases the cross section and moves the maximum to lower energies.

Pion angular and q^2 distributions are displayed in the other three panels of figure 21, where the results from a microscopic calculation following [211], but neglecting non-resonant background terms and using $C_5^A(0) = 1.2$, is compared with the predictions of the PCAC Rein–Sehgal model [219]. Outgoing pion distortion is only included in the right top panel, where the modifications of the Δ properties in the nuclear medium are also taken into account within the microscopical approach. In the bottom panels, plane waves for the outgoing pion and a free Δ resonance were employed. From the figure, we can conclude:

1. The Rein–Sehgal model predicts much larger and wider q^2 differential cross sections. As mentioned above, this is mainly due to the poor approximation assumed in this model for the elastic $\pi + A_Z|_{gs} \to \pi + A_Z|_{gs}$ angular differential cross section. The effects of this approximation decrease with the neutrino energy and atomic number, but they are still important for $E_\nu \sim 1.5 - 2$ GeV in a medium sized nucleus like calcium [259].
2. Regarding the outgoing pion distributions, the microscopic calculation is much more peaked around $\eta = E_\pi\left(1 - \cos\theta_\pi\right) = 0$ than the Rein–Sehgal model results, especially far from $q^2 = 0$. Terms that vanish at $q^2 = 0$, and that are not considered in PCAC based models, provide much more forward peaked pion angular distributions. This is also true for results obtained with pion distortion [259].

Finally we briefly review other approaches. The model of [258] starts from Lorentz-covariant effective field theories with nucleon, pion, $\Delta(1232)$ but also scalar (σ) and vector (ρ, ω) mesons as the relevant degrees of freedom, and exhibit a nonlinear realization of (approximate) $SU(2)_L \otimes SU(2)_R$ chiral symmetry. This is the same scheme as that employed in [189] for the neutrino-production of pions from nucleons. Special attention is paid to the power counting, which is shown to be valid only for quite low neutrino energies below 550 MeV. On the other hand, the approach of [124] shares many of the ingredients of previous models (in-medium Δ modification, effective Δ-hole interactions) but there, the coherent cross section is related to the coherent part of the nuclear response (mostly longitudinal). This response is obtained within the RPA approximation when the intermediate pion is placed on the mass shell and thus, some RPA corrections driven by short distance dynamics in the spin–isospin longitudinal channel are neglected. In the forward direction, the authors of [124] explicitly relate their forward neutrino coherent cross section to the elastic cross section of physical pions, as predicted by Adler's theorem [260], thus making contact with the PCAC based models

[15] The outgoing pion wave function is obtained in [211], as in [212, 256, 257], by solving the Klein–Gordon equation with a non-local pion–nucleus optical potential, based on the Δ-hole model plus some other low energy terms, that successfully describes the interaction of pions with nuclei at low and intermediate energies. This is an improvement with respect to the simpler eikonal approximation used for example in [255].

mentioned above (actually the results of [124] agree quite well, see [137], with those found in [261, 262] that use the elastic differential pion-carbon data). This infinite nuclear matter approach derived in [124] uses plain (undistorted) pion wave-functions. In spite of this, the obtained COHπ cross sections do not differ much [137] from those obtained with the microscopic models addressed above.

A different microscopic COHπ model is derived in [251] starting from a dynamical model in coupled channels, where the bare $N\Delta$ transition from a constituent quark model is renormalized by meson clouds. Pion distortion and Δ spreading potential effects are also taken into account. The free parameters in the spreading potential and pion–nucleus OP are fitted to pion–nucleus elastic scattering data. The results of this approach reasonably agree with those found in [211, 212] (see figures 8 and 9 of [137]).

To conclude, we stress once more that all microscopical theoretical models, though they lead to different cross sections, predict a value for the ratio $\sigma_{\mathrm{CC-COH}\pi^+}/\sigma_{\mathrm{NC-COH}\pi^0}$ in carbon that is always around 1.5 for $E_\nu \sim 0.8$ GeV, which is in clear contradiction with the SciBooNE measurement ($0.14^{+0.30}_{-0.28}$). This becomes an open problem and a challenge for both theory and experimental communities.

5.3. CC coherent kaon and antikaon production reactions

Here we briefly discuss the coherent production of charged kaons. Namely, we consider the $\Delta S = \pm 1$, Cabibbo suppressed, weak strangeness production reactions

$$\begin{aligned} \nu_l(k) + A_Z\big|_{gs}(p_A) &\to l^-(k') + A_Z\big|_{gs}(p'_A) + K^+(k_K), \\ \bar{\nu}_l(k) + A_Z\big|_{gs}(p_A) &\to l^+(k') + A_Z\big|_{gs}(p'_A) + K^-(k_K). \end{aligned} \tag{76}$$

These reactions have been theoretically studied in the recent work of [263] using a microscopic approach along the lines of the COHπ study of [211] described above. At the nucleon level, the model of [227, 264], presented in section 4.4.1, was implemented. The distortion of the outgoing kaons is treated in a quantum-mechanical way by solving the Klein–Gordon equation with realistic OPs accounting for the (very different) K and $\bar{K}$ interactions in the nuclear medium.

The resulting cross sections for incident muon neutrinos of 1–2 GeV are small, with cross sections per nucleon much smaller than the corresponding ones on free nucleons. This can be explained by the rather large momentum transferred to the nucleus (due to the large value of the kaon mass compared to the typical kaon momenta) which reduces drastically the nuclear form factors. At these large momentum transfers, the nuclear form factors depend strongly on the details of the proton and neutron density distributions. Angular kaon and lepton momentum distributions are forward peaked, as is normally the case in coherent processes. The cross section dependence on the atomic (Z) and mass numbers (A) of the target nuclei is shown in figure 22 for 1 GeV (anti)neutrinos. The isospin factors of the dominant CT mechanisms (see figures 16 and 17) suggest a quadratic dependence of the cross section with (A+Z) but no significant enhancement for heavy nuclei is observed, even if the distortion is neglected. To understand this, one should recall that heavier nuclei have narrower form factors, which causes a larger suppression at high momentum transfers. The error-bars in the full-model results represent the uncertainties in the model. The errors in the proton and neutron density

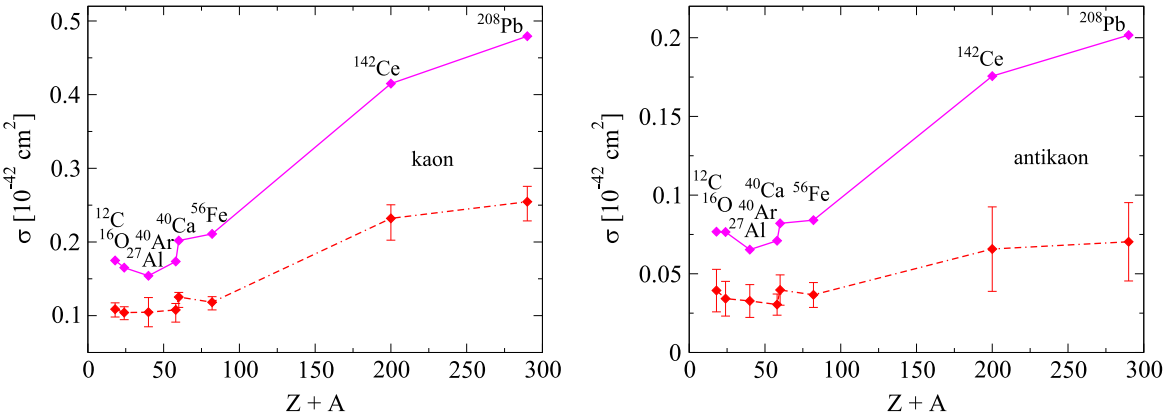

Figure 22. Predictions from the model of [263] for the coherent $K^{\pm}$ production cross-sections in several targets at an incident (anti)neutrino energy of 1 GeV. The solid (dashed) lines are obtained without (with) kaon distortion.

distributions, as well as a 10% one in M_F (equation (65)), accounting for the uncertainty in the elementary production model, have been propagated to the final results. In the case of $\bar{K}$ production, the uncertainty in the K^- distortion, which turns out to be the major error source, has also been estimated [263].

At higher energies, where the present model is not directly applicable, larger kaon momenta are present so that the suppressing role of the kaon mass is less important. A fast increase of the cross section is therefore expected. In view of this, measuring this reaction at MINERνA would be quite interesting.

5.4. NC coherent γ production reactions

The coherent contribution (NC COH γ), equation (68), is an important ingredient in a realistic description of NC photon emission on nuclear targets. At high energies, it was firstly studied in the early eighties [265, 266]. A discussion about these works can be found in section 5.5 of [236]. Here, we focus on the intermediate energy region, of relevance for the MiniBooNE and T2K experiments. At these energies, there exist three recent theoretical calculations of this reaction channel. The model of [236] mostly ignores nuclear corrections. The nucleus is treated as a scalar particle, including a nuclear form factor to ensure that the coherence is restricted to low-momentum transfers. The microscopical approaches of [258] and [238] are more robust and rely on the same formalism and approximations used to study COH π processes [211, 258]. In [238], the NCγ model on the nucleon is directly applied by summing the different amplitudes coherently. The total cross section is clearly dominated by the Δ (1232), with small corrections from D_{13} (1520) excitation (see figure 11 of [238]). Nucleon-pole contributions are negligible because the coherent kinematics favors a strong cancellation between the direct and crossed terms. The πEx terms vanish exactly for isospin symmetric nuclei because amplitudes for protons and neutrons cancel with each other. The results from the $\Delta P + C\Delta P + NP + CNP$ part of the model of [237, 258] are within the uncertainty band of those in [238] up to (anti) neutrino energies of 1.4–1.5 GeV.

Unlike π and ρ t-channel terms, the coherent contribution of the ωEx does not vanish for symmetric nuclei because amplitudes on protons and neutrons add up rather than cancel. In

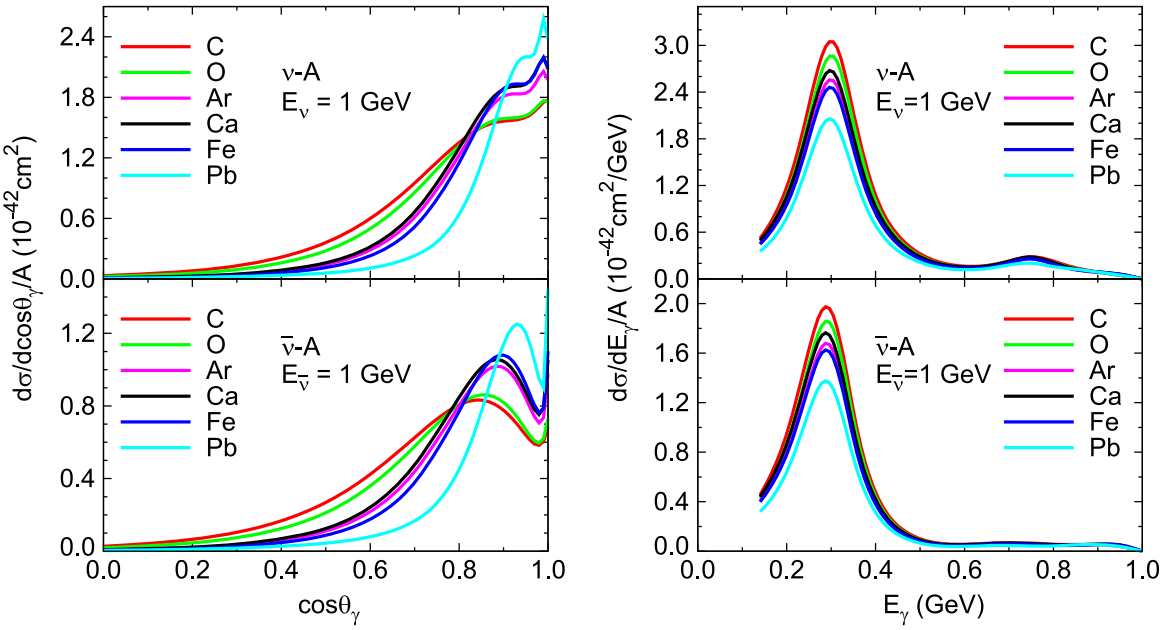

Figure 23. NC COHγ neutrino (top) and antineutrino (bottom) photon angular and energy differential distributions for various nuclei according to the model of [238].

[236] it was found that the COH ωEx mechanism plays a subdominant role at $E_\nu \sim 1$ GeV, compared to naive estimates, being suppressed by form factors and recoil. On the other hand, because of the strong energy dependence of the contact terms in [237], with couplings derived from the ρEx and ωEx amplitudes of [236], the NC COHγ cross section above $E_{\nu,\bar{\nu}} = 0.65$ GeV is dominated by these contact terms and not by the Δ. However, as discussed in section 4.4.2 in the nucleon case, the results are not only highly sensitive to unknown form factors but should also be constrained by unitarity.

There are two features that make the dynamics of NC COHγ processes substantially different to that governing the COHπ ones. First, the outgoing particle (γ) does not suffer from strong distortion effects during its way out of the nucleus, and, second, the axial contribution turns out to be purely transverse $\sim\left(\vec{k}_\gamma \times \vec{q}\ \right)$ and also vanishes when $\vec{q} = \vec{k}_\gamma$ (optimal configuration for the nuclear form factor), which corresponds to $q^2 = 0$. Therefore, the largest differential cross sections arise in kinematics that optimize the product of the amplitude squared of the elementary process times the nuclear form factor, as in pion coherent production reactions induced by electrons and photons [247, 248]. The photon angular dependence exhibited in the left panels of figure 23, obtained with the model of [238], should be understood from this perspective. Notice that θ_γ is the photon angle with respect to the direction of the incoming (anti) neutrino beam and not the angle formed by $\vec{q}$ and $\vec{k}_\gamma$, which is not observable. Indeed, for each θ_γ, an integration over all possible $\vec{q}$ is performed. The interference pattern between the direct dominant Δ mechanism, the cross Δ and the $N(1520)$-pole (weak excitation of this resonance and its subsequent decay into $N\gamma$) terms, also included in the elementary model employed in [238], strongly influences the angular distributions shown in figure 23. Neutrino (antineutrino) COHγ cross sections are about a factor 15 (10) smaller than the incoherent ones [238]. These

proportions are similar to those found for pion production reactions [184, 212] in spite of the suppression of the axial current for forward kinematics in COHγ reactions. This suppression is however partially compensated by the reduction of about a factor of two due to the strong distortion of the outgoing pion, which is not present in the photon case.

Predictions [238] for the outgoing photon energy distributions in various nuclei are displayed in the right panels of figure 23. The pronounced peak is produced by the dominant Δ resonance. The peak position does not appreciably change from nucleus to nucleus, but it gets wider as A increases. The second, smaller and broader peak that can be seen for neutrinos but not for antineutrinos corresponds to the excitation of the $D_{13}(1520)$ resonance. For the integrated cross sections it is found [238] that these neither scale with A, like the incoherent one approximately does, nor with A^2 as one would expect from the coherence of the dominant Δ mechanism.

6. MC generators

Neutrino beams are not mono-energetic and usually contain several flavors. In the experiments, it is necessary to identify the flavor of the interacting neutrino and reconstruct its direction and energy from the particles observed in the detectors. Therefore, a detailed knowledge of the final state after a neutrino interaction is essential to analyze and interpret the data. In order to evaluate the efficiency, resolution and purity of the selected event samples, or to establish the method to analyze the data, simulation program libraries, developed specifically for neutrino interactions, are extensively used. These libraries, which provide all the information on the produced particles for the different neutrino interaction mechanisms, are called MC neutrino event generators.

There are several generators available, such as ANIS [267], GENIE [268], GiBUU [86], NEGN [269], NEUT [270], NUANCE [206], FLUKA [271] or NuWRO [216]. Some of them have been developed by different experimental groups to be used in their analysis. There are several reasons why the different collaborations developed their own generators. The first reason is that the neutrino beam energy spectrum is specific for each experiment and thus, the dominant/relevant interaction modes could be quite different. Unfortunately, there is no *unified* framework able to describe all neutrino interactions in a broad energy range, so that each generator needs to combine various models. Sometimes rather simplified schemes are used to describe some interactions, which are not too relevant for a given experiment. The second reason is that the target nuclei and detectors used in each experiment are different as well. Furthermore, the detection efficiencies for each type of particle are detector dependent and can become quite different. A widespread strategy to deal with these challenges is to choose the underlying models according to the specific needs of the experiment and tune them from the data measured at the (near) detectors. These specialized generators are useful within a single experiment but, sometimes, their diversity makes the comparison of results from different experiments difficult. This also obscures the physical interpretation of the cross section data and slows down the development of more precise approaches. In order to avoid these kinds of problems, the GENIE collaboration undertook the development of a new MC aiming to cover all the relevant neutrino energy ranges. On the other hand, some theory groups have also developed generators to interpret the experimental data sets that have become available in recent years.

In general, an event generator is required to provide, for any neutrino flavor and energy, and target nucleus:

- the total cross section,
- the partial contributions to the cross section from each interaction mode,
- the energy and direction of all the produced particles, simulating particle re-interactions inside the target nucleus when necessary.

Usually, the procedure employed to simulate an event in the actual detector can be separated into several steps:

1. The target nucleus and the neutrino energy are selected, taking into account the composition of the detector, the total cross section for each material and the spectrum of the neutrino beam.
2. The four-momentum of the target nucleon and the position inside the nucleus where the neutrino interaction takes place are chosen.
3. The type of interaction (QE, pion production, etc) is selected according to the corresponding probabilities for the neutrino energy picked up in the first step.
4. The neutrino–nucleon interaction is simulated, and the four-momenta of the outgoing lepton, nucleon(s) and other particles are fixed using the differential cross section of the particular type of interaction considered.
5. The produced nucleons and mesons are followed along their path through the nucleus; their subsequent interactions are also simulated.

As mentioned, the total cross section is used in the first step. Generally, the generator creates a table of interaction probabilities, which are calculated as $\text{flux}\left(E_\nu\right) \times \sum_{\text{nuclear targets }(A)} \sigma_A\left(E_\nu\right) \times r_A$, where r_A is the relative abundance (weight) of type A nuclei. This energy-dependent interaction probability is used to determine the energy of the incoming neutrino that should be simulated. A similar strategy is adopted to select the target nucleus and the specific neutrino interaction considered for each event. Once the energy and target nucleus are fixed, the actual event simulation procedure starts, which is different for each generator depending on the choice of models. The initial nucleon momentum is selected using a probability density profile. The simplest form is a step function, deduced from a global Fermi-gas model. This probability density function could be corrected or re-weighted to take into account kinematical bounds such as Pauli-blocking in the final state. The position within the nucleus where the first neutrino interaction occurs is set assuming a uniform volume distribution. Starting from this position, the subsequent interactions of the produced (secondary) particles in their way out of the nucleus are simulated in a later stage. Next, the theoretical model for $\mathrm{d}\sigma/\mathrm{d}E_\ell \mathrm{d}\theta_\ell$ cross section is used to fix the four-momentum of the outgoing lepton. In the case of QE interactions, the momentum of the final nucleons are determined from energy-momentum conservation. If the first interaction is not QE, additional particles (mostly mesons) are also produced in this first step. All final-state hadrons interact in the nucleus and it is necessary to take into account secondary collisions. Although the initial positions of the particles are fixed from the location of the first interaction that originates the cascade, the actual starting point of each particle may be shifted to take into account the travel length in the nucleus, in the case of resonances, or the formation length of particles. One of the simplest ways to estimate the amount of this shift is to use the concept of the formation zone. Once the simulation of the secondary

interactions of hadrons is finished, some of the generators simulate also de-excitation gamma ray processes or (multi-)nucleon emission.

The simulation programs are carefully designed to deal with the different dynamical models, paying special attention to prevent any important interactions being missed and to avoid unwanted overlaps between different energy regimes. Some event generators incorporate rather old theoretical models to simulate neutrino interactions, even though more sophisticated schemes have recently become available. A first reason for this is that the generators need to simulate several nuclear targets, but sometimes the models are not applicable for all nuclei. Another reason is that the models often have limitations in the kinematic ranges where they can be reliably used, although this is no less true for the old approaches. Because the event generators have to cover the entire allowed phase space and be capable of simulating all the relevant exclusive channels, some models cannot be accommodated in them. Finally, to be able to produce millions of events, the generators have speed limitations that are not complied with by all theoretical descriptions.

As mentioned in section 3.2, to simulate CCQE and NCQE scattering, several generators still use the simple RgFG. This is because it is easy to implement and allows one to change the target nucleus by modifying just a few parameters. Recently, some of the generators have started to adopt some of the more advanced approaches, with spectral functions or the RlFG with RPA corrections discussed in section 3.2.

For single meson production via resonances, many generators implement the relativistic harmonic oscillator model of Rein–Sehgal [175]. Even though this approach underestimates significantly pion electroproduction data (see figure 14 in section 4.2 and the related discussion), it is still extensively used. Indeed, the code to calculate the helicity amplitudes was provided by the authors, it is easy to implement and includes higher energy resonances, which allows the extension of the model to simulate the resonant production of kaon, eta and multiple pions. Some authors [185] have improved the vector form factors for the dominant $\Delta(1232)$ resonance, taking advantage of the helicity amplitudes obtained from recent pion electroproduction data. Some modern generators, like GiBUU [86] and NuWRO [272], are using better models, which rely on pion electroproduction data for the vector part of the amplitudes, and on the neutrino pion production cross sections from the old ANL and BNL bubble chamber neutrino experiments to constrain the resonance axial-vector couplings.

For the simulation of multi-hadron production, DIS (neutrino-quark) is assumed. DIS differential cross sections can be expressed in terms of PDFs. These PDFs are fitted to various experimental data sets and provided as a library. These PDFs are not applicable in the low $q^2 \lesssim 0.8$ GeV^2, and low resonance mass ($W \lesssim 2$ GeV) regions. Therefore, some correction functions have been proposed in these kinematic regions [273]. There could also be some overlaps with the single meson production contributions depending on the implementation. These overlaps are usually avoided by limiting W and the multiplicity. The kinematics of hadrons produced in DIS, the so-called hadronization, is determined with the help of PYTHIA [274, 275], the standard library used in the high energy experiments. PYTHIA is also designed for large values of W, at least bigger than 2 GeV. Thus, most generators use a scaling function, known as KNO [276], whose parameters are also extracted from data.

The particles produced inside the nucleus may interact with the nucleons on their way out. These are the FSI addressed in different parts of this review. Most generators, except GiBUU and NUNDIS/NUNRES, simulate these rescatterings with a semi-classical cascade. In

particular, the pions are carefully treated because their interaction probability is rather high, once many of these are produced from resonance decay. Although the basic idea is the same in several generators, the actual implementations of the particle mean free paths, the determination of the rescattered particle kinematics, or the particle production multiplicities are substantially different in the various generators. GiBUU takes FSI into account using a semi-classical transport model in coupled channels, which was briefly described in section 4.3. Finally, NUNDIS/NURES simulates the rescattering in the framework of the FLUKA simulation package.

7. Concluding remarks

Neutrino interactions offer unique opportunities for exploring fundamental questions in astrophysics, nuclear and particle physics. One of these questions regards the neutrino oscillation phenomenon, which has been established over the last 15 years. Neutrino oscillation experiments are currently evolving from the discovery to the precision stage. Unavoidably, any oscillation experiment faces a major difficulty: the elusive nature of the neutrinos. The presence of neutrinos, being chargeless particles, can only be inferred by detecting the secondary particles created when the neutrinos interact with the nuclear targets used as detectors. A better understanding of the neutrino–nucleus interactions is then crucial to minimize systematic uncertainties in neutrino oscillation experiments. For nuclear physics this represents not only a challenge, but also an opportunity. Indeed, with the recent intense experimental activity a wealth of new more precise neutrino–nucleus cross section data have become available, and more are awaited in the future.

Most of the relevant event sample falls inside the poorly understood region of resonance excitation. Experiments like MiniBooNE and SciBooNE have produced good quality data for quasi-elastic scattering and pion production at intermediate energies. These data show interesting deviations from theoretical predictions. Some of them have found an explanation (CCQE, in terms of 2p2h excitations), but others still await a proper interpretation.

We have reviewed the recent progress in the physics of neutrino cross sections, highlighting the open questions revealed by the comparison with new experimental data. Among others, we have identified both incoherent and coherent pion production on nuclei as topical problems, where significant discrepancies between data and theoretical predictions exist and have not yet been understood. In the first case, state of the art microscopic approaches fail to describe the CC1π MiniBooNE differential and total cross sections: theoretical estimates are systematically below the data. Microscopic models predict a suppression in the pion spectra around the $\Delta(1232)$ resonance region, which is not seen in the experimental distribution of events. This points either to an incorrect theoretical description of pion FSI effects or to a misunderstanding of the actual (dynamical) origin of the events measured by MiniBooNE. Regarding coherent pion production, the SciBooNE measurement of the ratio $\sigma_{\mathrm{CC-COH}\pi^+}/\sigma_{\mathrm{NC-COH}\pi^0}$ on carbon is more than 4σ away from the bulk of the theoretical results, which are consistent with what is expected from the combination of PCAC and isospin invariance.

So far, more precise nuclear cross sections have not allowed us to gain insight into the axial hadron properties because of the intrinsic difficulties in the treatment of nuclear and FSI effects. The more than 30-year-old ANL and BNL low statistics deuterium pion production data are still nowadays the best source of information about the $N\Delta$ transition matrix element. New

measurements of neutrino cross sections on hydrogen and deuterium are thus absolutely necessary, even more when there is tension between ANL and BNL $p\pi^+$ data samples.

We should also stress that, to achieve the precision goals in neutrino oscillation measurements and to reliably extract information about the axial properties of the nucleon and baryon resonances, it is crucial that the current theoretical developments are implemented in the event generators used in the experimental data analysis. The strategy, adopted by some oscillation experiments, of fitting the new data with the parameters available in the MC event generators is dangerous in the long term.

The MINERνA experiment at FermiLab, fully dedicated to the measurement of neutrino cross sections on nuclear targets, has started to take data. This experiment will provide valuable information complementary to the findings of the Jefferson Lab with electrons, and stimulate productive activity in the field of neutrino cross sections in the coming years.

Acknowledgments

We thank M Barbaro, R Gran, E Hernandez and M J Vicente Vacas for their help with some of the figures included in this review. Research supported by the Spanish Ministerio de Economía y Competitividad and European FEDER funds under the contract FIS2011-28853-C02-02 and the Spanish Consolider-Ingenio 2010 Programme CPAN (CSD2007-00042), by Generalitat Valenciana under contract PROMETEO/2009/0090 and by the EU Hadron Physics2 project, grant agreement no. 227431.

References

[1] Bertulani C and Gade A 2010 *Phys. Rep.* **485** 195–259
[2] Volpe C 2013 *Ann. Phys. (Berlin)* **525** 588–99
[3] Ohlsson T 2013 *Rep. Prog. Phys.* **76** 044201
[4] Gallagher H, Garvey G and Zeller G 2011 *Annu. Rev. Nucl. Part. Sci.* **61** 355–78
[5] Morfin J G, Nieves J and Sobczyk J T 2012 *Adv. High Energy Phys.* **2012** 934597
[6] Kopeliovich B, Morfin J and Schmidt I 2013 *Prog. Part. Nucl. Phys.* **68** 314–72
[7] Formaggio J and Zeller G 2012 *Rev. Mod. Phys.* **84** 1307
[8] Fukuda Y *et al* (Super-Kamiokande Collaboration) 1998 *Phys. Rev. Lett.* **81** 1562–7
[9] Ashie Y *et al* (Super-Kamiokande Collaboration) 2005 *Phys. Rev.* D **71** 112005
[10] Abe K *et al* (Super-Kamiokande Collaboration) 2013 *Phys. Rev. Lett.* **110** 181802
[11] Wendell R *et al* (Super-Kamiokande Collaboration) 2010 *Phys. Rev.* D **81** 092004
[12] Ahn S H *et al* (K2K Collaboration) 2001 *Phys. Lett.* B **511** 178–84
[13] Adamson P *et al* (MINOS Collaboration) 2008 *Phys. Rev.* D **77** 072002
[14] Agafonova N *et al* (OPERA Collaboration) 2010 *Phys. Lett.* B **691** 138–45
[15] Abe K *et al* (T2K Collaboration) 2011 *Nucl. Instrum. Methods* A **659** 106–35
[16] Gran R *et al* (K2K Collaboration) 2006 *Phys. Rev.* D **74** 052002
[17] Bodek A and Yang U 2003 *AIP Conf. Proc.* **670** 110–7
[18] Nakayama S *et al* (K2K Collaboration) 2005 *Phys. Lett.* B **619** 255–62
[19] Hasegawa M *et al* (K2K Collaboration) 2005 *Phys. Rev. Lett.* **95** 252301
[20] Adamson P *et al* (MINOS Collaboration) 2013 *Phys. Rev. Lett.* **110** 251801
[21] Dorman M (MINOS Collaboration) 2009 *AIP Conf. Proc.* **1189** 133–8
[22] Agafonova N *et al* (OPERA Collaboration) 2013 *JHEP* **1311** 036
[23] Aguilar-Arevalo A *et al* (MiniBooNE Collaboration) 2010 *Phys. Rev.* D **81** 092005

[24] Aguilar-Arevalo A *et al* (LSND Collaboration) 2001 *Phys. Rev.* D **64** 112007
[25] Aguilar-Arevalo A *et al* (MiniBooNE Collaboration) 2013 *Phys. Rev.* D **88** 032001
[26] Katori T (MiniBooNE Collaboration) 2010 *AIP Conf. Proc.* **1222** 471–4
[27] Aguilar-Arevalo A *et al* (MiniBooNE Collaboration) 2011 *Phys. Rev.* D **83** 052009
[28] Aguilar-Arevalo A *et al* (MiniBooNE Collaboration) 2011 *Phys. Rev.* D **83** 052007
[29] Aguilar-Arevalo A *et al* (MiniBooNE Collaboration) 2010 *Phys. Rev.* D **82** 092005
[30] Aguilar-Arevalo A A *et al* (MiniBooNE Collaboration) 2010 *Phys. Rev.* D **81** 013005
[31] Aguilar-Arevalo A *et al* (MiniBooNE Collaboration) 2009 *Phys. Rev. Lett.* **102** 101802
[32] Aguilar-Arevalo A *et al* (MiniBooNE Collaboration) 2013 *Phys. Rev. Lett.* **110** 161801
[33] Altegoer J *et al* (NOMAD Collaboration) 1998 *Nucl. Instrum. Meth.* A **404** 96–128
[34] Astier P *et al* (NOMAD Collaboration) 2001 *Nucl. Phys.* B **611** 3–39
[35] Lyubushkin V *et al* (NOMAD Collaboration) 2009 *Eur. Phys. J.* C **63** 355–81
[36] Kullenberg C *et al* (NOMAD Collaboration) 2009 *Phys. Lett.* B **682** 177–84
[37] Tian X (NOMAD Collaboration) 2013 arXiv:1310.8547 [hep-ex]
[38] Astier P *et al* (NOMAD Collaboration) 2002 *Nucl. Phys.* B **621** 3–34
[39] Naumov D *et al* (NOMAD Collaboration) 2004 *Nucl. Phys.* B **700** 51–68
[40] Astier P *et al* (NOMAD Collaboration) 2002 *Phys. Lett.* B **526** 278–86
[41] Aunion J L A 2010 *PhD Thesis* Barcelona
[42] Katori T (MiniBooNE Collaboration, SciBooNE Collaboration) 2013 arXiv:1304.5325
[43] Hiraide K *et al* (SciBooNE Collaboration) 2008 *Phys. Rev.* D **78** 112004
[44] Kurimoto Y *et al* (SciBooNE Collaboration) 2010 *Phys. Rev.* D **81** 111102
[45] Nakajima Y *et al* (SciBooNE Collaboration) 2011 *Phys. Rev.* D **83** 012005
[46] Anderson C *et al* 2012 *J. Instrum.* **7** P10019
[47] Anderson C *et al* (ArgoNeuT Collaboration) 2012 *Phys. Rev. Lett.* **108** 161802
[48] Fields L *et al* (MINERvA Collaboration) 2013 *Phys. Rev. Lett.* **111** 022501
[49] Fiorentini G *et al* (MINERvA Collaboration) 2013 *Phys. Rev. Lett.* **111** 022502
[50] Abe K *et al* (T2K Collaboration) 2011 *Phys. Rev. Lett.* **107** 041801
[51] Abe K *et al* (T2K Collaboration) 2014 *Phys. Rev. Lett.* **112** 061802
[52] An F *et al* (Daya Bay Collaboration) 2014 *Phys. Rev. Lett.* **112** 061801
[53] Ahn J *et al* (RENO Collaboration) 2012 *Phys. Rev. Lett.* **108** 191802
[54] Abe Y *et al* (Double Chooz Collaboration) 2013 *Phys. Lett.* B **723** 66–70
[55] Nieves J, Amaro J E and Valverde M 2004 *Phys. Rev.* C **70** 055503
[56] Nieves J, Valverde M and Vicente Vacas M 2006 *Phys. Rev.* C **73** 025504
[57] Llewellyn Smith C 1972 *Phys. Rep.* **3** 261–379
[58] Bernard V, Kaiser N and Meissner U G 1992 *Phys. Rev. Lett.* **69** 1877–9
[59] Bernard V, Elouadrhiri L and Meissner U 2002 *J. Phys.* **G28** 1–35
[60] Liesenfeld A *et al* (A1 Collaboration) 1999 *Phys. Lett.* B **468** 20
[61] Gonzalez-Jimenez R, Caballero J and Donnelly T 2013 *Phys. Rep.* **524** 1–35
[62] Bodek A, Avvakumov S, Bradford R and Budd H S 2008 *Eur. Phys. J.* C **53** 349–54
[63] Crawford C *et al* 2010 *Phys. Rev.* C **82** 045211
[64] Masjuan P, Ruiz Arriola E and Broniowski W 2013 *Phys. Rev.* D **87** 014005
[65] Megias G, Amaro J, Barbaro M, Caballero J and Donnelly T 2013 *Phys. Lett.* B **725** 170–4
[66] Pate S and Trujillo D 2013 arXiv:1308.5694 [hep-ph]
[67] Gonzalez-Jimenez R, Ivanov M, Barbaro M, Caballero J and Udias J 2013 *Phys. Lett.* B **718** 1471–4
[68] Dharmapalan R *et al* (MiniBooNE Collaboration) 2013 arXiv:1310.0076 [hep-ex]
[69] Chen H *et al* (MicroBooNE Collaboration) 2007 *Fermilab Proposal* **0974** http://inspirehep.net/record/776376/files/fermilab-proposal-0974.PDF
[70] Leitner T, Alvarez-Ruso L and Mosel U 2006 *Phys. Rev.* C **74** 065502
[71] Fetter A L and Walecka J D 2003 *Quantum Theory of Many-Particle Systems* (New York: Dover)

[72] Smith R and Moniz E 1972 *Nucl. Phys.* B **43** 605
[73] Benhar O, Fabrocini A, Fantoni S and Sick I 1994 *Nucl. Phys.* A **579** 493–517
[74] Ciofi degli Atti C and Simula S 1996 *Phys. Rev.* C **53** 1689
[75] Fernandez de Cordoba P and Oset E 1992 *Phys. Rev.* C **46** 1697–709
[76] Kulagin S A and Petti R 2006 *Nucl. Phys.* A **765** 126–87
[77] Ciofi degli Atti C, Liuti S and Simula S 1990 *Phys. Rev.* C **41** R2474–8
[78] Gil A, Nieves J and Oset E 1997 *Nucl. Phys.* A **627** 543–98
[79] Benhar O, Farina N, Nakamura H, Sakuda M and Seki R 2005 *Phys. Rev.* D **72** 053005
[80] Benhar O and Meloni D 2007 *Nucl. Phys.* A **789** 379–402
[81] Ankowski A M and Sobczyk J T 2008 *Phys. Rev.* C **77** 044311
[82] Butkevich A 2012 *Phys. Rev.* C **85** 065501
[83] Ankowski A M and Sobczyk J T 2006 *Phys. Rev.* C **74** 054316
[84] Nieves J, Oset E and Garcia-Recio C 1993 *Nucl. Phys.* A **554** 509–53
[85] Shneor R *et al* (Jefferson Lab Hall A Collaboration) 2007 *Phys. Rev. Lett.* **99** 072501
[86] Buss O *et al* 2012 *Phys. Rep.* **512** 1–124
[87] Alberico W *et al* 1997 *Nucl. Phys.* A **623** 471–97
[88] Maieron C, Martinez M, Caballero J and Udias J 2003 *Phys. Rev.* C **68** 048501
[89] Butkevich A and Kulagin S A 2007 *Phys. Rev.* C **76** 045502
[90] Meucci A, Giusti C and Pacati F D 2004 *Nucl. Phys.* A **744** 307–22
[91] Benhar O *et al* 1991 *Phys. Rev.* C **44** 2328–42
[92] Leitner T, Buss O, Alvarez-Ruso L and Mosel U 2009 *Phys. Rev.* C **79** 034601
[93] Martinez M *et al* 2006 *Phys. Rev.* C **73** 024607
[94] Meucci A, Giusti C and Pacati F D 2011 *Phys. Rev.* D **84** 113003
[95] Boffi S, Giusti C and Pacati F 1993 *Phys. Rep.* **226** 1–101
[96] Udias J, Sarriguren P, Moya de Guerra E, Garrido E and Caballero J 1993 *Phys. Rev.* C **48** 2731–9
[97] Giusti C, Meucci A, Pacati F, Co' G and De Donno V 2011 *Phys. Rev.* C **84** 024615
[98] Giusti C, Meucci A, Pacati F, Caballero J and Udias J 2009 *AIP Conf. Proc.* **1189** 107–14
[99] Meucci A, Giusti C and Pacati F D 2004 *Nucl. Phys.* A **739** 277–90
[100] Meucci A, Barbaro M, Caballero J, Giusti C and Udias J 2011 *Phys. Rev. Lett.* **107** 172501
[101] Meucci A and Giusti C 2012 *Phys. Rev.* D **85** 093002
[102] Meucci A and Giusti C 2014 *Phys. Rev.* D **89** 057302
[103] González-Jiménez R *et al* 2013 *Phys. Rev.* C **88** 025502
[104] Leitner T, Alvarez-Ruso L and Mosel U 2006 *Phys. Rev.* C **73** 065502
[105] Meziani Z *et al* 1984 *Phys. Rev. Lett.* **52** 2130–3
[106] Meucci A, Capuzzi F, Giusti C and Pacati F D 2003 *Phys. Rev.* C **67** 054601
[107] Benhar O, Day D and Sick I 2008 *Mod. Phys. Rev.* **80** 189–224
[108] Fabrocini A and Fantoni S 1989 *Nucl. Phys.* A **503** 375–403
[109] Donnelly T and Sick I 1999 *Phys. Rev. Lett.* **82** 3212–5
[110] Donnelly T and Sick I 1999 *Phys. Rev.* C **60** 065502
[111] Amaro J E *et al* 2005 *Phys. Rev.* C **71** 015501
[112] Jourdan J 1996 *Nucl. Phys.* A **603** 117–60
[113] Caballero J *et al* 2005 *Phys. Rev. Lett.* **95** 252502
[114] Caballero J, Amaro J E, Barbaro M, Donnelly T and Udias J 2007 *Phys. Lett.* B **653** 366–72
[115] Antonov A *et al* 2011 *Phys. Rev.* C **83** 045504
[116] Amaro J E, Barbaro M, Caballero J and Donnelly T 2007 *Phys. Rev. Lett.* **98** 242501
[117] Singh S and Oset E 1992 *Nucl. Phys.* A **542** 587–615
[118] Kosmas T and Oset E 1996 *Phys. Rev.* C **53** 1409–15
[119] Singh S, Mukhopadhyay N C and Oset E 1998 *Phys. Rev.* C **57** 2687–92
[120] Sajjad Athar M, Ahmad S and Singh S 2006 *Nucl. Phys.* A **764** 551–68

[121] Athar M S, Ahmad S and Singh S 2005 *Eur. Phys. J.* A **24** 459–74
[122] Marteau J 1999 *Eur. Phys. J.* A **5** 183–90
[123] Marteau J, Delorme J and Ericson M 2000 *Nucl. Instrum. Meth.* A **451** 76–80
[124] Martini M, Ericson M, Chanfray G and Marteau J 2009 *Phys. Rev.* C **80** 065501
[125] Kim H c, Piekarewicz J and Horowitz C 1995 *Phys. Rev.* C **51** 2739–49
[126] Graczyk K M and Sobczyk J T 2003 *Eur. Phys. J.* C **31** 177–85
[127] Graczyk K M 2005 *Nucl. Phys.* A **748** 313–30
[128] Aguilar-Arevalo A *et al* (MiniBooNE Collaboration) 2009 *Phys. Rev.* D **79** 072002
[129] Alvarez-Ruso L, Buss O, Leitner T and Mosel U 2009 *AIP Conf. Proc.* **1189** 151–6
[130] Speth J, Klemt V, Wambach J and Brown G 1980 *Nucl. Phys.* A **343** 382–416
[131] Kolbe E, Langanke K, Krewald S and Thielemann F 1992 *Nucl. Phys.* A **540** 599–620
[132] Volpe C, Auerbach N, Colo G, Suzuki T and van Giai N 2000 *Phys. Rev.* C **62** 015501
[133] Jachowicz N, Heyde K, Ryckebusch J and Rombouts S 2002 *Phys. Rev.* C **65** 025501
[134] Pandey V, Jachowicz N, Ryckebusch J, van Cuyck T and Cosyn W 2014 *Phys. Rev.* C **89** 024601
[135] Amaro J E, Maieron C, Nieves J and Valverde M 2005 *Eur. Phys. J.* A **24** 343–53
[136] Katori T(MiniBooNE Collaboration) 2009 *AIP Conf. Proc.* **1189** 139–44
[137] Boyd S, Dytman S, Hernandez E, Sobczyk J and Tacik R 2009 *AIP Conf. Proc.* **1189** 60–73
[138] Sajjad Athar M, Chauhan S and Singh S 2010 *Eur. Phys. J.* A **43** 209–27
[139] Nieves J, Ruiz Simo I and Vicente Vacas M 2012 *Phys. Lett.* B **707** 72–75
[140] Shimizu K and Faessler A 1980 *Nucl. Phys.* A **333** 495–513
[141] Alberico W, Ericson M and Molinari A 1984 *Ann. Phys.* **154** 356
[142] Nieves J, Ruiz Simo I and Vicente Vacas M 2011 *Phys. Rev.* C **83** 045501
[143] Lovato A, Gandolfi S, Carlson J, Pieper S C and Schiavilla R 2014 *Phys. Rev. Lett.* **112** 182502
[144] Lovato A *et al* 2013 *Phys. Rev. Lett.* **111** 092501
[145] Benhar O, Lovato A and Rocco N 2013 arXiv:1312.1210 [nucl-th]
[146] Amaro J, Barbaro M, Caballero J, Donnelly T and Williamson C 2011 *Phys. Lett.* B **696** 151–5
[147] Martini M, Ericson M and Chanfray G 2011 *Phys. Rev.* C **84** 055502
[148] Amaro J, Barbaro M, Caballero J and Donnelly T 2012 *Phys. Rev. Lett.* **108** 152501
[149] Nieves J, Ruiz Simo I and Vicente Vacas M 2013 *Phys. Lett.* B **721** 90–93
[150] Martini M and Ericson M 2013 *Phys. Rev.* C **87** 065501
[151] Lalakulich O, Gallmeister K and Mosel U 2012 *Phys. Rev.* C **86** 014614
[152] Sobczyk J T 2012 *Phys. Rev.* C **86** 015504
[153] Kordosky M 2006 *Nucl. Phys. Proc. Suppl.* **159** 223–8
[154] Martini M, Ericson M and Chanfray G 2012 *Phys. Rev.* D **85** 093012
[155] Nieves J, Sanchez F, Ruiz Simo I and Vicente Vacas M 2012 *Phys. Rev.* D **85** 113008
[156] Martini M, Ericson M and Chanfray G 2013 *Phys. Rev.* D **87** 013009
[157] Lalakulich O and Mosel U 2012 *Phys. Rev.* C **86** 054606
[158] Mosel U, Lalakulich O and Gallmeister K 2013 *Phys. Rev. Lett.* **112** 151802
[159] Coloma P and Huber P 2013 *Phys. Rev. Lett.* **111** 221802
[160] Coloma P, Huber P, Jen C M and Mariani C 2013 *Phys. Rev.* D **89** 073015
[161] Gran R, Nieves J, Sanchez F and Vacas M J V 2013 *Phys. Rev.* D **88** 113007
[162] Cabibbo N, Swallow E C and Winston R 2003 *Annu. Rev. Nucl. Part. Sci.* **53** 39–75
[163] Singh S and Vicente Vacas M 2006 *Phys. Rev.* D **74** 053009
[164] Mintz S and Wen L 2007 *Eur. Phys. J.* A **33** 299–301
[165] Kuzmin K and Naumov V 2009 *Phys. Atom. Nucl.* **72** 1501–12
[166] Zhu S L, Puglia S and Ramsey-Musolf M 2001 *Phys. Rev.* D **63** 034002
[167] Alam M R, Chauhan S, Athar M S and Singh S 2013 *Phys. Rev.* D **88** 077301
[168] Kurimoto Y *et al* (SciBooNE Collaboration) 2010 *Phys. Rev.* D **81** 033004
[169] Campbell J *et al* 1973 *Phys. Rev. Lett.* **30** 335–9

[170] Radecky G *et al* 1982 *Phys. Rev.* D **25** 1161–73
[171] Kitagaki T *et al* 1986 *Phys. Rev.* D **34** 2554–65
[172] Schreiner P and von Hippel F 1973 *Phys. Rev. Lett.* **30** 339–42
[173] Fogli G L and Nardulli G 1979 *Nucl. Phys.* B **160** 116
[174] Fogli G L and Nardulli G 1980 *Nucl. Phys.* B **165** 162
[175] Rein D and Sehgal L M 1981 *Ann. Phys.* **133** 79–153
[176] Alvarez-Ruso L, Singh S and Vacas M V 1998 *Phys. Rev.* C **57** 2693–9
[177] Alvarez-Ruso L, Singh S and Vacas M V 1999 *Phys. Rev.* C **59** 3386–92
[178] Sato T, Uno D and Lee T 2003 *Phys. Rev.* C **67** 065201
[179] Paschos E A, Yu J Y and Sakuda M 2004 *Phys. Rev.* D **69** 014013
[180] Lalakulich O and Paschos E A 2005 *Phys. Rev.* D **71** 074003
[181] Lalakulich O, Paschos E A and Piranishvili G 2006 *Phys. Rev.* D **74** 014009
[182] Hernandez E, Nieves J and Valverde M 2007 *Phys. Rev.* D **76** 033005
[183] Hernandez E, Nieves J, Valverde M and Vacas M V 2010 *Phys. Rev.* D **81** 085046
[184] Hernandez E, Nieves J and Vacas M J V 2013 *Phys. Rev.* D **87** 113009
[185] Graczyk K M and Sobczyk J T 2008 *Phys. Rev.* D **77** 053001
[186] Graczyk K, Kielczewska D, Przewlocki P and Sobczyk J 2009 *Phys. Rev.* D **80** 093001
[187] Barbero C, Castro G L and Mariano A 2008 *Phys. Lett.* B **664** 70–77
[188] Barbero C, Castro G L and Mariano A 2014 *Phys. Lett.* B **728** 282–7
[189] Serot B D and Zhang X 2012 *Phys. Rev.* C **86** 015501
[190] MAID www.kph.uni-mainz.de/MAID
[191] Tiator L, Drechsel D, Kamalov S and Vanderhaeghen M 2011 *Eur. Phys. J. ST* **198** 141–70
[192] Feynman R, Kislinger M and Ravndal F 1971 *Phys. Rev.* D **3** 2706–32
[193] Berger C and Sehgal L 2007 *Phys. Rev.* D **76** 113004
[194] Graczyk K M and Sobczyk J T 2008 *Phys. Rev.* D **77** 053003
[195] Leitner T, Buss O, Mosel U and Alvarez-Ruso L 2008 *PoS NUFACT* **08** 009
[196] Paschos E and Schalla D 2011 *Phys. Rev.* D **84** 013004
[197] Kamano H, Nakamura S, Lee T S and Sato T 2012 *Phys. Rev.* D **86** 097503
[198] Nakamura S, Kamano H, Lee T S H and Sato T 2013 arXiv:1303.4152 [hep-ph]
[199] JLab https://hallcweb.jlab.org/resdata/database/jlabh2.txt
[200] Adler S L 1968 *Ann. Phys.* **50** 189–311
[201] Bijtebier J 1970 *Nucl. Phys.* B **21** 158–72
[202] Lalakulich O, Leitner T, Buss O and Mosel U 2010 *Phys. Rev.* D **82** 093001
[203] Kim H C, Schramm S and Horowitz C 1996 *Phys. Rev.* C **53** 2468–73
[204] Singh S, Vicente-Vacas M and Oset E 1998 *Phys. Lett.* B **416** 23–28
[205] Praet C, Lalakulich O, Jachowicz N and Ryckebusch J 2009 *Phys. Rev.* C **79** 044603
[206] Casper D 2002 *Nucl. Phys. Proc. Suppl.* **112** 161–70
[207] Lalakulich O and Mosel U 2013 *Phys. Rev.* C **87** 014602
[208] Leitner T, Lalakulich O, Buss O, Mosel U and Alvarez-Ruso L 2010 *AIP Conf. Proc.* **1222** 212–21
[209] Leitner T, Buss O, Mosel U and Alvarez-Ruso L 2009 *AIP Conf. Proc.* **1189** 207–12
[210] Leitner T, Buss O, Mosel U and Alvarez-Ruso L 2009 *Phys. Rev.* C **79** 038501
[211] Amaro J, Hernandez E, Nieves J and Valverde M 2009 *Phys. Rev.* D **79** 013002
[212] Hernandez E, Nieves J and Valverde M 2010 *Phys. Rev.* D **82** 077303
[213] Oset E and Salcedo L 1987 *Nucl. Phys.* A **468** 631–52
[214] Salcedo L, Oset E, Vicente-Vacas M and Garcia-Recio C 1988 *Nucl. Phys.* A **484** 557
[215] Gil A, Nieves J and Oset E 1997 *Nucl. Phys.* A **627** 599–619
[216] Juszczak C, Nowak J A and Sobczyk J T 2006 *Nucl. Phys. Proc. Suppl.* **159** 211–6
[217] Juszczak C 2009 *Acta Phys. Pol.* B **40** 2507–12
[218] Golan T, Juszczak C and Sobczyk J T 2012 *Phys. Rev.* C **86** 015505

[219] Rein D and Sehgal L M 1983 *Nucl. Phys.* B **223** 29
[220] Pinzon E 2013 *talk at NuFacT 13, Beijing, China*
[221] Aguilar-Arevalo A *et al* (MiniBooNE Collaboration) 2009 *Phys. Rev. Lett.* **103** 081801
[222] Rodriguez A *et al* (K2K Collaboration) 2008 *Phys. Rev.* D **78** 032003
[223] Sajjad Athar M, Chauhan S and Singh S 2010 *J. Phys.* G **37** 015005
[224] Lalakulich O and Mosel U 2013 *Phys. Rev.* C **88** 017601
[225] Mosel U, Lalakulich O and Gallmeister K 2014 *Phys. Rev.* D **89** 093003
[226] Dewan H 1981 *Phys. Rev.* D **24** 2369–78
[227] Alam M R, Simo I R, Athar M S and Vacas M V 2010 *Phys. Rev.* D **82** 033001
[228] Alam M R, Simo I R, Athar M S and Vicente Vacas M 2012 *Phys. Rev.* D **85** 013014
[229] Shrock R E 1975 *Phys. Rev.* D **12** 2049
[230] Adera G, van der Ventel B, van Niekerk D and Mart T 2010 *Phys. Rev.* C **82** 025501
[231] Alam M R, Simo I R, Athar M S, Alvarez-Ruso L and Vacas M J V 2013 arXiv:1303.5924 [hep-ph]
[232] Alam M R *et al* 2013 arXiv:1311.2293 [hep-ph]
[233] Lalakulich O, Gallmeister K and Mosel U 2012 *Phys. Rev.* C **86** 014607
[234] Ankowski A M, Benhar O, Mori T, Yamaguchi R and Sakuda M 2012 *Phys. Rev. Lett.* **108** 052505
[235] Aguilar-Arevalo A *et al* (MiniBooNE Collaboration) 2007 *Phys. Rev. Lett.* **98** 231801
[236] Hill R J 2010 *Phys. Rev.* D **81** 013008
[237] Zhang X and Serot B D 2013 *Phys. Lett.* B **719** 409–14
[238] Wang E, Alvarez-Ruso L and Nieves J 2014 *Phys. Rev.* C **89** 015503
[239] Harvey J A, Hill C T and Hill R J 2007 *Phys. Rev. Lett.* **99** 261601
[240] Harada M, Matsuzaki S and Yamawaki K 2011 *Phys. Rev.* D **84** 036010
[241] Zhang X and Serot B D 2012 *Phys. Rev.* C **86** 035502
[242] Hill R J 2011 *Phys. Rev.* D **84** 017501
[243] MiniBooNE 2012 http://www-boone.fnal.gov/for_physicists/data_release/nue_nuebar_2012/efficiency/MB_nu_nubar_combined_release.html
[244] Alvarez-Ruso L, Nieves J and Wang E 2013 arXiv:1304.2702 [nucl-th]
[245] Wang E, Alvarez-Ruso L and Nieves J 2014 in preparation
[246] Hiraide K (SciBooNE Collaboration) 2006 *Nucl. Phys. Proc. Suppl.* **159** 85–90
[247] Carrasco R, Nieves J and Oset E 1993 *Nucl. Phys.* A **565** 797–817
[248] Hirenzaki S, Nieves J, Oset E and Vicente-Vacas M 1993 *Phys. Lett.* B **304** 198–202
[249] Fernández de Córdoba P, Nieves J, Oset E and Vicente-Vacas M 1993 *Phys. Lett.* B **319** 416–20
[250] Leitner T, Mosel U and Winkelmann S 2009 *Phys. Rev.* C **79** 057601
[251] Nakamura S, Sato T, Lee T S, Szczerbinska B and Kubodera K 2010 *Phys. Rev.* C **81** 035502
[252] Kopeliovich B and Marage P 1993 *Int. J. Mod. Phys.* A **8** 1513–602
[253] Rein D and Sehgal L 2007 *Phys. Lett.* B **657** 207–9
[254] Paschos E, Kartavtsev A and Gounaris G 2006 *Phys. Rev.* D **74** 054007
[255] Singh S, Sajjad Athar M and Ahmad S 2006 *Phys. Rev. Lett.* **96** 241801
[256] Alvarez-Ruso L, Geng L, Hirenzaki S and Vicente Vacas M 2007 *Phys. Rev.* C **75** 055501
[257] Alvarez-Ruso L, Geng L and Vacas M V 2007 *Phys. Rev.* C **76** 068501
[258] Zhang X and Serot B D 2012 *Phys. Rev.* C **86** 035504
[259] Hernandez E, Nieves J and Vicente-Vacas M 2009 *Phys. Rev.* D **80** 013003
[260] Berger C and Sehgal L 2009 *Phys. Rev.* D **79** 053003
[261] Paschos E and Schalla D 2009 *Phys. Rev.* D **80** 033005
[262] Adler S L 1964 *Phys. Rev.* **135** B963–6
[263] Alvarez-Ruso L, Nieves J, Simo I R, Valverde M and Vicente Vacas M 2013 *Phys. Rev.* C **87** 015503
[264] Alam M R, Simo I R, Athar M S and Vicente Vacas M 2012 *Phys. Rev.* D **85** 013014
[265] Gershtein S, Komachenko Y Y and Khlopov M Y A 1981 *Sov. J. Nucl. Phys.* **33** 860
[266] Rein D and Sehgal L 1981 *Phys. Lett.* B **104** 394–8

[267] Gazizov A and Kowalski M P 2005 *Comput. Phys. Commun.* **172** 203–13
[268] Andreopoulos C *et al* 2010 *Nucl. Instrum. Meth.* A **614** 87–104
[269] Autiero D 2005 *Nucl. Phys. Proc. Suppl.* **139** 253–9
[270] Hayato Y 2009 *Acta Phys. Pol.* B **40** 2477–89
[271] Battistoni G, Sala P, Lantz M, Ferrari A and Smirnov G 2009 *Acta Phys. Pol.* B **40** 2491–505
[272] Nowak J A 2006 *Phys. Scr.* **T127** 70–72
[273] Bodek A and Yang U 2003 *J. Phys.* G **29** 1899–906
[274] Sjostrand T, Mrenna S and Skands P Z 2006 *J. High Energy Phys.* **0605** 026
[275] Sjostrand T, Mrenna S and Skands P Z 2008 *Comput. Phys. Commun.* **178** 852–67
[276] Koba Z, Nielsen H B and Olesen P 1972 *Nucl. Phys.* B **40** 317–34